

KfK 4696
April 1990

High Resolution Shock-Capturing Scheme for Numerical Simulation of Plasma-Shock Interaction

N. K. Gupta, C. D. Munz, B. Goel
Institut für Neutronenphysik und Reaktortechnik

Kernforschungszentrum Karlsruhe GmbH
Zentralbibliothek

11. JULI 1990

Kernforschungszentrum Karlsruhe

KERNFORSCHUNGSZENTRUM KARLSRUHE
Institut für Neutronenphysik und Reaktortechnik

KfK 4696

***High Resolution Shock-Capturing Scheme for Numerical Simulation
of Plasma-Shock Interaction***

by

N.K. GUPTA*, C.D. MUNZ and B. GOEL

Kernforschungszentrum Karlsruhe GmbH
Zentralbibliothek

* on leave from Theoretical Physics Division, Bhabha Atomic Research Centre
Trombay, Bombay-400 085, India

Kernforschungszentrum Karlsruhe GmbH, Karlsruhe

Als Manuskript vervielfältigt
Für diesen Bericht behalten wir uns alle Rechte vor

Kernforschungszentrum Karlsruhe GmbH
Postfach 3640, 7500 Karlsruhe 1

ISSN 0303-4003

Abstract

This report describes a one dimensional hydrodynamic computer code in Lagrangean geometry based on high resolution upwind schemes. The code has 1st order as well as 2nd order upwind scheme options and can accommodate any given, analytical or tabular equation of state. The code is tested against a number of test problems for which either analytical or numerical solutions from well tested computer codes or both are available in literature. A brief summary of these comparisons is presented in this report. The predictions of this code are compared with the result of the often used von-Neumann prescription of shock capturing. The results of the present code are free from unphysical oscillations which are typical of von-Neumann procedure. The code is used to simulate the 1-dimensional hydrodynamic and thermodynamic behaviour of plasma irradiated by an intense ion beam. The absence of the spurious oscillations in the results of the present code is especially advantageous to study the effects of temporal non-uniformities of the beam. The second order upwind scheme resolves shocks much steeper than the 1st order one and is therefore recommended for shock wave experiment analysis. For a typical pinch reflex diode pulse of proton beam on aluminium target upwind results predict compressions of about 10 - 15 % higher as compared to von-Neumann procedure. The upwind results are believed to be closer to reality because this method does not involve any artificial pressure term.

Ein Shock-Capturing Verfahren hoher Genauigkeit zur numerischen Simulation von Plasma-Stoßwellen Wechselwirkungen

Zusammenfassung

Dieser Bericht beschreibt ein eindimensionales Rechenprogramm in Lagrange Koordinaten, welches eine numerische Methode hoher Genauigkeit benutzt. Im Programm besteht die Wahl zwischen Upwind-Verfahren erster und zweiter Ordnung; beliebig vorgegebene Zustandsgleichungen - in analytischer oder auch tabellarischer Form - können verwendet werden. Das Programm wurde anhand einer Reihe von Testproblemen überprüft, für welche analytische oder auch numerische Resultate von anderen Codes vorliegen. Ein kurzer Überblick über diese Vergleiche ist in diesem Bericht enthalten. Die Resultate mit diesem Programm werden verglichen mit denen, welche mit der oft benutzten von Neumann Methode der Stoßwellenapproximation erzielt wurden. Es zeigte sich, daß die Resultate des hier beschriebenen Codes frei von unphysikalischen Oszillationen sind, welche typischerweise beim von Neumann Verfahren auftreten. Das Programm wird benutzt zur Simulation des eindimensionalen hydro- und thermodynamischen Verhaltens eines Plasmas, welches durch einen hochenergetischen Ionenstrahl erzeugt wird. Das Fehlen der numerischen Oszillationen in den Resultaten dieses Programmes erweist sich als besonders vorteilhaft beim Studium der Auswirkungen von zeitlichen Änderungen des Strahles. Das Verfahren zweiter Ordnung löst Stoßwellen sehr viel besser auf und wird deshalb auch zur Analyse von Stoßwellen-Experimenten benutzt. Für einen typischen Protonenstrahl aus einer Pinch Reflex Diode auf ein Aluminiumtarget liefert der Code eine um 10 - 15 % höhere Kompression im Vergleich zu dem von Neumann Verfahren. Da in dem Upwind-Verfahren keine künstlichen Druckterme benutzt werden, trauen wir diesen Resultaten mehr.

Table of Contents

1. Introduction	1
2. Basic Equations	5
3. High Resolution Numerical Schemes for Shock Capturing	9
3.1 First Order Upwind Scheme	9
3.2 Second Order Accurate Scheme	12
3.3 Solution for the Source Equation	15
4. Energy Source Term and Equation of State	17
5. Validation of the Computer Code	21
6. Results and Discussions	25
6.1 A Constant Pressure Pulse	25
6.2 Proton Beam Incident on Aluminium Slab	27
6.2.1 Square Pulse of Proton Beam	27
6.2.2 KALIF Proton Beam	28
7. Summary and Conclusions	29
8. References	31
Appendix A: An Upwind Scheme for One Fluid Two Temperature Model of Plasma	35
Appendix B: Numerical Structure of the Code	39
Appendix C: A Sample Input and Output	49

1. Introduction

The need for an efficient and accurate numerical simulation of shock wave, contact discontinuity etc. is well known. A discontinuity in state variables (density, pressure, particle velocity etc.) requires special attention in numerical calculations. The classical method, proposed by von-Neumann and Richtmyer⁽¹⁾, consists of introducing a purely artificial dissipative mechanism of such a form and strength that the discontinuity in state variables is replaced by a smooth transition extending over a small number (say three or four) of space intervals. For one dimensional problems they proposed an artificial viscous pressure q to be added to the physical pressure term, of the form

$$q = \begin{cases} b \cdot \eta \rho (\nabla u)^2 & \text{if } \nabla u < 0 \\ 0 & \text{otherwise} \end{cases} \quad (1.1)$$

Here ρ denotes the fluid density, u is the particle velocity with its gradient ∇u . η is a geometry dependent factor defined as

$$\eta = \left\{ \frac{\nabla u}{\nabla \cdot u} \right\} \quad (1.2)$$

This factor reduces to unity for plane geometry. b in equation (1.1) is an empirical constant determining the strength of the artificial viscosity q . The quadratic dependence on ∇u instead of linear dependence as observed in normal viscosity ensures that this term is small away from the shock. Also expression (1.1) ensures that the artificial viscosity is absent during the expansion of the fluid.

The suitability and limitations of the von-Neumann procedure of artificial viscosity can be seen from figure 1.1. In this figure we show the space profiles of the density and the pressure at various times of evolution for two test problems in plane geometry. The first test problem (Figs. 1.1a and 1.1b) consists of a constant pressure applied at the right boundary of a 1.25×10^{-4} meter thick aluminium slab. This leads to a single shock wave moving towards the left, which is reflected at the fixed left boundary. The second test problem (Figs. 1.1c and 1.1d) has its initial conditions given by

$$(\rho, u, p)^t = \begin{cases} (1.0, 0.0, 1.0)^t & \text{for } R < R_0 \\ (0.125, 0.0, 0.1)^t & \text{for } R > R_0 \end{cases} \quad (1.3)$$

This is a benchmark problem for shock wave calculations proposed by Sod⁽²⁾ in 1978. Its exact solution consists of a shock wave propagating in the right direction ($R > R_0$), a rarefaction wave moving to the left ($R < R_0$) and a contact discontinuity separating the two. The results of the space profiles of density and pressure at various time steps are shown in Figs. (1.1c) and (1.1d) respectively for this problem. The parameter $b = 1.0$ for the calculations presented in this figure. From this figure we observe that, although the artificial viscous pressure (1.1) resolves the shock wave and the contact discontinuity well, it introduces some unphysical oscillations. The magnitude of these oscillations depend on the strength of artificial viscosity determined by the empirical parameter b . In Figs. (1.2) and (1.3) we show the effect of this parameter for these two test problems. Fig. (1.2a) shows the density profiles for a constant pressure pulse with $b = 0.2$ while figure (1.2b) shows the density profiles for Sod's problem with the same value of b . Fig. 1.2a clearly demonstrates that a low value for the viscous pressure leads to high oscillations. Fig. (1.2b) again shows large oscillations at the shock wave, but the rarefaction wave is smooth. This is as expected because no artificial viscosity is required for a rarefaction wave. Figs. (1.2c) and (1.2d) show the density profiles for the two test problems with high value of the artificial viscosity. Fig. (1.2c) shows that the unphysical oscillations can be suppressed but now the shock wave is spread over more meshes. However, it is not always possible to suppress the unphysical oscillations completely. Few kinks near the shock persist even with a high value of b (Fig. (1.2d)). Moreover, too high a value for artificial viscosity may falsify the results. For example, if the pressure pulse is caused by any oscillating particle or laser beam it may suppress some of the real oscillations associated with the beam. Also one can not be sure that at the point of interest the artificial viscous pressure is zero because a small gradient in velocity will be amplified by the empirical factor b . In addition it is well known⁽³⁾ that the von-Neumann method leads to high temperatures at contact discontinuity-shock interactions and at the point of shock reflection. This is demonstrated from the space profiles of temperatures shown in figure 1.3. We observe that the average temperature at shock reflection for $b = 0.2$ (Fig. 1.3a) is nearly equal to 1.0 eV. However, for $b = 3.0$ (Fig. 1.3c) this value is 1.3 eV increased by about 30 %. This shows that an increase in the magnitude of artificial viscous pressure leads to an increase in the temperature at the shock reflection. Similarly the magnitude of the jump in temperature at $R = 0.27$ in Fig. 1.3d is more than the corresponding jump in average temperature in Fig. 1.3b. This implies that an increase in the artificial viscous pressure leads to an increase in temperature at the contact discontinuity also. These observations are further supported by many other numerical

simulations which will be presented later in section 6. Implication of these observations will also be discussed in that section. In some cases (e.g. where a sequence of shock waves of different strengths move and interact with one another) it can be a very tedious job to obtain an optimum value for the parameter b .

The need for a better technique to calculate the state variables at discontinuities is obvious from the above discussion. It is also clear that for the analysis of experiments designed to study the effects of time and space fluctuations in beam power the von-Neumann procedure is not suitable and one needs a numerical procedure which could capture shocks within a few meshes without introducing any unphysical oscillations. In recent years a class of new shock-capturing schemes has been developed which possess the above mentioned qualities. These schemes, usually referred to as "high resolution" schemes, have the following properties: (i) They are at least second order accurate on the smooth part of the flow; (ii) they sharply resolve discontinuities without generating spurious oscillations; (iii) they do not need artificial viscosity or other empirical prescription for shock capturing. The main building block of these schemes is an upwind scheme based on the exact⁽⁴⁾ or an approximate⁽⁵⁾ 'Riemann Solver'. A review of these schemes is given in Ref. 5 - 7. All numerical procedures describing shock structures must have some degree of dissipation to control the numerical instabilities. The 'high resolution' methods inherently possess the needed dissipation through the type of difference operator used to approximate the governing equations while the von-Neumann procedure artificially adds a new viscous term. For the former, the dissipation is related to the eigenvalue-eigenvector structure of the governing equations while for the latter no such relationship exist. As a result, in the von-Neumann procedure some components of the solution may be destroyed in an attempt to control the dissipation⁽⁸⁾.

Based on these high resolution schemes, we have developed a hydrodynamic code ESCALA (Efficient Shock Capturing code in Lagrangean geometry). This report describes this code and the method used. In section 2 we present the basic equations solved in Lagrangean geometry. Section 3 presents the numerical scheme for the 1st order and 2nd order upwind options of the code while section 4 is devoted to the special treatment for an EOS other than ideal gas law. Evaluation of the source term is also discussed in this section. Section 5 gives a summary of the test problems simulated for the validation of the code. In section 6 we present the main results and discussions. Also present in this section are the

results of simulation of the KALIF proton beam. Finally, in section 7 we present a summary and the conclusions. Appendix A gives a procedure for the two temperature (electron and ion), one fluid simulations of target plasma. The numerical structure of the code ESCALA is described in appendix B. A sample input and output is presented in appendix C.

2. Basic Equations

The basic equations governing the thermodynamics and hydrodynamics of fluids are the conservation equations for energy, momentum and mass. In many of the shock wave experiments where high temperatures are not achieved the one fluid one temperature model of the plasma is sufficient. We restrict ourselves to such a case as most of the high resolution schemes developed so far consider only one energy equation. An approximate new formulation for the two temperature model is described in the appendix A.

The one temperature, one fluid conservation equations in Lagrangean geometry can be written as:

Energy conservation:

$$\left(\frac{\partial U}{\partial T}\right)_p \frac{\partial T}{\partial t} + \left(\frac{\partial U}{\partial p}\right)_T \frac{\partial p}{\partial t} + p \frac{\partial V}{\partial t} = S \quad (2.1)$$

Momentum conservation:

$$\frac{\partial u}{\partial t} = -\frac{1}{\rho} \nabla p \equiv -r^\alpha \frac{\partial p}{\partial m} \quad (2.2)$$

Mass conservation:

$$\frac{\partial r}{\partial t} = u(r, t) \quad (2.3)$$

In these equations the symbols U , T , ρ , p and S respectively denote total internal energy, temperature, density, total pressure and total energy source. The specific volume V is the inverse of the fluid density ρ . The particle velocity $u(r, t)$ is related to the Lagrangean coordinate r through the mass conservation equation (2.3). The mass coordinate m is related to the volume coordinate v as

$$dm = \frac{1}{V} dv \quad (2.4)$$

where the volume element dv is defined as

$$dv = \frac{1}{\alpha + 1} d(r^{\alpha+1}) \quad (2.5)$$

The geometry factor α takes the values of 0, 1 and 2 for plane, cylindrical and spherical geometries. These equations are completed through the equation of state which relates pressure and internal energy to the fluid density and temperature.

The high resolution upwind schemes start with the governing equations in conservation form, i.e. a vector equation of the form

$$\frac{\partial W}{\partial t} + \frac{\partial}{\partial m} [F(W)] = Q(W) \quad (2.6)$$

where W is the vector of conserved state quantities and $F(W)$ is the vector of their fluxes. To write equations (2.1) - (2.3) in the conservation form (i.e. in the form of 2.6) we note that using Eqs. (2.4) and (2.5), the mass conservation equation (2.3) can be written as

$$\frac{\partial V}{\partial t} - \frac{\partial}{\partial m} (r^\alpha u) = 0 \quad (2.7)$$

with specific volume V as a conserved state variable and $-r^\alpha u$ as its corresponding flux. Similarly, the momentum balance equation (2.2) can be written as

$$\frac{\partial u}{\partial t} + \frac{\partial}{\partial m} (r^\alpha p) = \frac{\alpha p V}{r} \quad (2.8)$$

This equation is also in conservation form (conserved state variable u with the corresponding flux as $r^\alpha p$) since the term on the right hand side $\alpha p V/r$ can be treated as a source term. This term is inversely proportional to the product pr for the curved geometries and is zero for the plane geometry. This term represents the additional momentum contribution due to the geometry convergence effects in curved geometries.

Using Eq. (2.7) energy conservation equation (2.1) can be written as

$$\frac{\partial U}{\partial t} + \frac{\partial}{\partial m} (p r^\alpha u) - r^\alpha u \frac{\partial p}{\partial t} = S \quad (2.9)$$

where the total derivative of the internal energy (depends on t and r) is defined as

$$\frac{\partial U}{\partial t} = \left(\frac{\partial U}{\partial \Gamma} \right)_{\rho} \frac{\partial \Gamma}{\partial t} + \left(\frac{\partial U}{\partial \rho} \right)_{\Gamma} \cdot \frac{\partial \rho}{\partial t} \quad (2.10)$$

Recognising $-r^{\alpha} \partial p / \partial m$ as $\partial u / \partial t$ (Eq. 2.2), the equation (2.9) can be written in the conservation form

$$\frac{\partial E}{\partial t} + \frac{\partial}{\partial m} (r^{\alpha} p u) = S \quad (2.11)$$

with the conserved variable E , the total specific energy, defined as

$$E = U + \frac{1}{2} u^2 \quad (2.12)$$

and $r^{\alpha} p u$ as its flux. Thus combining Eqs. (2.7), (2.8) and (2.12) and denoting the combined vector equation by (2.6), we identify the state vector W and the flux vector $F(W)$ as

$$W = (V, u, E)^t \quad (2.13)$$

and

$$F(W) = (-r^{\alpha} u, r^{\alpha} p, r^{\alpha} u p)^t \quad (2.14)$$

The source vector $Q(W)$ is recognised as

$$Q(W) = \left(0, \frac{\alpha V p}{r}, S \right)^t \quad (2.15)$$

Equation (2.6) together with the definitions (2.13) - (2.15) is the required equation to develop any upwind scheme. However, these schemes require signal velocities (or characteristic velocities) given by the theory of characteristics. For this we rewrite (2.6) in the quasilinear form

$$\frac{\partial W}{\partial t} + A(W) \frac{\partial W}{\partial m} = Q \quad (2.16)$$

where $A(W)$ denotes the Jacobian matrix $dF(W)/dW$. For $F(W)$ and W as defined by equations (2.14) and (2.13) we have

$$A(W) = r^a \begin{bmatrix} 0 & -1 & 0 \\ \frac{\partial p}{\partial V} & -u \frac{\partial p}{\partial U} & \frac{\partial p}{\partial U} \\ u \frac{\partial p}{\partial V} & p - u^2 \frac{\partial p}{\partial U} & u \frac{\partial p}{\partial U} \end{bmatrix} \quad (2.17)$$

The eigenvalues of A are

$$\lambda_1 = -Cr^a, \lambda_2 = 0, \lambda_3 = Cr^a \quad (2.18)$$

which give the required characteristic velocities. Here C denotes the Lagrangean sound speed defined as

$$C^2 = p \frac{\partial p}{\partial U} - \frac{\partial p}{\partial V} \quad (2.19)$$

which is related to the Eulerian sound speed C_E by

$$C = C_E/V \quad (2.20)$$

For ideal gas law

$$C^2 = \gamma p/V \quad (2.21)$$

where the adiabatic exponent γ is the ratio of the specific heat at constant pressure to the specific heat at constant volume.

In the following section we describe the numerical scheme used to solve the vector equation (2.6). We may remark here that although the scheme described in the next section is for one-dimensional geometry, its generalization to 2 or 3 dimensions is straightforward using the well tested method of directional splitting(9, 10).

3. High Resolution Numerical Schemes for Shock Capturing

In this section we describe the numerical procedure adopted to solve the inhomogeneous equation (2.6). We use the method of operator splitting⁽¹⁰⁾, i.e. we decompose Eq. (2.6) into the homogeneous system

$$\frac{dW}{dt} + \frac{d}{dm} [F(W)] = 0 \quad (3.1)$$

and a system containing the sources

$$\frac{dW}{dt} = Q(W, r, t) \quad (3.2)$$

In each time step these equations are solved one after the other. In the following subsections we describe the upwind schemes to solve (3.1) and (3.2). Sections 3.1 and 3.2 respectively contain the 1st order and 2nd order upwind scheme for the homogeneous equation (3.1), while section 3.3 describes the source treatment.

3.1 First Order Upwind Scheme

The main building block of a shock-capturing scheme used here is the upwind scheme described below. This scheme chooses the direction of differencing locally according to the direction of the nonlinear wave propagation. As a first order upwind scheme we use the Godunov-type of scheme as proposed by Harten, Lax and van Leer⁽⁷⁾ and by Einfeldt⁽⁵⁾. We introduce a grid as shown in figure 3.1 and use the short hand notation;

$$\Delta m_i = m_{i+1/2} - m_{i-1/2} \quad (3.3)$$

$$I_i = \left[m_{i-1/2}, m_{i+1/2} \right] \quad (3.4)$$

where I_i denotes the mass mesh interval. The centre of a mass mesh is denoted by subscript i , while a half integer subscript $i + 1/2$ denotes the edge of the mass mesh. The time step is denoted by the subscript n . Simple arithmetic average is used to relate the edge points to the centre of the mesh, e.g.

$$m_{i+1/2} = \frac{1}{2} (m_i + m_{i+1}) . \quad (3.5)$$

A shock capturing numerical method is formulated in the form

$$W_i^{n+1} = W_i^n - \frac{t_{n+1} - t_n}{\Delta m_i} (G_{i+1/2}^n - G_{i-1/2}^n) \quad (3.6)$$

which preserves the integral of the conserved variables. The sum, difference or integral of a vector is defined by applying this operation to each component of the vector. Here, W_i^n is an approximation for the average value of the solution W in the grid zone I_i at time t_n

$$\frac{1}{I_i} \int_{I_i} W(m, t_n) dm . \quad (3.7)$$

The numerical flux G is a function of two arguments

$$G_{i+1/2}^n \doteq G(W_i^n, W_{i+1}^n) \quad (3.8)$$

and it approximates the flux vector $F(W)$ defined by equation (2.14). We note that the conservation form of equation (3.1) is preserved by its finite difference form as given by Eq. (3.6). This is important for the shock capturing property because this guaranties the correct propagation rate of the discrete shock profile independent from the grid zone size.

In Godunov-type upwind differencing schemes, the cell averages are advanced in time by first solving a Riemann problem. The Riemann problem is an initial value problem with initial data of the form

$$W(\kappa, 0) = \begin{cases} W_L & \text{for } \kappa < 0 \\ W_R & \text{for } \kappa > 0 \end{cases} \quad (3.9)$$

where κ here denotes the independent variable (m in our case of Lagrangean geometry). The average W_i^{n+1} at the next time level $t^{n+1} = t^n + \Delta t$ is obtained as

$$W_i^{n+1} = \frac{1}{I_i} \int_0^{I_i/2} R_{i-1/2}^n \left(\frac{m}{\Delta t} \right) dm + \frac{1}{I_i} \int_{-I_i/2}^0 R_{i+1/2}^n \left(\frac{m}{\Delta t} \right) dm \quad (3.10)$$

where $R_{i \pm 1/2}^n [(m - m_{i \pm 1/2}) / (t - t_n)]$ is the solution of the Riemann problem at the cell interface $m_{i \pm 1/2}$. To save computational effort a number of schemes have been proposed where one replaces $R_{i \pm 1/2}^n$ by an approximate (instead of exact) Riemann solution. We adopt the scheme proposed by Einfeldt⁽⁵⁾ for the equations of compressible gas dynamics in Eulerian form. This scheme was originally formulated by Harten, Lax and van Leer⁽⁷⁾. We will refer this scheme as HLLC scheme. Writing the analogous scheme in Lagrangean geometry gives the numerical fluxes G as

$$G(W_i, W_{i+1}) = \frac{1}{2} [F(W_i) + F(W_{i+1})] - \frac{C_{i+1/2}}{2} (W_{i+1} - W_i) \quad (3.11)$$

where $C_{i+1/2}$ is an appropriate approximation for the Lagrangean signal velocity (Eq. 2.18). We omit the time superscript n as long as no misunderstanding arises. A simple expression for the signal velocity is

$$C_{i+1/2} = (C_i + C_{i+1})/2 \quad (3.12)$$

which leads to stable solutions as long as the shock waves are not too strong. Another averaging which works for strong shocks as well, is based on the Roe's mean value^(5, 11). For an ideal gas equation of state this is given by

$$C_{i+1/2}^2 = \frac{V_i \sqrt{V_i} C_i^2 + V_{i+1} \sqrt{V_{i+1}} C_{i+1}^2}{\sqrt{V_i V_{i+1}} (\sqrt{V_i} + \sqrt{V_{i+1}})} + \frac{\gamma-1}{2} \frac{(u_{i+1} - u_i)^2}{\sqrt{V_i V_{i+1}} (\sqrt{V_i} + \sqrt{V_{i+1}})^2} \quad (3.13)$$

Thus, with flux vector as defined by Eq. 2.14, we can finally write down the upwind scheme for the state variables V , u and E as

$$V_i^{n+1} = V_i^n - \frac{\Delta t}{2\Delta m_i} \left[r_{i-1}^n u_{i-1}^n - r_{i+1}^n u_{i+1}^n - C_{i+1/2}^n (V_{i+1}^n - V_i^n) + C_{i-1/2}^n (V_i^n - V_{i-1}^n) \right] \quad (3.14)$$

$$u_i^{n+1} = u_i^n - \frac{\Delta t}{2\Delta m_i} \left[\left(r_{i+1}^a p_{i+1}^n - r_{i-1}^a p_{i-1}^n \right) - C_{i+1/2}^n \left(u_{i+1}^n - u_i^n \right) + C_{i-1/2}^n \left(u_i^n - u_{i-1}^n \right) \right] \quad (3.15)$$

and

$$E_i^{n+1} = E_i^n - \frac{\Delta t}{2\Delta m_i} \left[\left(r_{i+1}^a u_{i+1}^n p_{i+1}^n - r_{i-1}^a u_{i-1}^n p_{i-1}^n \right) - C_{i+1/2}^n \left(E_{i+1}^n - E_i^n \right) + C_{i-1/2}^n \left(E_i^n - E_{i-1}^n \right) \right] \quad (3.16)$$

As equations (3.13) - (3.16) represent a fully explicit scheme, the time interval Δt has to satisfy the stability condition

$$\text{Max} \left\{ \frac{\Delta t}{\Delta m_i} \cdot C_i \right\} \leq 1 \quad (3.17)$$

which is the well known CFL⁽¹⁾ condition. This guaranties that the information moves no further than the grid zone thickness during one time step.

3.2 Second Order Accurate Scheme

In this section we describe a shock capturing scheme which is second order accurate on smooth parts of the flow. It is based on the ideas of Godunov⁽⁴⁾ and van Leer⁽¹³⁾ and is usually called MUSCL⁽¹⁴⁾ type scheme. The main building block is an upwind scheme as described in the previous section. The basic idea of Godunov⁽⁴⁾ in the construction of a first order upwind scheme was the assumption that the state variables are piecewise constant in each grid zone (solid lines in figure 3.2). Godunov then obtained an approximation of the solution at a next time level calculating the fluxes between the grid zones using the exact solution of a Riemann problem. (In the previous section we have described a Godunov type 1st order upwind scheme where the exact solution of the Riemann problem is replaced by an approximate one.) A second order scheme is obtained by replacing the piecewise constant assumption of Godunov by a piecewise linear

one (dotted lines in figure 3.2). This idea is due to van Leer(13). The piecewise linear representation of the state variables in a grid zone is obtained through a monotonic preserving interpolation of the form

$$W^n(m) = W_i^n + S_i^n(m - m_i) \quad m_{i-1/2} \leq m \leq m_{i+1/2} \quad (3.18)$$

where, as earlier, the subscript i denotes the value at the grid zone centre. The calculation of the vector of slopes S_i^n will be described later. We denote the right and left boundary values in each zone by $W_{i\pm}^n$ (Fig. 3.2). From equation (3.18) we obtain these boundary values as

$$W_{i\pm}^n = W_i^n \pm \frac{\Delta m_i}{2} S_i^n \quad (3.19)$$

These values are advanced to time $t_{n+1/2}$ using a Taylor expansion as

$$W_{i\pm}^{n+1/2} = W_{i\pm}^n - \frac{\Delta t}{2\Delta m_i} \left[F_{i+}^n - F_{i-}^n \right] \quad (3.20)$$

where

$$F_{i\pm}^n = F(W_{i\pm}^n) \quad (3.21)$$

This half time step establishes a second order accuracy in time. It only considers the development in time of the flow inside the grid zones. No fluxes between different cells are taken into account. We calculate the fluxes between the grid zones during the time step Δt using the upwind scheme described in the previous section (sec. 3.1) and obtain the state variables at the next time step as

$$W_i^{n+1} = W_i^n - \frac{\Delta t}{\Delta m_i} \left[G(W_{i+}^{n+1/2}, W_{(i+1)-}^{n+1/2}) - G(W_{(i-1)+}^{n+1/2}, W_{i-}^{n+1/2}) \right] \quad (3.22)$$

where the numerical flux function G is as defined for the 1st order upwind scheme, e.g.

$$G(W_{i+}^{n+1/2}, W_{(i+1)-}^{n+1/2}) = \frac{1}{2} \left[F(W_{(i+)}^{n+1/2}) + F(W_{(i+1)-}^{n+1/2}) \right] - \frac{C_{i+1/2}^{n+1/2}}{2} \left[W_{(i+1)-}^{n+1/2} - W_{i+}^{n+1/2} \right] \quad (3.23)$$

where

$$C_{i+1/2}^{n+1/2} = \left(C_{i+}^{n+1/2} + C_{(i+1)-}^{n+1/2} \right) / 2 \quad (3.24)$$

analogous to Eq. (3.12). In the same way, one can also define this quantity analogous to Eq. (3.13).

This completes the numerical algorithm for one time step except for the definitions of the appropriate slopes in each grid zone. There are several ways to calculate the slopes. One can calculate them either in terms of the conservative variables V , u and E or in terms of the primitive variables ρ , u and p . We use the conservative variables. This choice ensures the positivity of V and E . A simple form of slope calculation for each variable was proposed by van-Leer:

$$S = S(a, b) = \begin{cases} \frac{2ab}{a+b} & a \cdot b > 0 \\ 0 & \text{otherwise} \end{cases} \quad (3.25)$$

where a , b stand for the right and left hand differences e.g. for the first variable

$$a = \frac{V_{i+1} - V_i}{m_{i+1} - m_i} ; b = \frac{V_i - V_{i-1}}{m_i - m_{i-1}} \quad (3.26)$$

This form of slope calculation, though simple, sometimes leads to small oscillations (see sections 5 and 6 of this report). A better form of the slope calculation proposed by Roe(11, 12) is

$$S = \frac{a}{|a|} \cdot \text{Max} \cdot \left\{ \left| \text{Minmod}(a, S_k b) \right| , \left| \text{Minmod}(S_k a, b) \right| \right\} \quad (3.27)$$

where the Minmod function is defined as

$$\text{Minmod}(a, b) = \begin{cases} a & |a| \leq |b| ; ab > 0 \\ b & |a| > |b| ; ab > 0 \\ 0 & ab \leq 0 \end{cases} \quad (3.28)$$

S_k is a constant which takes a value between one and two. A value of 1.4 is used for the results presented in this report. This value can be changed by the input.

3.3 Solution for the Source Equation

In each time step, the state variable vector W as obtained by solving the homogeneous equation (3.1) has to be corrected for the sources by solving the source equation (3.2). For a weak source one can use a fully explicit method where one writes

$$W_i^{n+1} = W_i^n + \Delta t Q(r_i, t_n, W_i^n) \quad (3.29)$$

Here W_i^n on the right hand side of this equation denotes the solution of a homogeneous equation as described in sections 3.1 and 3.2. In cases where the source term Q depends very strongly on the state vector W and time t one should use a fully implicit scheme

$$W_i^{n+1} = W_i^n + \Delta t Q(r_i, t_{n+1}, W_i^{n+1}) \quad (3.30)$$

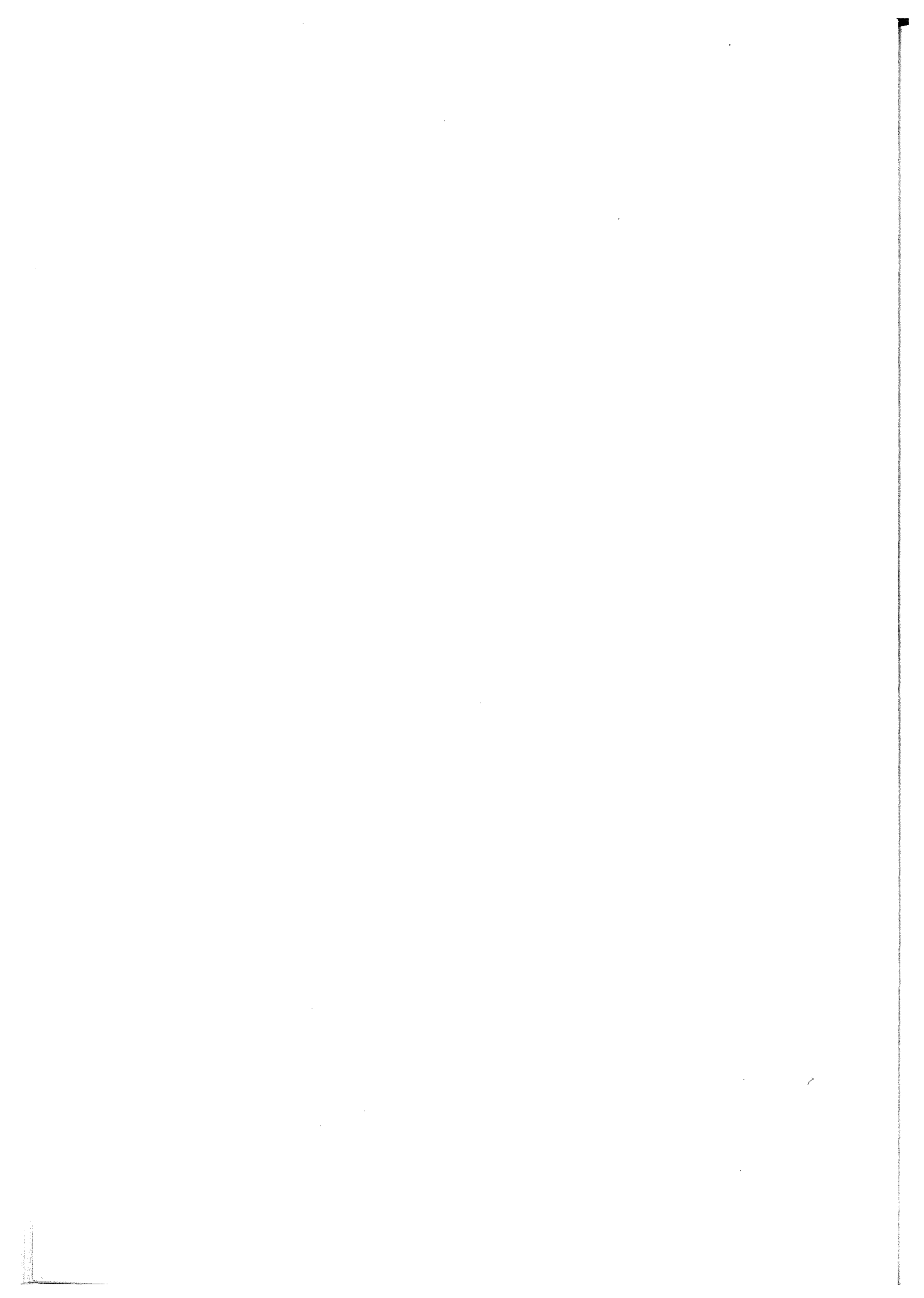
or a combination of explicit and implicit schemes. Equation (3.30) requires an iteration and hence more computational efforts. For an intermediate case one can use the predictor-corrector⁽¹⁵⁾ method. In this method we first obtain the 1st order predictor

$$\tilde{W}_i^{n+1} = W_i^n + \Delta t \cdot Q(r_i, t_n, W_i^n) \quad (3.31)$$

and then the 2nd order corrector

$$W_i^{n+1} = W_i^n + \frac{\Delta t}{2} \left[Q(r_i, t_n, W_i^n) + Q(r_i, t_{n+1}, \tilde{W}_i^{n+1}) \right] \quad (3.32)$$

To increase the accuracy, the second order corrector step should be repeated with the value of W_i^{n+1} on the left hand side of Eq. (3.32) taken as \tilde{W}_i^{n+1} . Usually one or two iterations are sufficient. The present version of the code has only a fully explicit treatment of the source (Eq. 3.29). Other methods need a modification to the code.



4. Energy Source Term and Equation of State

The energy source term S in Eq. (2.1) contains all the sources; internal as well as external. For a typical hydrodynamic simulation of the plasma, the source term can be formally written as

$$S = H + Y - J + X \quad (4.1)$$

where H represents the flow of heat due to thermal conduction, Y is the rate of thermonuclear energy release, J is the rate of radiation loss from the plasma and X denotes the rate of external energy source (e.g. Laser or ion beam energy deposited to the plasma). For an accurate evaluation of the source term a knowledge of average degree of ionization is essential. We use the Thomas-Fermi model(16) to calculate it. In the following we briefly describe the various contribution to the source term which are calculated in the code. They are adopted from KATACO(17).

The heat conduction term is calculated as

$$H = \frac{1}{\rho} \nabla \cdot \kappa \nabla T \quad (4.2)$$

where ρ is the plasma density. The thermal conductivity coefficient κ is written as

$$\kappa = \kappa_i + \kappa_e \quad (4.3)$$

The ion contribution κ_i is given as

$$\kappa_i = 4.55 \times 10^{-11} T^{5/2} (\log \Lambda)^{-1} [\bar{A} \bar{Z}^{-2}]^{1/2} (\bar{Z}^2)^{-1} \cdot \epsilon \delta \quad (4.4)$$

with

$$\epsilon \delta = 0.43 \bar{Z} / (3.44 + \bar{Z} + 0.26 \log \bar{Z}) \quad (4.5)$$

The coulomb logarithm Λ is given by

$$\Lambda = 1.24 \times 10^6 T^{3/2} n_e^{-1/2} / \bar{Z} \quad (4.6)$$

In these expressions Z denotes the average ion-charge, A is the average atomic number of the plasma and n_e denotes the electron number density. The electron thermal conductivity coefficient is 'free streaming limited' and is written as

$$\kappa_e = \kappa'_e \left[1 + (a \lambda_e / T) \frac{dT}{dx} \right]^{-1} \quad (4.7)$$

where λ_e is the electron mean free path

$$\lambda_e = 5.7 \times 10^7 T^2 / n_e \bar{Z}^2 \quad (4.8)$$

and 'a' is the free streaming constant. The default value of this constant is 0.0. Any other value for this constant can be specified by the user through the input data. The electron thermal conductivity coefficient κ'_e is given as

$$\kappa'_e = 1.955 \times 10^{-9} T^{5/2} (\log \Lambda)^{-1} \bar{Z} \cdot \epsilon \delta / \bar{Z}^2 \quad (4.9)$$

The radiation loss from the plasma is considered to be dominated by Bremsstrahlung radiation emitted by the electron and the term J in Eq. (4.1) is written as

$$J = 8.5 \times 10^{-14} n_e T^{1/2} \bar{Z}^2 / A \quad (4.10)$$

All these expressions for the energy source terms are in the units of Watts/Kg. The ion beam energy deposition term X is calculated using the computer code EDEPOS(18). The contribution due to thermonuclear fusion energy Y is calculated by numerically integrating the microscopic fusion cross sections over the Maxwellian distribution. The microscopic fusion X-sections are obtained from the Mott's barrier penetration formula in conjunction with the Breit-Wigner formula for the nuclear resonances(17).

The source term S strongly depends on the plasma temperature. In the upwind schemes described in section 3, the conservative variable is the total energy $E = U + 1/2 u^2$. Thus in addition to the Equation of State (EOS) in the standard form

$$p = p(\rho, T) ; U = U(\rho, T) \quad (4.11)$$

we also need the inverse EOS as

$$T = T(U, \rho) \quad (4.12)$$

For ideal gas law, these equations can be written as

$$p = \frac{k_B T \rho}{M_p A} (1 + \bar{Z}) \quad (4.13)$$

$$U = \frac{k_B T}{M_p A} \left[\frac{1}{\gamma_i - 1} + \frac{\bar{Z}}{\gamma_e - 1} \right] \quad (4.14)$$

$$T = \frac{M_p A U}{k_B} \left[\frac{1}{\gamma_i - 1} + \frac{\bar{Z}}{\gamma_e - 1} \right]^{-1} \quad (4.15)$$

where k_B is the Boltzmann constant, M_p is the proton mass and γ_i and γ_e respectively denote the ion and electron adiabatic exponents. However, the ideal gas laws have limited applications. The code can accommodate any given EOS, in analytical or tabular form (e.g. SESAME tables). For any given EOS (other than ideal gas) we use the following new scheme.

Total pressure p and total internal energy U for a given temperature and density are read from the given EOS-tables. Using these values we obtain two space, time, density and temperature dependent parameters

$$\gamma_1 = 1.0 + \frac{p \cdot \rho}{U} \quad (4.16)$$

$$\gamma_2 = 1.0 + \frac{k_B T}{M_p A} \frac{(1 + \bar{Z})}{U} \quad (4.17)$$

and an effective parameter

$$\gamma_{\text{eff}} = \text{Max} \cdot \{\gamma_1, \gamma_2\} \quad (4.18)$$

To calculate the signal velocities we use expression (2.19) if accurate values of pressure derivatives are available in the EOS data. Otherwise we use the ideal gas expression (2.21) with γ therein replaced by γ_{eff} given by Eq. (4.18) and pressure as obtained through the given EOS. Another place where EOS is used is the evaluation of the average signal velocity at the mesh boundary using the Roe's mean value (Eq. 3.13). For any given EOS, we still use the expression (3.13) but γ therein is replaced by a parameter $\bar{\gamma}$ defined as

$$\bar{\gamma} = \text{Max} \cdot \left\{ \gamma_{\text{eff}}^i, \gamma_{\text{eff}}^{i+1} \right\} \quad (4.19)$$

where γ_{eff}^i and $\gamma_{\text{eff}}^{i+1}$ are the values of parameter γ_{eff} (Eq. 4.18) for the i_{th} and $(i + 1)_{\text{th}}$ mesh zone. This procedure guarantees that the signal velocity is not underestimated.

To obtain the temperature from the internal energy, we use the inverse EOS data in the form (4.12) if available. In case the inverse EOS data are not available we use the derivative dU/dT to estimate the change in temperature ΔT for a given change in internal energy ΔU over one time step Δt . For this procedure one should assure that the derivative dU/dT does not change significantly in the time step Δt . In case it does so, one has to reduce the time step Δt .

5. Validation of the Computer Code

For the purpose of validation of the computer code, a number of test problems were chosen for which either analytical or numerical solutions from well tested codes or both are available in the literature. The first such test problem is the Sod's shock tube problem described in Section 1. In this case the solution consists of a shock wave, a rarefaction wave and a contact discontinuity. For this problem, in addition to the analytical solution, the numerical solutions using the upwind scheme proposed by Harten, Lax, van Leer⁽⁷⁾ and Einfeldt⁽⁵⁾ (referred to as HLL scheme); the Godunov's⁽⁴⁾ scheme as well as Roe's^(11,12) scheme are available. The differences between the results of Godunov's and Roe's schemes are small. Therefore we use only Godunov's results for the purpose of comparison. In figures 5.1 to 5.3 we compare the 1st order and 2nd order upwind schemes described in this report with the analytical solution, HLL scheme and Godunov's schemes. The three figures respectively show the space profiles of density, pressure and particle velocity. In these figures, the curves on the left hand side marked a and b respectively give the profile taken from ref. 5 while on the right hand side the curves marked c and d are the results obtained by using the present computer code with 1st and 2nd order upwind schemes. The van-Leer prescription (Eq. 3.25) is used to calculate slopes for the 2nd order methods. In the figures marked a and b, the solid lines give the analytical solution while the open circles represent the results of the HLL or the Godunov's scheme. Although these results from the literature are available only for one typical time step, we have shown the space profiles for a number of time steps in Figs. 5.1c and d. The 2nd order upwind scheme resolves shocks more sharply as compared to the 1st order upwind scheme. The comparison with the analytical solutions show that the corners are rounded off. The constant state between the contact discontinuity and the shock has been obtained. The shock wave resolution is much sharper as compared to the contact discontinuity. The strong dissipation of the contact discontinuity as compared to the analytical solution is known for first order upwind schemes. This can be corrected in a modified scheme by adding a correction term to the numerical flux (Eqs. 3.11 and 3.23). The correction term depends on the eigenvectors of the Jacobian matrix and at present the code is being modified to incorporate these corrections. In general, the code simulates the time evolution of various waves in this shock tube problem well. Small oscillations observed in figure 5.3d can be removed by using a better slope. This is demonstrated in figure 5.4 where we show the space profiles of velocity

(analogous to fig. 5.3d) as obtained by using the Roe's prescription for calculation of the slope (Eq. 3.27) with the constant $S_k = 1.3$. We observe that, except for a kink at an earlier time, the oscillations are almost completely removed.

The second test problem we examine is the one proposed by Lax(19). The initial conditions of this Riemann problem are

$$(\rho, u, p)^t = \begin{cases} (0.445, 0.698, 3.528)^t & R < 0.5 \\ (0.5, 0.0, 0.571)^t & R > 0.5 \end{cases} \quad (5.1)$$

Note that for this problem we have an initial jump in the particle velocity as well in addition to the jump in the density and the pressure which were present in the Sod's problem discussed above. This problem was also calculated using the 1st order and the 2nd order upwind options of the present code and results are compared with the analytical solution as well as the numerical solution from HLLC scheme, Godunov's scheme and Roe's scheme. In general a good agreement was observed. As a representative result we show the comparison of the space profiles of density and pressure with the analytical solution and the HLLC scheme. The figures (5.5a) and (5.5b) respectively show the density and pressure profiles as obtained by the analytical solution (solid lines) and by the HLLC scheme (open circles). Figures (5.5c) and (5.5d) show the corresponding profiles obtained by using the code described in this report with 1st order upwind scheme. Various curves in figures (5.5c) and (5.5d) correspond to different time of evolution. Note that the compression obtained agrees well with analytical and HLLC schemes. The shape of the space profiles also agrees well with HLLC solutions.

In the increasing order of complexity, the third test problem we consider here is one in which a shock wave interacts with a contact discontinuity (Munz Problem, Ref. 14). Such a problem appears when the initial conditions are of the type

$$(\rho, u, p)^t = \begin{cases} (\rho_1, u_1, 10.0)^t & \text{for } R < 0.3 \\ (1.0, -1.0, 0.1)^t & \text{for } 0.3 < R < 0.6 \\ (10.0, -1.0, 0.1)^t & \text{for } R > 0.6 \end{cases} \quad (5.2)$$

Here we have a jump in density, velocity and pressure at $R = 0.3$ and a second jump in density at $R = 0.6$. The values of the constants ρ_1 and u_1 are so chosen that a shock wave is generated at $R = 0.3$ moving towards right without the

corresponding backwards moving rarefaction wave. The values of ρ_1 and u_1 so obtained using the well known Rankine-Hugniot relations are

$$\rho_1 = \sqrt{\frac{9801}{1202}} - 1 \quad (5.3)$$

$$u_1 = 601/106 \quad (5.4)$$

The analytical solution of this problem on space-time ($R - t$) diagram is of the type shown in figure 5.6. A shock wave initiated at $R = 0.3$ moves towards right while a contact discontinuity initiated at $R = 0.6$ moves towards left. These waves interact producing two shock waves and a contact discontinuity.

This problem was calculated using the 1st order upwind option of the code. The results are compared with the analytical solution and the numerical solution from the Roe's upwind scheme in figure 5.7. In this figure we show space profiles of density and particle velocity. In figures (5.6a) and (5.6b) the solid line represents the analytical results while filled circles give the corresponding values using Roe's method. Our results for the density and particle velocity at various time steps are shown in figures 5.7c and 5.7d respectively. The code simulates this problem also fairly well. As compared to Roe's calculations (Figs. 5.7a & 5.7b) our results show more dissipation. This is expected because the results presented in this figure are of 1st order upwind scheme while Roe's results are from a 2nd order method. We have already seen (Figs. 5.1 - 5.3) that the 2nd order procedure resolves the state discontinuities more sharply.

Finally, as an example of testing the code for curved geometries, we consider a cylindrically converging shock wave problem which was first proposed by Payne(21). The initial conditions for this problem are

$$(\rho, u, p)^t = \begin{cases} (1.0, 0.0, 1.0)^t & \text{for } R \leq 1 \\ (4.0, 0.0, 4.0)^t & \text{for } R > 1 \end{cases} \quad (5.5)$$

These conditions generate a shock with initial strength 1.93, a contact discontinuity and an expansion fan. This problem was again calculated using the 1st order and 2nd order upwind scheme options of the present code. Results are compared with the other available calculations(21, 22) in figures 5.8 and 5.9. In these figures we show the space profiles of density and pressure at various time

steps. Curves marked a refer to the computations of Payne (redrawn by Lapidus), the curves marked b denote the computations of Lapidus⁽²²⁾ using the 'Cartesian method' based on Lax differencing. Curves marked c and d show our results for the 1st order and the 2nd order options. The numbers on the curves indicate the relative value of the time. These times do not correspond to the values given in the part a and b of the figures 5.8 and 5.9. Note that in our calculations $R = 0.01$ is the fixed centre instead of 0.0. Also the normalization of pressure in our case is different. Our results do not show spurious oscillations present in the Lapidus computations. In general, the shape of the profiles agrees well.

These test problems clearly validate the present computer code. In the first 3 test problems, our results were compared with the analytical solution and with the other numerical results based on similar (upwind type) schemes. The absence of oscillations in our results as compared to the Lapidus results where the conventional finite-difference methods (not upwind schemes) are used demonstrate the superiority of upwind schemes over the conventional finite difference method. This point is further examined in the following section.

6. Results and Discussions

In the previous section we have shown that the results of present code are absent of numerical oscillation and results match qualitatively well with the results of either analytical or previous computer calculations(12, 14). In fact the superiority of the method used here over the conventional methods have been demonstrated. In the following we make an attempt to compare quantitatively the results of the present code with those of KATACO(17). The code KATACO uses the von-Neumann viscous pressure. The physics model and transport coefficients in the present code and KATACO are the same. Thus the difference in the results of the two codes should be due to the difference in the numerical method alone.

6.1 A Constant Pressure Pulse

A pressure pulse constant in time at one boundary of the target leads to a single shock wave moving away from this boundary without generation of a rarefaction wave. The target consists of an aluminium slab of solid density at room temperature and of a thickness of 1.25×10^{-4} meters. At the right boundary we apply a constant pressure of 10^{11} Pascal. The left boundary is assumed to be fixed so that effects of shock reflection at this boundary can be seen. In figures 6.1a to 6.1d we show the space profiles of density at time intervals of 3 ns, 6 ns, 9 ns, 12 ns, 15 ns and 18 ns obtained by using the code KATACO and different options of the present code. Fig. 6.1a presents the results using the code KATACO (i.e. von-Neumann procedure for shock capturing with the parameter $b = 1.0$) while figures 6.1b to 6.1d give the results using the present code. For Fig. 6.1b, the 1st order upwind scheme described in section 3.1 was used while the second order upwind scheme of section 3.2 is used for figures (6.1c) and (6.1d). For figure 6.1c, the van-Leer prescription (Eq. 3.25) is used while Roe's prescription (Eq. 3.27) is used to calculate the slopes for Fig. 6.1d. The sets of figures 6.2a - 6.2d, 6.3a - 6.3d and 6.4a - 6.4d present the corresponding space profiles for pressure, particle velocity and temperature. The unphysical oscillations in the state variables (density, pressure, velocity and temperature) which are typical of the von-Neumann procedure used in the code KATACO disappear. Small oscillations are seen in figures 6.1c, 6.2c, 6.3c and 6.4c but they are easily removed by using a proper slope calculation as can be seen from figs. 6.1d, 6.2d, 6.3d and 6.4d respectively.

At the shock reflection the upwind schemes (Figs. 6.4b - 6.4d) predict a temperature less than 1.0 eV while the von-Neumann procedure (Fig. 6.4a) gives a higher temperature (> 1.0 eV). This is expected. As observed earlier, the 2nd order upwind scheme resolves shocks more sharply as compared to 1st order upwind schemes. A quantity which is measured experimentally is the shock speed. Shock speed obtained from data presented in Figs. 6.1 - 6.4 is 7.06 Kms/sec for von-Neumann method and 7.07 Kms/sec for upwind schemes. The expression for shock speed as obtained from Hugoniot relations⁽²⁵⁾ is

$$S = V_0 \sqrt{\frac{p_1 - p_0}{V_0 - V_1}} \quad (6.1)$$

where p_0, V_0 are the pressures and specific volumes for the uncompressed region while p_1, V_1 are the corresponding values for the compressed region. For $p_1 = 1.0 \times 10^{11}$ Pa, $p_2 = 8.6 \times 10^8$ Pa, $V_1 = 3.7 \times 10^{-4}$ m³ and $V_2 = 9.56 \times 10^{-5}$ m³ (Figs. 6.1 and 6.2) equation (6.1) gives the shock speed as 7.063 km/s which agrees very well with values obtained from the results of the code. Hugoniot relations also give an expression for the particle velocity v_p as

$$v_p = \sqrt{(p_1 - p_0)(V_0 - V_1)} \quad (6.2)$$

Substituting p_1 and V_1 from Figs. 6.2 and 6.1 we get $v_p = 5.238$ km/s which agrees very well with the particle velocity space profiles shown in set of figures 6.3.

These values are for the ideal gas EOS and therefore can not be compared with experimental data. To calculate the shock speed in solid aluminium the above calculation is repeated using the SESAME tables EOS data. In figures 6.5a - 6.5d we present the space profiles of density, pressure, particle velocity and temperature for a pressure pulse of 10^{11} Pascal. The first order upwind scheme is used for these results. We obtain a shock speed of 10.47 km/s. The corresponding experimental value is 10.0 km/s⁽²⁶⁾. The code overestimates the shock speed by about 5 %. The large data base on high pressure experiments can be fitted to an expression of the form

$$S = a + v_p \quad (6.3)$$

where S is the shock velocity and a, b are the two constants to be determined from experiments. For aluminium, the best fitted value of these constants⁽²⁶⁾ lie between 5.15 - 5.38 for a and 1.29 - 1.37 for b .

Numerical simulations using the new code were carried out for the pressure pulse of magnitude varying from 10^{10} to 10^{12} Pascal in aluminium. SESAME table EOS data are used for all these simulations. The results are summarised in figure 6.6 where we plot shock speed against the particle speed. From this figure we obtain the constants a and b of equation (6.3) as 5.64 and 1.30 respectively. Both these coefficients are within 5 % of the experimental values.

6.2 Proton Beam Incident on Aluminium Slab

For the results presented so far the shock waves were generated either by a constant pressure at the boundary (section 6.1) or by initial data (section 5.2). In this section we consider cases where the shock waves are generated as a result of high power proton beam incident on the surface of the target. The target is the same as in section 6.1. The left boundary is kept fixed to simulate the effects of shock reflection. As our main aim in these simulations is to compare the upwind schemes with the von-Neumann procedure, for the sake of convenience we use ideal gas EOS. A fully explicit scheme described in section 5 is used to treat the source. We consider two time profiles for the proton beam. The first one consists of an idealised square pulse while the second profile corresponds to the proton beam obtained from the pinch reflex diode at KALIF⁽²³⁾. The main results are presented below.

6.2.1 Square Pulse of Proton Beam

A beam of 1.6 MeV protons with 0.164 TW/cm^2 power is incident on the target. Numerical simulations are carried out up to 18 ns when the reflected shock is moving backwards. The ion energy deposition code EDEPOS⁽¹⁸⁾ is used to calculate the energy deposition of the beam in the target. The results of simulation by computer code KATACO are presented in set of figures 6.7. Here the figures 6.7a, 6.7b, 6.7c and 6.7d respectively show the space profiles of density, pressure, particle velocity and temperature at 3, 6, 9, 12, 15 and 18 ns of time. The corresponding results using the new computer code are presented in figures 6.8 and 6.9. Figures 6.8 give the results for 1st order upwind scheme while figures 6.9 give the corresponding results for the 2nd order upwind scheme with

van-Leer prescription to calculate the slopes. These figures show that the proton beam generates a forward moving shock wave and the ablation of outer target layers leads to a drop in the density of outer meshes. As observed earlier, the upwind schemes are better in the sense that the spurious oscillations in the density, pressure, particle velocity and temperature profiles disappear. The space profiles of 1st order upwind schemes are more flat because of inherent dissipation (and hence the robust nature) in these schemes. As was expected, the temperature predictions by KATACO are higher than those by upwind schemes. There is some difference in the temperature estimates of 1st order and 2nd order schemes too. This is attributed to higher dissipation in the 1st order methods. We believe that the temperature estimates by the 2nd order upwind scheme (Fig. 6.9d) are closer to reality as the von-Neumann method gives higher temperatures at the shock reflection as discussed earlier.

6.2.2 KALIF Proton Beam Pulse

Our final calculations are for a realistic proton beam generated at the KALIF using the pinch reflex diode⁽²³⁾. The beam is incident on the target at an average angle of 150° and its time profile is shown in Fig. 6.10. The solid line in this figure gives the beam energy in MeV while the dotted line shows the profile of beam current at the target in units of terra amperes/sq. meter. The energy deposition code EDEPOS⁽¹⁸⁾ is used to calculate the energy deposition of the beam. Ideal gas EOS was used for these calculations. The main results of these calculations are presented in figures 6.11 to 6.13. Here we show the space profiles of density, pressure, particle velocity and temperature at timesteps of 5, 10, 15, 20, 25 and 30 ns. These figures show the results using the code KATACO, 1st order upwind and 2nd order upwind schemes respectively. A comparison of these figures shows that the upwind schemes predict higher compressions by about 15 % as compared to the KATACO. We also observe higher temperatures in KATACO simulations because of the use of von-Neumann viscous pressure.

Finally we have resimulated a typical KALIF dE/dx experiment⁽²³⁾. In this experiment the KALIF beam shown in Fig. 6.10 was incident on a 12.5 micro-meter thick aluminium target. The energy of the protons coming out of the target was measured. The simulations with the present code as well as the KATACO (Fig. 6.14) reproduce the experimental results within the experimental uncertainties.

7. Summary and Conclusions

Most of the hydrodynamic simulations of targets involving strong shocks used up to now are haunted with spurious numerical oscillations. This is due to an inadequate treatment of shocks in hydrocodes. For example in the code KATACO, like most codes in the field of inertial confinement fusion, von-Neumann's viscous pressure (Eq. 1.1) is used to treat shocks. The value of the numerical constant b influences the amplitude of numerical oscillations. Increasing the viscous pressure by increasing this numerical constant of Eq. 1.1 can reduce these oscillations to a great extent. This procedure causes a spread of the shock over a larger number of meshes thus introducing an uncertainty in the position of the shock. Moreover the material properties at the shock reflection also experience spurious modifications. Appreciable differences in the temperature are observed (Fig. 1.3). In simulation of the experiments performed at KALIF these numerical oscillations can mask the temporal beam structure and can smooth them out. Hence the above procedure destroys the information of beam nonuniformity.

To remedy this drawback different shock capturing schemes have been developed in the literature⁽³⁻⁶⁾. We use a high resolution shock capturing scheme proposed recently⁽⁵⁾ for the equations of compressible gas dynamics in Eulerian form to develop an Efficient Shock Capturing hydro code in LAgrangean geometry (ESCALA). This is a one dimensional one temperature code. The physical models and constants in the code are basically the same as in the KArlsruhe Target Code (KATACO). A variety of equations of state (ideal gas analytical equations of state formulas as described in the documentation of code KATACO as well as tabulated EOS e.g. the SESAME library) can be used. The upwind schemes require energy, momentum and mass balance equations (Eqs. 2.1 - 2.3) in conservation form. The Jacobian matrix and its eigenvalues are obtained as estimates of the signal velocity. The code described in this report contains two upwind schemes which are first and second order accurate in the smooth part of the state variables. The first order upwind scheme shows no numerical oscillations but a comparatively large dissipation of shock is observed. If the second order upwind scheme of shock capturing is used a sharp shock is observed. Though in general the results are free from spurious numerical oscillations there are still examples where some small oscillations do persist. In these cases a better prescription for the calculation of slope has to be used (see Sec. 5).

The code has been validated by calculating 4 different test problems, 3 in plane and one in cylindrical geometry. The results have been compared with the analytical solution and with the results of other numerical simulations with well tested codes(5, 14).

Finally we have compared the results of the present code with those of KATACO. The physics between the two codes being the same, the difference between the two results should be due to the difference in the numerical method. The comparison was done for a constant pressure pulse, a constant particle beam and a KALIF proton beam. As expected the code KATACO with its von-Neumann artificial viscosity method predicts somewhat higher temperatures and lower compressions than the present code with its upwind shock capturing scheme. Simulations with constant pressure pulse of 10^{11} Pascal and SESAME equation of state give a shock velocity of 10.47.

To conclude we remark that the results of the present code are basically free from spurious numerical oscillations and can be used to analyse shock wave experiments at KALIF. We recommend to use the 2nd order upwind option with Roe's prescription for shock calculation.

Acknowledgements

One of the authors (N.K. Gupta) thanks Prof. Keßler and Dr. Fröhlich for giving the opportunity to work at this laboratory.

8. References

1. R.D. Richtmyer and K.W. Morton, *Difference Methods for Initial-Value Problems*, 2nd edition, John Wiley and Sons, New York/London/Sydney, 1976
2. G.A. Sod, A Survey of Several Finite Difference Methods for Systems of Non-linear Hyperbolic Conservation Laws, *J. Comput. Phys.* 27 (1978) 1
3. E. Halter, *On Numerical Methods for Compressible Non-viscous Fluid Flow; a Comparison*, KfK-3804 (1984)
4. S.K. Godunov, Finite-Difference Method for Numerical Computation of Discontinuous Solutions of the Equations of Fluid Dynamics, *Mat. Sbornik* 47 (1959), 271 - 306
5. B. Einfeldt, On Godunov-Type Methods for Gas Dynamics, *SIAM J. Numer. Anal.* 25 (1988), 294 - 318
6. A. Harten, On a Class of High Resolution Total-Variation-Stable Finite Difference Schemes, *SIAM J. Numer. Anal.* 21 (1984) 1 - 23
7. A. Harten, P.D. Lax and B. van Leer, On Upstream Differencing and Godunov-type Schemes for Hyperbolic Conservation Laws, *SIAM Rev.* 25 (1983) 35 - 62
8. R.W. Mac Cormack, Current Status of Numerical Solution of the Navier-Stokes equations, AIAA-85-0032 (1985)
9. P. Woodward, P. Colella, The numerical simulation of Two-Dimensional Fluid Flow with Strong Shocks, *J. Comput. Phys.* 54 (1984) 115 - 173
10. G.I. Marchuk, *Methods of Numerical Mathematics*, Springer-Verlag, New York/Heidelberg/Berlin (1975)
11. P.L. Roe, Approximate Riemann Solvers, Parameter Vectors, and Difference Schemes, *J. Comput. Phys.* 43 (1981) 357 - 372

12. P.L. Roe, The Use of the Riemann Problem in Finite-Difference Schemes, Lecture notes in Physics 141, Springer Verlag (1981), 354 - 359
13. B. van Leer, Towards the Ultimate Conservative Difference Scheme-V, A Second-order Sequel to Godunov's Method, J. Comput. Phys. 32 (1979) 101 - 136
14. C.D. Munz, On the Construction and Comparison of Two-Step Schemes for the Euler Equations, in Finite Approximation in Fluid Mechanics (E.H. Hirschel Ed.), Note on Numerical Fluid Mechanics 14, Vieweg (1986), 195 - 217
15. J. Stoer and R.R. Bulirsch, Einführung in die Numerische Mathematik, Springer, New York/Heidelberg/Berlin (1978)
16. R.M. More, In Atomic and Molecular Physics of Controlled Thermonuclear Fusion (Ed. C.J. Joachain and D.E. Post), Plenum Press, New York (1983) 399 - 440
17. B. Kiefer, B. Goel, W. Höbel and K. Kufner, KATACO, program description, unpublished report
18. B.P. Goel, G.A. Moses and R. Peterson, Proton Stopping in Thin Aluminium Slabs, Laser and Particle Beams, 5 (1987) 907
19. P.D. Lax, Weak Solutions of Nonlinear Hyperbolic Equations and their Numerical Computation, Comm. Pure Appl. Math. 7 (1954) 159 - 193
20. C.D. Munz, On the Numerical Dissipation of High Resolution Schemes for Hyperbolic Conservation Laws, J. Comput. Phys. 77 (1988) 18 - 39
21. R.B. Payne, A Numerical Method for a Converging Cylindrical Shock, J. Fluid Mechanics 2 (1957) 185
22. A. Lapidus, Computation of Radially Symmetric Shocked Flows, J. Comput. Phys. 8 (1971) 106 - 188

23. B. Goel and H. Bluhm, Determination of Proton Slowing Power in Hot Plasma at KALIF, *J. De Physique* C 7 (1988) 169 - 176
24. B. van Leer, On the Relation Between the Upwind Differencing Schemes of Godunov, Engquist-Osher and Roe, *SIAM J. Sci. Stat. Comp.* 5 (1984) 1 - 20
25. Ya. B. Zel'dovich and Yu. P. Raizer, *Elements of Gas Dynamics and Classical Theory of Shock Waves*, Academic Press, New York (1968)
26. S.P. Marsh (Editor), *LASL Shock Hugoniot Data*, University of California Press, Berkeley, Los Angeles, London (1980)



APPENDIX A

An Upwind Scheme for One Fluid, Two Temperature Model of Plasma

In this appendix we present an outline of the upwind scheme for two temperature (electron and ion) one fluid model of plasma. In this model, the conservation equations are

Ion Energy Conservation

$$\left(\frac{\partial U_i}{\partial T_i}\right)_\rho \frac{\partial T_i}{\partial t} + \left(\frac{\partial U_i}{\partial \rho}\right)_{T_i} \frac{\partial \rho}{\partial t} + p_i \frac{\partial V}{\partial t} = S_i \quad (\text{A.1})$$

Electron Energy Conservation

$$\left(\frac{\partial U_e}{\partial T_e}\right)_\rho \frac{\partial T_e}{\partial t} + \left(\frac{\partial U_e}{\partial \rho}\right)_{T_e} \frac{\partial \rho}{\partial t} + p_e \frac{\partial V}{\partial t} = S_e \quad (\text{A.2})$$

Momentum Conservation

$$\frac{\partial u}{\partial t} = -\frac{1}{\rho} \nabla p_t = -r^a \frac{\partial p_t}{\partial m} \quad (\text{A.3})$$

Mass conservation

$$\frac{dr}{dt} = u(r, t) \quad (\text{A.4})$$

Various symbols are as defined in section 2 of the text. The subscript i and e now refer to the ion and electron respectively. The total pressure p_t is a sum of electron and ion pressure. Although electrons and ions are assumed to be at different temperatures, they move with common velocity u . This assumption is necessary to avoid any charge separation (Quasi-neutrality condition of the plasma) and is an essential feature of the one fluid model. Accordingly we have only one momentum balance equation and the Lagrangian coordinates are moved with the common velocity u (Eq. A.4). The energy equation is split into two, one for electrons and the other for ions.

For an upwind scheme, it is necessary to reduce equations (A.1) - (A.4) to the conservation form. Eqs. (A.3) and (A.4) are the same as the corresponding equations in the one temperature model (section 2 of the text) and cause no problem. However, to reduce (A.1) and (A.2) to conservation form we define two auxiliary parameters u_i and u_e through the equations

$$\frac{\partial u_i}{\partial t} = - \frac{1}{\rho} \nabla p_i = - r^a \frac{\partial p_i}{\partial m} \quad (\text{A.5})$$

$$\frac{\partial u_e}{\partial t} = - \frac{1}{\rho} \nabla p_e = - r^a \frac{\partial p_e}{\partial m} \quad (\text{A.6})$$

Now a procedure similar to one described in section 2 of the text reduces the Eqs. (A.1) and (A.2) to

$$\frac{\partial U_i}{\partial t} + \frac{\partial}{\partial m} (p_i r^a u) + u \frac{\partial u_i}{\partial t} = S_i \quad (\text{A.7})$$

and

$$\frac{\partial U_e}{\partial t} + \frac{\partial}{\partial m} (p_e r^a u) + u \frac{\partial u_e}{\partial t} = S_e \quad (\text{A.8})$$

From the inspection of these equations it is clear that they can be reduced to the conservation form if we define two new functions ψ_i and ψ_e such that they satisfy

$$u \frac{\partial \psi_\eta}{\partial t} = \frac{\partial \psi_\eta}{\partial t} \quad (\eta = i, e) \quad (\text{A.9})$$

and then we get the required vector equation

$$\frac{\partial W}{\partial t} + \frac{\partial}{\partial m} [F(W)] = Q \quad (\text{A.10})$$

where the conserved variable vector W , the flux vector F and source vector Q are defined as

$$W = (V, u, E_i^*, E_e^*)^t \quad (\text{A.11})$$

$$F(W) = (- r^a u, r^a p_t, r^a u p_i, r^a u p_e)^t \quad (\text{A.12})$$

$$Q = (0, a p_t V/r, S_i, S_e)^t \quad (\text{A.13})$$

where

$$E_{i,e}^* = U_{i,e} + \psi_{i,e} \quad (\text{A.14})$$

Thus we observe that the conserved energy variables are now related to internal energy with the additional functions $\psi_{i,e}$ which are obtained as a solution of the auxiliary equation (A.9) which in turn requires a solution of Eqs. (A.5) and (A.6). The situation can be greatly simplified if we assume that

$$u_{i,e} = \frac{p_{i,e}}{p_t} \cdot u \quad (\text{A.15})$$

The justification for the assumption (A.15) is the similar form of equations governing $u_{i,e}$ and u (Eqs. A.5, A.6 and A.3). Under this assumption $\psi_{i,e}$ is given by

$$\psi_{i,e} = \left(\frac{p_{i,e}}{p_t} \right) \cdot \frac{1}{2} u^2 \quad (\text{A.16})$$

and thus $E_{i,e}^*$ has a form very similar to the total energy $E_{i,e}$ except for a factor $p_{i,e}/p_t$ with the kinetic energy part. We note that if $p_i = p_e = p_t$, then $\psi_{i,e} = 1/2 u^2$. This is expected because in this case the homogeneous parts of energy Eqs. (A.1) and (A.2) are identical and the conserved variables are the same in form as in section 2 of the text. On the other hand, if $p_i = p_e = p_t/2$, then $\psi_{i,e} = u^2/4$.

Once we have reduced our basic equations to the conservation form, the remaining procedure is straightforward. In this case, the Jacobian matrix is a 4 x 4 matrix and is given as

$$J = r^a \begin{bmatrix} 0 & -1 & 0 & 0 \\ \frac{\partial p_t}{\partial V} & -u \frac{\partial p_t}{\partial U_t} & \frac{\partial p_t}{\partial U_i} & \frac{\partial p_t}{\partial U_e} \\ u \frac{\partial p_i}{\partial V} & p_i - \frac{p_i}{p_t} u^2 \frac{\partial p_i}{\partial U_i} & u \frac{\partial p_i}{\partial U_i} & u \frac{\partial p_i}{\partial U_e} \\ u \frac{\partial p_e}{\partial V} & p_e - \frac{p_e}{p_t} u^2 \frac{\partial p_e}{\partial U_e} & u \frac{\partial p_e}{\partial U_e} & u \frac{\partial p_e}{\partial U_e} \end{bmatrix} \quad (\text{A.17})$$

where U_t is the sum of ion and electron internal energies U_i and U_e . The eigenvalues of this matrix are

$$\lambda_1 = \lambda_2 = 0 ; \lambda_3 = Cr^a , \lambda_4 = - Cr^a \quad (\text{A.18})$$

where the Lagrangean sound speed C is given by

$$C^2 = \frac{\partial p_t}{\partial U_t} \cdot \left\{ u^2 \left(\frac{\partial p_t}{\partial U_t} - \frac{p_e}{p_t} \frac{\partial p_e}{\partial U_e} - \frac{p_i}{p_t} \frac{\partial p_i}{\partial U_i} \right) \right\} + p_t \frac{\partial p_t}{\partial U_t} - \frac{\partial p_t}{\partial V} \quad (\text{A.19})$$

In the limit $p_i = p_e \rightarrow p_t$, Eq. (A.19) reduces to Eq. (2.19) of the text, as is expected. Thus the procedure described in section 3 can be generalised to this case in a straightforward manner. Naturally, we now require separate EOS data for ions and electrons.

APPENDIX B

Numerical Structure of the Computer Code

The overall structure of the code ESCALA is kept similar to that of KATACO⁽¹⁷⁾. In this section we describe those features of the code which are either new or significantly different from those of KATACO. A new namelist '&UPWIND' is introduced with its variables as described in Table B.1. A schematic flow diagram of the program is shown in Fig. B.1. The subroutines enclosed by a dotted line in this figure are the new subroutines introduced in ESCALA and are not there in KATACO.

The sequence of calling the other subroutines by the modified subroutines STEPON and MOTN2 are described in Figure B.2. The calling sequence for the new subroutine MEDUPW is given in Table B.2. Even though the present version of the code simulates the plasma as a one temperature fluid, a provision exists for the future modifications incorporating the two temperature model (see Appendix A). As a result various variables in the code are defined for the electrons and ions separately. These variables are included in the five new common blocks which are defined in Table B.3.

Table B.1: Description of the variables in the namelist &UPWIND

Name	Type	Default	Description
NEOS	I	1	<p>= 1 for ideal gas EOS</p> <p>= 2 for KATACO EOS</p> <p>> 2 for SESAME EOS. In this case, it is equal to the material number for SESAME table</p>
NUPW	I	2	<p>= 0 for von-Neumann prescription (Eq. 1.1) for shocks (i.e. KATACO)</p> <p>= 1 for the 1st order upwind option</p> <p>= 2 for the 2nd order upwind option</p> <p>= 3 for 1st order method for first 25 time steps and then the second order method.</p>
SLPK	R	1.4	<p>is used only when NUPW = 2 and is the value of constant S_k for the calculation of slopes (see Eq. 3.27). A zero value for this constant implies the van-Leer prescription (Eq. 3.25) for the calculation of the slope.</p>
RHSLD	R	2.7E3	<p>solid density of the target material used only when NEOS = 2.</p>

Table B.2: Sequence of subroutines called by MEDUPW

UPWIND:	Controls the flow of upwind scheme calculations
TMPENR:	Converts fluid temperature to total energy
EOSIG:	Ideal gas equation of state
EOSRG:	SESAME table equation of state
SIGNU:	Calculates the signal velocities
SOLVE1:	Solves the hydrodynamic equations using 1st order upwind scheme
SOLVE2:	Solves the hydrodynamic equations using the 2nd order upwind scheme
SHELL:	Restricts the motion of coordinates till a thermal or pressure wave arises
ENRTMP:	Converts total energy to temperature
MOVE:	Moves the coordinate
BFLUX:	Calculates the conserved variables at the mesh boundaries
UPDATE:	Updates the conserved variables to 1/2 time step for a 2nd order accuracy in time
SOURCE:	Calculates the total source term for the energy balance equation

Table B.4: Description of common block variables used by the code ESCALA in addition to the KATACO common blocks. \$ stands for an array.

COMMON /UPW1/

1. SQI(\$) Source term for ions
2. SQE(\$) Source term for electrons
3. SQP(\$) External source term for momentum if present
4. ENRI1(\$) Total energy of ions at current time
5. ENRE1(\$) Total energy of electrons at current time
6. ENRI3(\$) Total energy of ions at next time step
7. ENRE3(\$) Total energy of electrons at next time step
8. SUP(\$) Positive signal velocity
9. SUN(\$) Negative signal velocity
10. ATM(\$) Effective atomic mass number of ions
11. ATZ(\$) Effective atomic charge number of ions

COMMON /UPW2/

1. TE1(\$) Electron temperature at current time
2. TE3(\$) Electron temperature at next time step
3. TI1(\$) Ion temperature at current time
4. TI3(\$) Ion temperature at next time step
5. RHO1(\$) Density at current time
6. RHO3(\$) Density at next time step
7. ZAI(\$) Dummy array not used

Table B.4 (contd.)

8.	R1(\$)	Mesh coordinates at current time
9.	R3(\$)	Mesh coordinates at next time step
10.	U1(\$)	Particle velocity at current time
11.	U3(\$)	Particle velocity at next time step
12.	AMASS(S)	Mass mesh interval Δm
13.	V1(\$)	Volume at current time
14.	V3(\$)	Volume at next time
15.	PI1(\$)	Ion pressure at current time
16.	PI3(\$)	Ion pressure at next time step
17.	PE1(\$)	Electron pressure at current time
18.	PE3(\$)	Electron pressure at next time step
19.	PT1(\$)	Total pressure at current time
20.	PT3(\$)	Total pressure at next time step
21.	EINTI(\$)	Internal energy of ions
22.	EINTE(\$)	Internal energy of electrons
23.	Q1(\$)	Dummy array not used
24.	Q3(\$)	Dummy array not used
25.	SPV1(\$)	Specific volume at current time
26.	SPV3(\$)	Specific volume at next time step
27.	SLOPV(\$)	Slope of specific volume
28.	SLOPE(\$)	Slope of the total specific energy

Table B.4 (contd.)

- 29. SLOPU(\$) Slope of particle velocity
- 30. SLOPEE(\$) Slope of the total specific energy for electrons
- 31. SLOPEI(\$) Slope of the total specific energy for ions

COMMON /UPW3/

- 1. DT Time interval Δt
- 2. GAMA Average ratio of specific heats
- 3. GAMAI Ratio of specific heats for ions
- 4. GAMAE Ratio of specific heats for electrons
- 5. AKB Boltzmann constant
- 6. AMH Proton mass
- 7. ALM Dummy variable not used
- 8. SLPK Constant S_k for slope calculations
- 9. BFL Left boundary condition parameter
- 10. BFR Right boundary condition parameter
- 11. RHSLD Solid density of target material

COMMON /UPW4/

- 1. MESH Total number of space meshes
- 2. IGEOM Geometry factor
- 3. NGEOM IGEOM - 1
- 4. NJP1 MESH + 1

Table B.4 (contd.)

- 5. NUPW Upwind scheme option parameter
- 6. NEOS Equation of state option parameter

COMMON /UPW5/

- 1. BV1(2, \$) Specific volume at mesh boundaries for current time
- 2. BV2(2, \$) Specific volume at mesh boundaries for next half time step
- 3. BU1(2, \$) Particle velocity at mesh boundaries for current time
- 4. BU2(2, \$) Particle velocity at mesh boundaries for next half time step
- 5. BEI1(2, \$) Ion energy at mesh boundaries for current time
- 6. BEI2(2, \$) Ion energy at mesh boundaries for next half time step
- 7. BEE1(2, \$) Electron energy at mesh boundaries for current time
- 8. BEE2(2, \$) Electron energy at mesh boundaries for next half time step
- 9. BPT1(2, \$) Total pressure at mesh boundaries for current time
- 10. BPT2(2, \$) Total pressure at mesh boundaries for next half time step
- 11. BPI1(2, \$) Ion pressure at mesh boundaries for current time
- 12. BPI2(2, \$) Ion pressure at mesh boundaries for next half time step
- 13. BPE1(2, \$) Electron pressure at mesh boundaries for current time
- 14. BPE2(2, \$) Electron pressure at mesh boundaries for next half time step
- 15. BCP(2, \$) Positive signal velocity at mesh boundaries for current time
- 16. BCP(2, \$) Positive signal velocity at mesh boundaries for next half time step

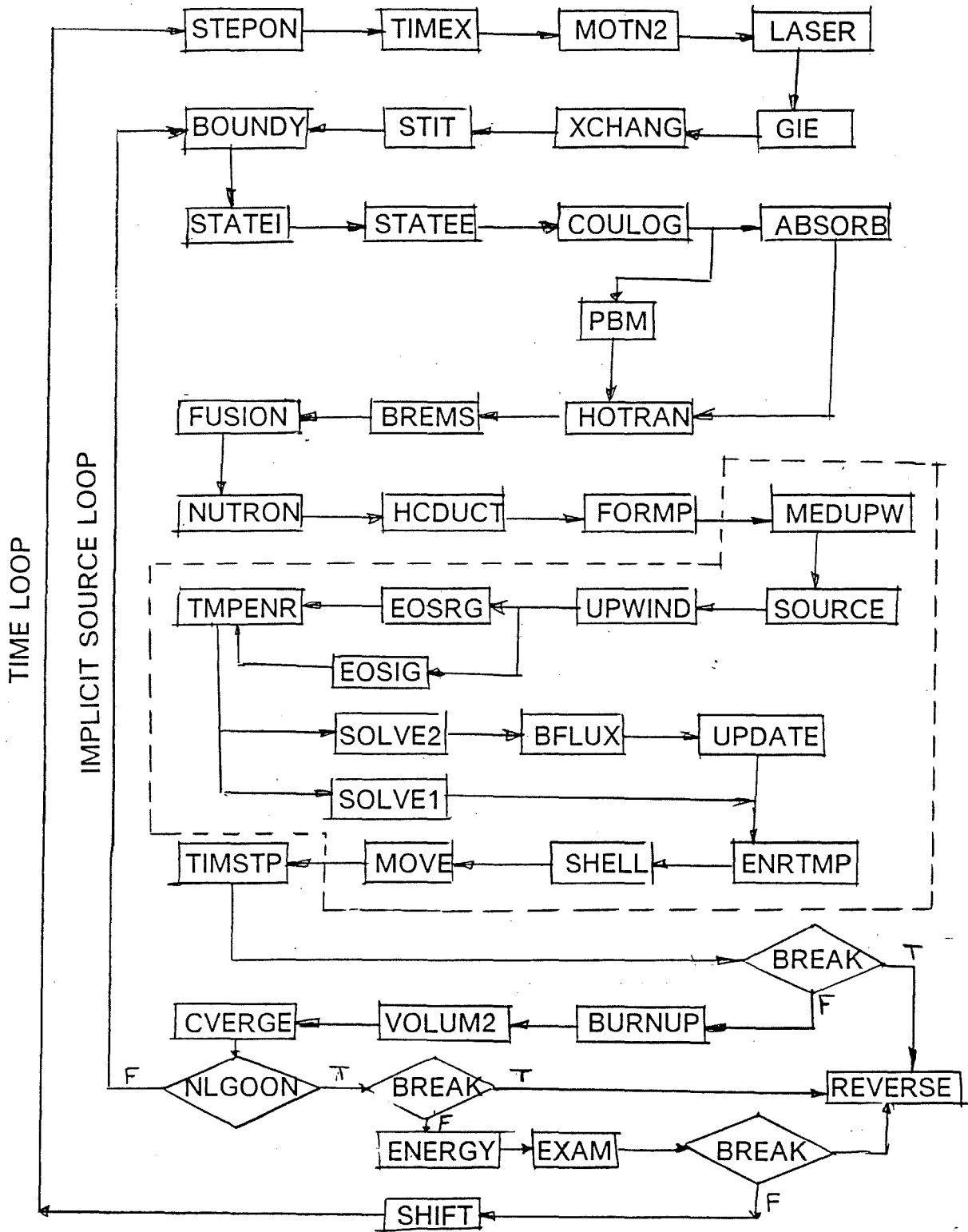


Fig. B.1: Schematic flow diagram of ESCALA

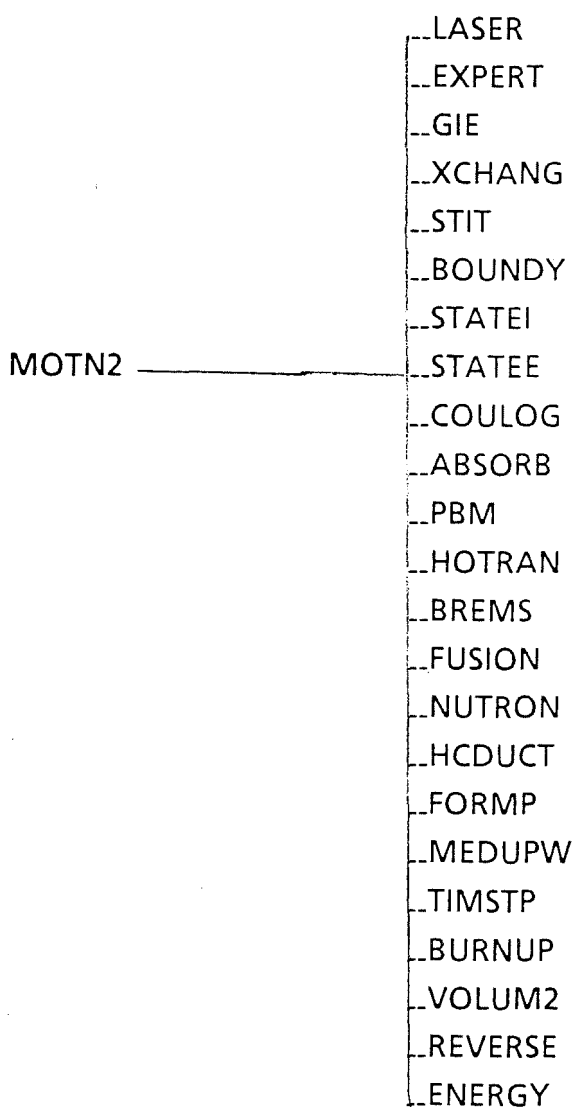
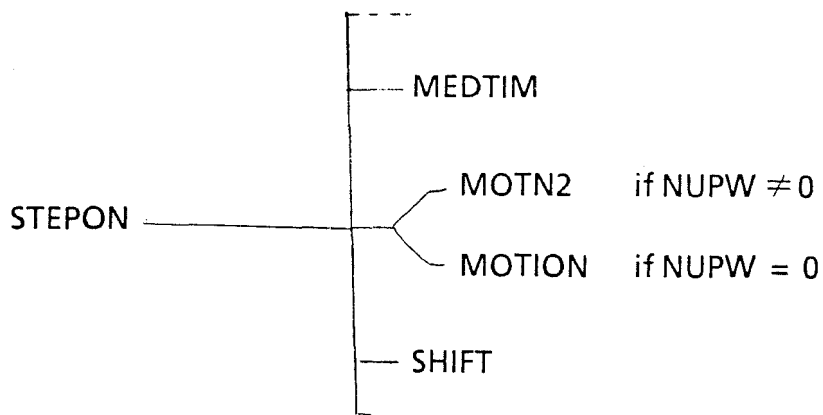


Fig. B.2: Sequence of subroutines called by STEPON and MOTN2

APPENDIX C

A Sample Input and Output

```

//INR265C JOB (0265,101,POD7N),GUPTA,MSGLEVEL=(1,1),REGION=4096K,
// NOTIFY=INR265,MSGCLASS=H,TIME=(2,59)
//**MAIN ORG=RM003
// EXEC TSO
ERASE 'INR265.PLOTEASY.PRD100.IG10'
/*
/**
/**MAIN LINES=30
/*******
// EXEC F7CLG,LIB=NUSYS,PARM.C='NOINSOURCE,NOMAP',PARM.L='MAP,LIST'
//C.SYSPRINT DD DUMMY
//C.SYSINC DD DISP=SHR,DSN=INR265.ESCALA.FORT
//C.SYSIN DD DISP=SHR,DSN=INR265.ESCALA.FORT(UPWIND)
// DD DISP=SHR,DSN=INR265.ESCALA.FORT(PLOTM)
// DD DISP=SHR,DSN=INR265.ESCALA.FORT(MPTIME)
//** DD DISP=SHR,DSN=INR265.MEDUPW.FORT(PBM)
// DD DISP=SHR,DSN=INR265.ESCALA.FORT(MEDUSA)
//C.SYSUT1 DD UNIT=SYSDA,SPACE=(TRK,100)
//C.SYSUT2 DD UNIT=SYSDA,SPACE=(TRK,100)
//L.MODA DD DISP=SHR,DSN=INR265.MEDUSA.LOAD
//L.SYSIN DD *
INCLUDE LOAD(EOSCAL)
ENTRY MAIN
/**----- PLOT INTERFACE
//G.FT03F001 DD DISP=SHR,DSN=INR609.EOS86.DATA,LABEL=(,,IN)
//G.FT11F001 DD DISP=SHR,DSN=TSO265.PLOT.DATA
//G.FT12F001 DD DISP=(NEW,CATLG),DCB=DCB.VBS,
// DSN=INR265.PLOTEASY.PRD100.IG10,
// VOL=SER=BAT00C,UNIT=DISK,SPACE=(TRK,(2,1),RLSE)
//G.FT15F001 DD DSN=INR265.MEDUSA.PLOT,DISP=SHR
/**DCB=(RECFM=VBS,BLKSIZE=19069,LRECL=19000),
/**UNIT=DISK,VOL=SER=BAT000,SPACE=(TRK,(20,20))
//G.FT24F001 DD DISP=SHR,DSN=INR528.LIBOPA.DATA,LABEL=(,,IN)
/**-----
//G.FT26F001 DD UNIT=SYSDA,DISP=(NEW,PASS),SPACE=(TRK,(100,25)),
// DCB=(RECFM=FBA,BLKSIZE=13300,LRECL=133)
//G.FT27F001 DD UNIT=SYSDA,DISP=(NEW,PASS),SPACE=(TRK,(100,25)),
// DCB=(RECFM=FBA,BLKSIZE=13300,LRECL=133)
//G.SYSIN DD *
** KALIF DE/DX EXPERIMENT *****
****PINCH REFLEX DIODE ** SESAME EOS *****
N. GUPTA KFK KARLRUHE
*****
&NEWRUN NRUN=9000,NPRNT=5,DELTAT=12.0E-11,TSTOP=75.1E-9,
MESH=20,
NLPBM=.TRUE.,NLBTHI=.FALSE.,IMODEL=1,BNDRY=0.0,
NDUMP=400,NLHCPY=.FALSE.,NHDCPY=10,NLBURN=F
TEINI=300.,TIINI=300.,NLBRMS=F,
NGEOM=1,
PIQ(58)=1.0,
PIQ(71)=1.0,PIQ(72)=1.0,SAHA=1.0
NLPFE=T,NLPFI=T,STATE=3.0,NP3=1,
DTOUT=15.0E-09,AK0=5.0,
AK1=0.01,AK2=0.01,AK3=0.01,AK4=0.01,
&END
&CPATR NLALTR=F,NPRCPT=-100,MDIR=4,MNG=4,MODE=1,MX1=1,MX2=45,
ZDPSI=1.0E-1,ZCUT=0.1,
&END
&BMPAR IBOPT=4,NBEAM=1,IBPRNT=1,
BEAMA=1.,12.,12.,12.,BEAMZ=1.,6.,6.,6.,ANGLE=15.0,
BEAMT= 0.00000, 8.92229, 11.74646, 17.78508, 20.40561,
22.83992, 25.06212, 27.88670, 29.70119, 34.73541,
45.22810, 48.04987, 52.26790, 73.,
BEAMV(1,1)= 0.20188, 1.00702, 1.09169, 1.11967, 1.17608,
1.40680, 1.51033, 1.59971, 1.64202, 1.68889,
2.03700, 2.09340, 2.00841, 1.1,
BEAMC(1,1)= 0.05582, 0.33336, 0.45571, 0.63445, 0.73326,
0.83205, 0.9, 1.00141, 1.03900, 1.15654, 1.29738,
1.34904, 1.40069, 1.47986,
BEAMTF=1.0E-09, BEAMCF=0.53E09, BEAMVF=1.0E6
&END
&TARGET NZONE=1,
RINI=0.0E-3
NCEL=20,
THICK= 1.25E-4,
RHO= 2.7E3,2.7E3,
MISCH=1,1
ATW(1,1)=27.0,27.0,
ZN(1,1)=13.,13.,
FRC(1,1)=1.,1.,
&END
&UPWIND NUPW= 2,NEOS=3712,SLPK=1.4,RHSLD=2.7E3,
&END

```

```

00010400
00010500
00010600
00010700
00010800

```



```

//INR265C JOB (0265,101,POD7N),GUPTA,MSGLEVEL=(1,1),REGION=4096K,
// NOTIFY=INR265,MSGCLASS=H,TIME=(2,59)
//**MAIN ORG=RM003
// EXEC TSO
ERASE 'INR265.PLOTEASY.PRD100.IG10'
/*
/**
//**
//**MAIN LINES=30
//*****
// EXEC F7CLG,LIB=NUSYS,PARM.C='NOINSOURCE,NOMAP',PARM.L='MAP,LIST'
//C.SYSPRINT DD DUMMY
//C.SYSINC DD DISP=SHR,DSN=INR265.ESCALA.FORT
//C.SYSIN DD DISP=SHR,DSN=INR265.ESCALA.FORT(UPWIND)
// DD DISP=SHR,DSN=INR265.ESCALA.FORT(PLOTM)
// DD DISP=SHR,DSN=INR265.ESCALA.FORT(MPTIME)
//** DD DISP=SHR,DSN=INR265.MEDUPW.FORT(PBM)
// DD DISP=SHR,DSN=INR265.ESCALA.FORT(MEDUSA)
//C.SYSUT1 DD UNIT=SYSDA,SPACE=(TRK,100)
//C.SYSUT2 DD UNIT=SYSDA,SPACE=(TRK,100)
//L.MODA DD DISP=SHR,DSN=INR265.MEDUSA.LOAD
//L.SYSIN DD *
INCLUDE LOAD(EOSCAL)
ENTRY MAIN
//***----- PLOT INTERFACE
//G.FT03F001 DD DISP=SHR,DSN=INR609.EOS86.DATA,LABEL=(,,IN)
//G.FT11F001 DD DISP=SHR,DSN=TSO265.PLOT.DATA
//G.FT12F001 DD DISP=(NEW,CATLG),DCB=DCB.VBS,
// DSN=INR265.PLOTEASY.PRD100.IG10,
// VOL=SER=BAT00C,UNIT=DISK,SPACE=(TRK,(2,1),RLSE)
//G.FT15F001 DD DSN=INR265.MEDUSA.PLOT,DISP=SHR
//**DCB=(RECFM=VBS,BLKSIZE=19069,LRECL=19000),
//**UNIT=DISK,VOL=SER=BAT000,SPACE=(TRK,(20,20))
//G.FT24F001 DD DISP=SHR,DSN=INR528.LIBOPA.DATA,LABEL=(,,IN)
//***
//G.FT26F001 DD UNIT=SYSDA,DISP=(NEW,PASS),SPACE=(TRK,(100,25)),
// DCB=(RECFM=FBA,BLKSIZE=13300,LRECL=133)
//G.FT27F001 DD UNIT=SYSDA,DISP=(NEW,PASS),SPACE=(TRK,(100,25)),
// DCB=(RECFM=FBA,BLKSIZE=13300,LRECL=133)
//G.SYSIN DD *
** KALIF DE/DX EXPERIMENT *****
****PINCH REFLEX DIODE ** SESAME EOS *****
N. GUPTA KFK KARLRUHE
*****
&NEWRUN NRUN=9000,NPRNT=5,DELTAT=12.0E-11,TSTOP=75.1E-9,
MESH=20,
NLPBM=.TRUE.,NLBTHI=.FALSE.,IMODEL=1,BNDRY=0.0,
NDUMP=400,NLHCPY=.FALSE.,NHDCPY=10,NLBURN=F
TEINI=300.,TIINI=300.,NLBRMS=F,
NGEOM=1,
PIQ(58)=1.0,
PIQ(71)=1.0,PIQ(72)=1.0,SAHA=1.0
NLPFE=T,NLPFI=T,STATE=3.0,NP3=1,
DTOUT=15.0E-09,AK0=5.0,
AK1=0.01,AK2=0.01,AK3=0.01,AK4=0.01,
&END
&CPATR NLALTR=F,NPRCPT=-100,MDIR=4,MNG=4,MODE=1,MX1=1,MX2=45,
ZDPSI=1.0E-1,ZCUT=0.1,
&END
&BMPAR IBOPT=4,NBEAM=1,IBPRNT=1,
BEAMA=1.,12.,12.,12.,BEAMZ=1.,6.,6.,6.,ANGLE=15.0,
BEAMT= 0.00000, 8.92229, 11.74646, 17.78508, 20.40561,
22.83992, 25.06212, 27.88670, 29.70119, 34.73541,
45.22810, 48.04987, 52.26790, 73.,
BEAMV(1,1)=0.20188, 1.00702, 1.09169, 1.11967, 1.17608,
1.40680, 1.51033, 1.59971, 1.64202, 1.68889,
2.03700, 2.09340, 2.00841, 1.1,
BEAMC(1,1)=0.05582, 0.33336, 0.45571, 0.63445, 0.73326,
0.83205, 0.9, 1.00141, 1.03900, 1.15654, 1.29738,
1.34904, 1.40069, 1.47986,
BEAMTF=1.0E-09, BEAMCF=0.53E09, BEAMVF=1.0E6
&END
&TARGET NZONE=1,
RINI=0.0E-3
NCEL=20,
THICK= 1.25E-4,
RHO= 2.7E3,2.7E3,
MISCH=1,1
ATW(1,1)=27.0,27.0,
ZN(1,1)=13.,13.,
FRC(1,1)=1.,1.,
&END
&UPWIND NUPW= 2,NEOS=3712,SLPK=1.4,RHSLD=2.7E3,
&END

```

```

//INR265C JOB (0265,101,POD7N),GUPTA,MSGLEVEL=(1,1),REGION=4096K,
// NOTIFY=INR265,MSGCLASS=H,TIME=(2,59)
//**MAIN ORG=RM003
// EXEC TSO
ERASE 'INR265.PLOTEASY.PRD100.IG10'

```

```

00010400
00010500
00010600
00010700
00010800

```

```

/*
//**
//**MAIN LINES=30
//*****
// EXEC F7CLG,LIB=NUSYS,PARM.C='NOINSOURCE,NOMAP',PARM.L='MAP,LIST'
//C.SYSRINT DD DUMMY
//C.SYSINC DD DISP=SHR,DSN=INR265.ESCALA.FORT
//C.SYSIN DD DISP=SHR,DSN=INR265.ESCALA.FORT(UPWIND)
//          DD DISP=SHR,DSN=INR265.ESCALA.FORT(PLOTM)
//          DD DISP=SHR,DSN=INR265.ESCALA.FORT(MPTIME)
//**        DD DISP=SHR,DSN=INR265.MEDUPW.FORT(PBM)
//          DD DISP=SHR,DSN=INR265.ESCALA.FORT(MEDUSA)
//C.SYSUT1 DD UNIT=SYSDA,SPACE=(TRK,100)
//C.SYSUT2 DD UNIT=SYSDA,SPACE=(TRK,100)
//L.MODA DD DISP=SHR,DSN=INR265.MEDUSA.LOAD
//L.SYSIN DD *
INCLUDE LOAD(EOSCAL)
ENTRY MAIN

```

```

//*****-----PLOT INTERFACE
//G.FT03F001 DD DISP=SHR,DSN=INR609.EOS86.DATA,LABEL=(,,IN)
//G.FT11F001 DD DISP=SHR,DSN=TSO265.PLOT.DATA
//G.FT12F001 DD DISP=(NEW,CATLG),DCB=DCB.VBS,
//          DSN=INR265.PLOTEASY.PRD100.IG10,
//          VOL=SER=BAT00C,UNIT=DISK,SPACE=(TRK,(2,1),RLSE)
//G.FT15F001 DD DSN=INR265.MEDUSA.PLOT,DISP=SHR
//**DCB=(RECFM=VBS,BLKSIZE=19069,LRECL=19000),
//**UNIT=DISK,VOL=SER=BAT000,SPACE=(TRK,(20,20))
//G.FT24F001 DD DISP=SHR,DSN=INR528.LIBOPA.DATA,LABEL=(,,IN)
//*****
//G.FT26F001 DD UNIT=SYSDA,DISP=(NEW,PASS),SPACE=(TRK,(100,25)),
//          DCB=(RECFM=FBA,BLKSIZE=13300,LRECL=133)
//G.FT27F001 DD UNIT=SYSDA,DISP=(NEW,PASS),SPACE=(TRK,(100,25)),
//          DCB=(RECFM=FBA,BLKSIZE=13300,LRECL=133)
//G.SYSIN DD *

```

```

** KALIF DE/DX EXPERIMENT *****
****PINCH REFLEX DIODE ** SESAME EOS *****
N. GUPTA KFK KARLRUHE
*****

```

```

&NEWRUN NRUN=9000,NPRNT=5,DELTAT=12.0E-11,TSTOP=75.1E-9,
MESH=20,
NLPBM=.TRUE.,NLBTHI=.FALSE.,IMODEL=1,BNDRY=0.0,
NDUMP=400,NLHCPY=.FALSE.,NHDCPY=10,NLBURN=F,
TEINI=300.,TIINI=300.,NLBRMS=F,
NGEOM=1,
PIQ(58)=1.0,
PIQ(71)=1.0,PIQ(72)=1.0,SAHA=1.0,
NLPFE=T,NLPFI=T,STATE=3.0,NP3=1,
DTOUT=15.0E-09,AK0=5.0,
AK1=0.01,AK2=0.01,AK3=0.01,AK4=0.01,

```

```

&END
&CPATR NLALTR=F,NPRCPT=-100,MDIR=4,MNG=4,MODE=1,MX1=1,MX2=45,
ZDPSI=1.0E-1,ZCUT=0.1,
&END

```

```

&BMPAR IBOPT=4,NBEAM=1,IBPRNT=1,
BEAMA=1.,12.,12.,12.,BEAMZ=1.,6.,6.,6.,ANGLE=15.0,
BEAMT=
0.00000, 8.92229, 11.74646, 17.78508, 20.40561,
22.83992, 25.06212, 27.88670, 29.70119, 34.73541,
45.22810, 48.04987, 52.26790, 73.,
BEAMV(1,1)=0.20188, 1.00702, 1.09169, 1.11967, 1.17608,
1.40680, 1.51033, 1.59971, 1.64202, 1.68889,
2.03700, 2.09340, 2.00841, 1.1,
BEAMC(1,1)=0.05582, 0.33336, 0.45571, 0.63445, 0.73326,
0.83205, 0.9, 1.00141, 1.03900, 1.15654, 1.29738,
1.34904, 1.40069, 1.47986,
BEAMTF=1.0E-09, BEAMCF=0.53E09, BEAMVF=1.0E6

```

```

&END
&TARGET NZONE=1,
RINI=0.0E-3
NCEL=20,
THICK= 1.25E-4,
RHO= 2.7E3,2.7E3,
MISCH=1,1
ATW(1,1)=27.0,27.0,
ZN(1,1)=13.,13.,
FRC(1,1)=1.,1.,
&END
&UPWIND NUPW= 2,NEOS=3712,SLPK=1.4,RHSLD=2.7E3,
&END

```

OLYMPUS SYSTEM
IBM 370/165 VERSION I 17/12/73 HARWELL
0.1 BASIC CONTROL DATA SET
0.2 STANDARD DATA ACCEPTED
0.3 ENTER RUN CONTROL

P R O G R A M M E D U K A
+++++

** KALIF DE/DX EXPERIMENT *****

****PINCH REFLEX DIODE ** SESAME EOS *****

N. GUPTA KFK KARLRUHE

** KALIF DE/DX EXPERIMENT *****

 LOGICAL NLBTHI IS .FALSE., THAT MEANS THAT THE TABULATED VALUES OF BETHE AVERAGE ION. POT. < I > ARE USED

BNDRY	LEFT	RIGHT
0.0	FIXED	FREE

ZONE	NCEL	RHO	THICK	MISCH
1	20	0.2700E+04	0.1250E-03	1

1. ZONE:

MISCH	ATW	ZN	FRC
1	27.000	13.000	1.000

DESCRIPTION:

FRC == FRACTION, ATW == ATOMIC WEIGHT, ZN == ATOMIC NUMBER, XMASS == AVERAGED ATOMIC WEIGHT, XZ == AVERAGED ATOMIC NUMBER

- NOT INCLUDING HYDROGEN & HELIUM -

CALCULATED RADII R1 STARTING FROM FIRST RADIUS RINI = 0.0000

CELL	RADIUS	DENSITY	MISCH	FRC1	FRC2	FRC3	ATW1	ATW2	ATW3	ZN1	ZN2	ZN3	XMASS	XZ
1	0.0000E+00	0.27000E+04	1	1.00	0.00	0.00	27.000	0.000	0.000	13.00	0.00	0.00	27.000	13.000
2	0.6250E-05	0.27000E+04	1	1.00	0.00	0.00	27.000	0.000	0.000	13.00	0.00	0.00	27.000	13.000
3	0.1250E-04	0.27000E+04	1	1.00	0.00	0.00	27.000	0.000	0.000	13.00	0.00	0.00	27.000	13.000
4	0.1875E-04	0.27000E+04	1	1.00	0.00	0.00	27.000	0.000	0.000	13.00	0.00	0.00	27.000	13.000
5	0.2500E-04	0.27000E+04	1	1.00	0.00	0.00	27.000	0.000	0.000	13.00	0.00	0.00	27.000	13.000
6	0.3125E-04	0.27000E+04	1	1.00	0.00	0.00	27.000	0.000	0.000	13.00	0.00	0.00	27.000	13.000
7	0.3750E-04	0.27000E+04	1	1.00	0.00	0.00	27.000	0.000	0.000	13.00	0.00	0.00	27.000	13.000
8	0.4375E-04	0.27000E+04	1	1.00	0.00	0.00	27.000	0.000	0.000	13.00	0.00	0.00	27.000	13.000
9	0.5000E-04	0.27000E+04	1	1.00	0.00	0.00	27.000	0.000	0.000	13.00	0.00	0.00	27.000	13.000
10	0.5625E-04	0.27000E+04	1	1.00	0.00	0.00	27.000	0.000	0.000	13.00	0.00	0.00	27.000	13.000
11	0.6250E-04	0.27000E+04	1	1.00	0.00	0.00	27.000	0.000	0.000	13.00	0.00	0.00	27.000	13.000
12	0.6875E-04	0.27000E+04	1	1.00	0.00	0.00	27.000	0.000	0.000	13.00	0.00	0.00	27.000	13.000
13	0.7500E-04	0.27000E+04	1	1.00	0.00	0.00	27.000	0.000	0.000	13.00	0.00	0.00	27.000	13.000
14	0.8125E-04	0.27000E+04	1	1.00	0.00	0.00	27.000	0.000	0.000	13.00	0.00	0.00	27.000	13.000
15	0.8750E-04	0.27000E+04	1	1.00	0.00	0.00	27.000	0.000	0.000	13.00	0.00	0.00	27.000	13.000
16	0.9375E-04	0.27000E+04	1	1.00	0.00	0.00	27.000	0.000	0.000	13.00	0.00	0.00	27.000	13.000
17	0.1000E-03	0.27000E+04	1	1.00	0.00	0.00	27.000	0.000	0.000	13.00	0.00	0.00	27.000	13.000
18	0.1062E-03	0.27000E+04	1	1.00	0.00	0.00	27.000	0.000	0.000	13.00	0.00	0.00	27.000	13.000
19	0.1125E-03	0.27000E+04	1	1.00	0.00	0.00	27.000	0.000	0.000	13.00	0.00	0.00	27.000	13.000
20	0.1187E-03	0.27000E+04	1	1.00	0.00	0.00	27.000	0.000	0.000	13.00	0.00	0.00	27.000	13.000

TIMESTEP NUMBER 0

TIME = 0.000000E+00

DELTA T = 8.5878596E-11

DELTA T DETERMINED BY CONDITION 1 AT MESHPOINT 20

BOUNDARY : R = 1.2500E-04 U = 0.0000E+00 P = 1.0000E-60 TI = 0.0000E+00 TE = 0.0000E+00 SOUND SPEED = 7.2777E+02

ENERGIES : THERMAL 1.60880E+05 KINETIC 0.00000E+00 NUCLEAR 0.00000E+00 ERROR 0.00000E+00 RHO R 1.68749E-01

BEAM POWER : 5.97254E+12 WATTS TOTAL INCIDENT ENERGY 0.00000E+00 JOULES
TOTAL ENERGY COUPLED 2.56457E+02 JOULES

POSITION OF FIRST CELL 0.00000E+00

Table with 10 columns: CELL NO, COORDINATES M, THICKNESS M, HYDRO D Y N A M I C VELOCITY, PRESSURE, DENSITY, TEMPERATURE (KEV) ION, ELECTRON, AVERAGE CHARGE, SOURCE (P.T.S.). Rows 1-20 show cell parameters, with row 20 marked as *****.

Table with 10 columns: #, SPEC POWER (WATT/KG), DEP ENERGY (JOULE/M2), BEAM POWER (WATT/M2), ION EN DEP (KEV), ION ENERGY (KEV), ION #2 ENGY (KEV), ION #3 ENGY (KEV), ION #4 ENGY (KEV). Includes a total ion energy deposited row and an ion current row.

TIMESTEP NUMBER 990

TIME = 1.5016596E-08

DELTA T = 3.7453873E-11

DELTA T DETERMINED BY CONDITION 2 AT MESHPOINT 18

BOUNDARY : R = 1.0708E+00 U = 1.0856E+01 P = 1.0079E+06 TI = 2.0661E+04 TE = 2.0661E+04 SOUND SPEED = 1.0333E+04

ENERGIES : THERMAL 8.13501E+05 KINETIC 1.47803E+02 NUCLEAR 0.00000E+00 ERROR -1.41238E+06 RHO R 1.22624E-01

BEAM POWER : 3.24114E+14 WATTS TOTAL INCIDENT ENERGY 2.23077E+06 JOULES

TOTAL ENERGY COUPLED 2.22603E+06 JOULES

POSITION OF FIRST CELL 0.00000E+00

CELL NO	COORDINATES M	THICKNESS M	H Y D R O D Y N A M I C		DENSITY	TEMPERATURE (KEV)		AVERAGE CHARGE	SOURCE (P.T.S.)
			VELOCITY	PRESSURE		ION	ELECTRON		
1	-6.2499E-05	0.0000E+00	0.0000E+00	2.4469E+05	2.7000E+03	2.5862E-05	2.5862E-05	2.4646	0.0000E+00
2	-5.6249E-05	0.0000E+00	0.0000E+00	2.4469E+05	2.7000E+03	2.5862E-05	2.5862E-05	2.4646	0.0000E+00
3	-4.9999E-05	0.0000E+00	0.0000E+00	2.4469E+05	2.7000E+03	2.5862E-05	2.5862E-05	2.4646	0.0000E+00
4	-4.3749E-05	0.0000E+00	0.0000E+00	2.4469E+05	2.7000E+03	2.5862E-05	2.5862E-05	2.4646	0.0000E+00
5	-3.7499E-05	0.0000E+00	0.0000E+00	2.4469E+05	2.7000E+03	2.5862E-05	2.5862E-05	2.4646	0.0000E+00
6	-3.1249E-05	0.0000E+00	-1.4677E-03	3.9525E+05	2.7000E+03	2.5862E-05	2.5862E-05	2.4646	0.0000E+00
7	-2.4999E-05	0.0000E+00	-7.3985E-03	7.1869E+05	2.7000E+03	2.5862E-05	2.5862E-05	2.4646	0.0000E+00
8	-1.8749E-05	0.0000E+00	-1.6706E-02	1.0685E+06	2.7001E+03	2.5862E-05	2.5862E-05	2.4647	0.0000E+00
9	-1.2499E-05	0.0000E+00	-3.0614E-02	1.4486E+06	2.7001E+03	2.5862E-05	2.5862E-05	2.4647	0.0000E+00
10	-6.2497E-06	0.0000E+00	-5.1154E-02	2.0307E+06	2.7001E+03	2.5862E-05	2.5862E-05	2.4647	0.0000E+00
11	0.0000E+00	0.0000E+00	-7.2282E-02	2.7411E+06	2.7002E+03	2.5862E-05	2.5862E-05	2.4647	0.0000E+00
12	6.2496E-06	0.0000E+00	-9.7987E-02	3.7677E+06	2.7002E+03	2.5862E-05	2.5862E-05	2.4647	0.0000E+00
13	1.2499E-05	0.0000E+00	-1.5918E-01	5.6617E+06	2.7004E+03	2.5862E-05	2.5862E-05	2.4648	5.1803E+01
14	1.8748E-05	0.0000E+00	-3.5566E-01	8.7111E+06	2.7005E+03	2.5865E-05	2.5865E-05	2.4649	3.2105E+02
15	2.4997E-05	0.0000E+00	-1.1125E+00	1.6358E+07	2.7009E+03	2.5885E-05	2.5885E-05	2.4650	6.9119E+03
16	3.1245E-05	0.0000E+00	-5.1806E+00	4.8658E+07	2.7015E+03	2.6254E-05	2.6254E-05	2.4652	4.9009E+05
17	3.7491E-05	0.0000E+00	-6.6133E+01	4.7854E-20	2.2408E+03	4.0285E-05	4.0285E-05	2.2678	3.6117E+10
18	4.5022E-05	0.0000E+00	-6.5669E+01	1.5522E+09	3.1146E+02	1.3335E-03	1.3335E-03	1.0534	3.2252E+15
19	9.9202E-05	0.0000E+00	6.2099E+01	7.6215E+07	5.2444E+00	2.3221E-03	2.3221E-03	1.3243	8.8490E+15
20	3.3169E-03	0.0000E+00	7.1405E+01	1.0129E+06	1.5810E-02	1.7854E-03	1.7854E-03	1.9662	7.1325E+15
*****	1.0708E+00								

#	SPEC POWER (WATT/KG)	DEP ENERGY (JOULE/M2)	BEAM POWER (WATT/M2)	ION EN DEP (KEV)	ION ENERGY (KEV)	ION #2 ENGY (KEV)	ION #3 ENGY (KEV)	ION #4 ENGY (KEV)
1	0.0000E+00	0.0000D+00	0.0000D+00	0.0000D+00	0.0000D+00			
2	0.0000E+00	0.0000D+00	0.0000D+00	0.0000D+00	0.0000D+00			
3	0.0000E+00	0.0000D+00	0.0000D+00	0.0000D+00	0.0000D+00			
4	0.0000E+00	0.0000D+00	0.0000D+00	0.0000D+00	0.0000D+00			
5	0.0000E+00	0.0000D+00	0.0000D+00	0.0000D+00	0.0000D+00			
6	0.0000E+00	0.0000D+00	0.0000D+00	0.0000D+00	0.0000D+00			
7	0.0000E+00	0.0000D+00	0.0000D+00	0.0000D+00	0.0000D+00			
8	0.0000E+00	0.0000D+00	0.0000D+00	0.0000D+00	0.0000D+00			
9	0.0000E+00	0.0000D+00	0.0000D+00	0.0000D+00	0.0000D+00			
10	0.0000E+00	0.0000D+00	0.0000D+00	0.0000D+00	0.0000D+00			
11	0.0000E+00	0.0000D+00	0.0000D+00	0.0000D+00	0.0000D+00			
12	0.0000E+00	0.0000D+00	0.0000D+00	0.0000D+00	0.0000D+00			
13	0.0000E+00	0.0000D+00	0.0000D+00	0.0000D+00	0.0000D+00			
14	0.0000E+00	0.0000D+00	0.0000D+00	0.0000D+00	0.0000D+00			
15	0.0000E+00	0.0000D+00	0.0000D+00	0.0000D+00	0.0000D+00			
16	0.0000E+00	0.0000D+00	0.0000D+00	0.0000D+00	3.5527D-15			
17	0.0000E+00	0.0000D+00	1.0403D-03	0.0000D+00	3.5527D-15			
18	3.2252E+15	2.0384D+03	5.4264D+13	1.8531D+02	1.8531D+02			
19	8.8490E+15	5.5929D+03	2.0371D+14	5.1034D+02	6.9565D+02			
20	7.1325E+15	4.5080D+03	3.2411D+14	4.1119D+02	1.1068D+03			
		TOTAL ION ENERGY DEPOSITED (KEV)		1.1068E+03				
		----- ION CURRENT (AMP/M2) -----			2.9283E+08			

TIMESTEP NUMBER 1813

TIME = 3.0002877E-08

DELTA T = 2.0235064E-11

DELTA T DETERMINED BY CONDITION 3 AT MESHPOINT 15

BOUNDARY : R = 1.0916E+00 U = 5.8221E+01 P = 3.8249E+06 TI = 4.4406E+04 TE = 4.4406E+04 SOUND SPEED = 2.0239E+04

ENERGIES : THERMAL 4.23349E+06 KINETIC 3.40143E+04 NUCLEAR 0.00000E+00 ERROR -6.89305E+06 RHO R 1.03354E-01

BEAM POWER : 9.11898E+14 WATTS TOTAL INCIDENT ENERGY 1.11733E+07 JOULES
TOTAL ENERGY COUPLED 1.11606E+07 JOULES

POSITION OF FIRST CELL 0.00000E+00

Table with 10 columns: CELL NO, COORDINATES M, THICKNESS M, H Y D R O VELOCITY, D Y N A M I C PRESSURE, DENSITY, TEMPERATURE (KEV) ION, TEMPERATURE (KEV) ELECTRON, AVERAGE CHARGE, SOURCE (P.T.S.). Rows 1-20 show cell data, ending with ***** 1.0916E+00.

Table with 8 columns: #, SPEC POWER (WATT/KG), DEP ENERGY (JOULE/M2), BEAM POWER (WATT/M2), ION EN DEP (KEV), ION ENERGY (KEV), ION #2 ENGY (KEV), ION #3 ENGY (KEV), ION #4 ENGY (KEV). Rows 1-20 show energy deposition data, ending with TOTAL ION ENERGY DEPOSITED (KEV) 1.6448E+03 and ION CURRENT (AMP/M2) 5.5440E+08.

109

TIMESTEP NUMBER 2674

TIME = 4.5003478E-08

DELTA T = 1.7920762E-11

DELTA T DETERMINED BY CONDITION 1 AT MESHPOINT 12

BOUNDARY : R = 1.1176E+00 U = 1.3185E+02 P = 4.5605E+06 TI = 1.0087E+05 TE = 1.0087E+05 SOUND SPEED = 2.2318E+04

ENERGIES : THERMAL 1.54763E+07 KINETIC 6.68178E+05 NUCLEAR 0.00000E+00 ERROR -1.20392E+07 RHO R 8.17896E-02

BEAM POWER : 1.39230E+15 WATTS TOTAL INCIDENT ENERGY 2.82009E+07 JOULES
TOTAL ENERGY COUPLED 2.81837E+07 JOULES

POSITION OF FIRST CELL 0.00000E+00

Table with 9 columns: CELL NO, COORDINATES M, THICKNESS M, H Y D R O D Y N A M I C VELOCITY, PRESSURE, DENSITY, TEMPERATURE (KEV) ION, ELECTRON, AVERAGE CHARGE, SOURCE (P.T.S.). Rows 1-20 show cell parameters, ending with ***** and 1.1177E+00.

Table with 9 columns: #, SPEC POWER (WATT/KG), DEP ENERGY (JOULE/M2), BEAM POWER (WATT/M2), ION EN DEP (KEV), ION ENERGY (KEV), ION #2 ENGY (KEV), ION #3 ENGY (KEV), ION #4 ENGY (KEV). Rows 1-20 show energy deposition data, ending with TOTAL ION ENERGY DEPOSITED (KEV) 2.0295E+03 and ION CURRENT (AMP/M2) 6.8601E+08.

101

TIMESTEP NUMBER 3999

TIME = 6.0004481E-08

DELTA T = 1.0835941E-11

DELTA T DETERMINED BY CONDITION 1 AT MESHPOINT 2

BOUNDARY : R = 1.1502E+00 U = 2.1951E+02 P = 9.1844E+06 T1 = 1.2707E+05 TE = 1.2707E+05 SOUND SPEED = 3.2066E+04

ENERGIES : THERMAL 2.50404E+07 KINETIC 2.32764E+06 NUCLEAR 0.00000E+00 ERROR -2.21828E+07 RHO R 6.57315E-02

BEAM POWER : 1.26546E+15 WATTS TOTAL INCIDENT ENERGY 4.95680E+07 JOULES
TOTAL ENERGY COUPLED 4.95509E+07 JOULES

POSITION OF FIRST CELL 0.00000E+00

CELL NO	COORDINATES M	THICKNESS M	H Y D R O D Y N A M I C		DENSITY	TEMPERATURE (KEV)		AVERAGE CHARGE	SOURCE (P.T.S.)
			VELOCITY	PRESSURE		ION	ELECTRON		
1	-5.0678E-05	0.0000E+00	0.0000E+00	4.2116E+10	3.5008E+03	1.5375E-04	1.5375E-04	2.7573	-3.1212E+06
2	-4.5857E-05	0.0000E+00	8.4158E+01	4.1644E+10	3.4942E+03	1.5230E-04	1.5230E-04	2.7551	-3.4042E+06
3	-4.1028E-05	0.0000E+00	1.6739E+02	4.0731E+10	3.4818E+03	1.4914E-04	1.4914E-04	2.7509	1.1684E+06
4	-3.6181E-05	0.0000E+00	2.4849E+02	3.9507E+10	3.4633E+03	1.4641E-04	1.4641E-04	2.7447	3.2417E+06
5	-3.1309E-05	0.0000E+00	3.2709E+02	3.8002E+10	3.4376E+03	1.4528E-04	1.4528E-04	2.7361	6.7655E+06
6	-2.6400E-05	0.0000E+00	3.9979E+02	3.6243E+10	3.4026E+03	1.4775E-04	1.4775E-04	2.7242	2.8546E+07
7	-2.1440E-05	0.0000E+00	4.6013E+02	3.4715E+10	3.3525E+03	1.6306E-04	1.6306E-04	2.7071	2.6608E+06
8	-1.6407E-05	0.0000E+00	4.9926E+02	3.2452E+10	3.2558E+03	1.7663E-04	1.7663E-04	2.6735	5.6295E+07
9	-1.1224E-05	0.0000E+00	5.3934E+02	3.2169E+10	3.1205E+03	2.0373E-04	2.0373E-04	2.6251	6.4953E+08
10	-5.8158E-06	0.0000E+00	5.5099E+02	2.7550E+10	2.9016E+03	3.0740E-04	3.0740E-04	2.5437	1.6498E+10
11	0.0000E+00	0.0000E+00	4.6102E+02	2.8162E+10	2.5083E+03	7.1045E-04	7.1045E-04	2.3957	1.3257E+11
12	6.7277E-06	0.0000E+00	2.3217E+02	2.3484E+10	1.8190E+03	1.4470E-03	1.4470E-03	2.1218	9.0915E+11
13	1.6005E-05	0.0000E+00	-6.9055E+01	2.2772E+10	1.0145E+03	2.9338E-03	2.9338E-03	1.8023	1.6041E+12
14	3.2639E-05	0.0000E+00	-7.0093E+01	1.9199E+10	5.1243E+02	4.8291E-03	4.8291E-03	1.7398	2.7050E+12
15	6.5571E-05	0.0000E+00	5.0059E+02	1.5223E+10	2.4322E+02	7.3749E-03	7.3749E-03	2.0404	6.3580E+12
16	1.3495E-04	0.0000E+00	2.8234E+03	1.4650E+10	1.2420E+02	1.1171E-02	1.1171E-02	2.7226	-1.0428E+12
17	2.7082E-04	0.0000E+00	7.5300E+03	1.3860E+10	8.2514E+01	1.3975E-02	1.3975E-02	3.2627	8.2899E+15
18	4.7533E-04	0.0000E+00	1.1266E+04	4.1701E+09	2.2483E+01	1.3886E-02	1.3886E-02	3.6806	2.5870E+16
19	1.2259E-03	0.0000E+00	8.6708E+03	1.8805E+08	1.0589E+00	1.1704E-02	1.1704E-02	4.3475	1.9915E+16
20	1.7162E-02	0.0000E+00	2.6837E+03	9.1886E+06	1.4894E-02	1.0956E-02	1.0956E-02	5.7296	2.0905E+16
*****	1.1502E+00								

#	SPEC POWER (WATT/KG)	DEP ENERGY (Joule/M2)	BEAM POWER (WATT/M2)	ION EN DEP (KEV)	ION ENERGY (KEV)	ION #2 ENGY (KEV)	ION #3 ENGY (KEV)	ION #4 ENGY (KEV)
1	0.0000E+00	0.0000D+00	0.0000D+00	0.0000D+00	0.0000D+00			
2	0.0000E+00	0.0000D+00	0.0000D+00	0.0000D+00	0.0000D+00			
3	0.0000E+00	0.0000D+00	0.0000D+00	0.0000D+00	0.0000D+00			
4	0.0000E+00	0.0000D+00	0.0000D+00	0.0000D+00	0.0000D+00			
5	0.0000E+00	0.0000D+00	0.0000D+00	0.0000D+00	0.0000D+00			
6	0.0000E+00	0.0000D+00	0.0000D+00	0.0000D+00	0.0000D+00			
7	0.0000E+00	0.0000D+00	0.0000D+00	0.0000D+00	0.0000D+00			
8	0.0000E+00	0.0000D+00	0.0000D+00	0.0000D+00	0.0000D+00			
9	0.0000E+00	0.0000D+00	0.0000D+00	0.0000D+00	0.0000D+00			
10	0.0000E+00	0.0000D+00	0.0000D+00	0.0000D+00	0.0000D+00			
11	0.0000E+00	0.0000D+00	0.0000D+00	0.0000D+00	0.0000D+00			
12	0.0000E+00	0.0000D+00	0.0000D+00	0.0000D+00	0.0000D+00			
13	0.0000E+00	0.0000D+00	0.0000D+00	0.0000D+00	0.0000D+00			
14	0.0000E+00	0.0000D+00	0.0000D+00	0.0000D+00	0.0000D+00			
15	0.0000E+00	0.0000D+00	0.0000D+00	0.0000D+00	3.5527D-15			
16	0.0000E+00	0.0000D+00	2.6930D-03	0.0000D+00	3.5527D-15			
17	8.3008E+15	1.5178D+03	1.3992D+14	1.8459D+02	1.8459D+02			
18	2.5870E+16	4.7304D+03	5.7658D+14	5.7605D+02	7.6063D+02			
19	1.9915E+16	3.6416D+03	9.1268D+14	4.4339D+02	1.2040D+03			
20	2.0905E+16	3.8226D+03	1.2655D+15	4.6540D+02	1.6694D+03			
	TOTAL ION ENERGY DEPOSITED (KEV)			1.6694E+03				
----- ION CURRENT (AMP/M2) -----				7.5802E+08				

TIMESTEP NUMBER 4789

TIME = 7.5019898E-08

DELTA T = 3.3872377E-11

DELTA T DETERMINED BY CONDITION 1 AT MESHPOINT 9

BOUNDARY : R = 1.1944E+00 U = 3.1678E+02 P = 1.4706E+07 TI = 1.5344E+05 TE = 1.5344E+05 SOUND SPEED = 4.1278E+04

ENERGIES : THERMAL 2.84323E+07 KINETIC 4.05424E+06 NUCLEAR 0.00000E+00 ERROR -3.09522E+07 RHO R 6.03465E-02

POSITION OF FIRST CELL 0.00000E+00

CELL NO	COORDINATES M	THICKNESS M	H Y D R O D Y N A M I C		DENSITY	TEMPERATURE (KEY)		AVERAGE CHARGE	SOURCE (P.T.S.)
			VELOCITY	PRESSURE		ION	ELECTRON		
1	-6.5634E-05	0.0000E+00	0.0000E+00	1.3048E+09	2.7307E+03	3.3873E-05	3.3873E-05	2.4769	-1.9446E+03
2	-5.9455E-05	0.0000E+00	4.2020E+01	1.4616E+09	2.7361E+03	3.3823E-05	3.3823E-05	2.4791	2.8227E+04
3	-5.3287E-05	0.0000E+00	8.0421E+01	1.7510E+09	2.7443E+03	3.4488E-05	3.4488E-05	2.4824	1.4334E+05
4	-4.7138E-05	0.0000E+00	1.1502E+02	2.2896E+09	2.7545E+03	3.8144E-05	3.8144E-05	2.4864	4.4344E+05
5	-4.1012E-05	0.0000E+00	1.3966E+02	2.7122E+09	2.7503E+03	4.6908E-05	4.6908E-05	2.4847	1.8794E+06
6	-3.4876E-05	0.0000E+00	1.5579E+02	3.5888E+09	2.7419E+03	6.4575E-05	6.4575E-05	2.4814	1.0507E+07
7	-2.8722E-05	0.0000E+00	1.6881E+02	4.6416E+09	2.6708E+03	9.9209E-05	9.9209E-05	2.4528	2.7892E+07
8	-2.2403E-05	0.0000E+00	1.8953E+02	5.2958E+09	2.5139E+03	1.4305E-04	1.4305E-04	2.3879	9.9102E+07
9	-1.5691E-05	0.0000E+00	2.2775E+02	6.2703E+09	2.3750E+03	2.0667E-04	2.0667E-04	2.3280	1.9305E+09
10	-8.5852E-06	0.0000E+00	1.6644E+02	6.4868E+09	1.9656E+03	4.2305E-04	4.2305E-04	2.1363	3.5329E+10
11	0.0000E+00	0.0000E+00	7.0217E+01	9.3750E+09	1.3973E+03	1.0279E-03	1.0279E-03	1.8621	1.4132E+11
12	1.2076E-05	0.0000E+00	1.6568E+02	9.7480E+09	8.9809E+02	1.9037E-03	1.9037E-03	1.6213	6.1546E+11
13	3.0866E-05	0.0000E+00	5.4820E+02	1.1739E+10	5.2830E+02	3.4041E-03	3.4041E-03	1.5539	9.4109E+11
14	6.2809E-05	0.0000E+00	1.3938E+03	1.1208E+10	3.0146E+02	5.1834E-03	5.1834E-03	1.7029	1.0705E+12
15	1.1879E-04	0.0000E+00	2.5038E+03	9.7920E+09	1.6223E+02	7.2374E-03	7.2374E-03	2.0438	1.9974E+12
16	2.2281E-04	0.0000E+00	4.5325E+03	8.6982E+09	8.1232E+01	1.0106E-02	1.0106E-02	2.6447	1.6125E+12
17	4.3055E-04	0.0000E+00	9.3671E+03	8.5202E+09	5.3010E+01	1.3217E-02	1.3217E-02	3.2800	-4.7439E+12
18	7.4889E-04	0.0000E+00	1.4524E+04	3.4376E+09	1.6740E+01	1.4587E-02	1.4587E-02	3.9099	-1.7223E+12
19	1.7570E-03	0.0000E+00	1.1770E+04	2.0723E+08	8.6406E-01	1.3967E-02	1.3967E-02	4.9345	4.9665E+10
20	2.1287E-02	0.0000E+00	3.7602E+03	1.4706E+07	1.4385E-02	1.3228E-02	1.3228E-02	6.3620	8.6388E+08
*****	1.1946E+00								

*** BEAM SWITCHED OFF AT STEP 4726 TIME 7.2995590E-08 POWER 8.62900E+14 ENERGY 6.34387E+07 R(ABS) 7.74517E-04

***** E N D O F J O B *****
TIMESTEP = 4792 NOUT = 6 TIME = 7.51215E-08
MESH = 20 TIMESTEP = 4792 YIELD = 0.000E+00

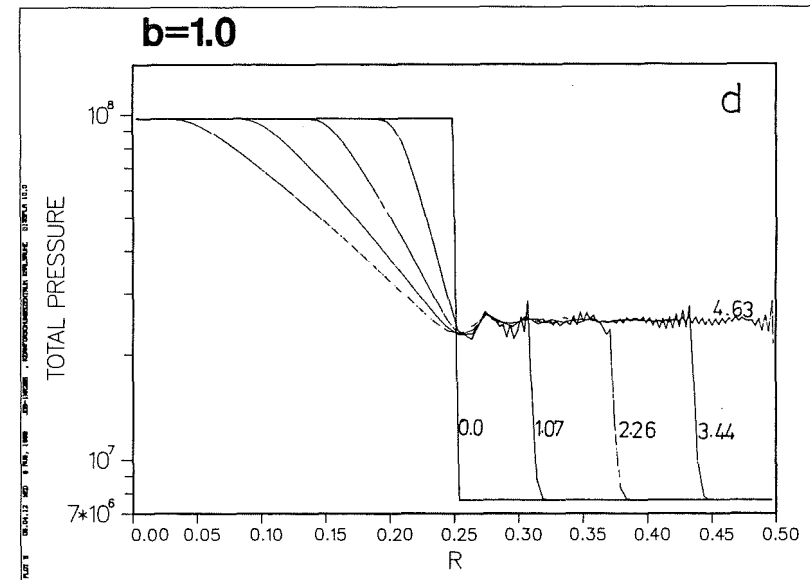
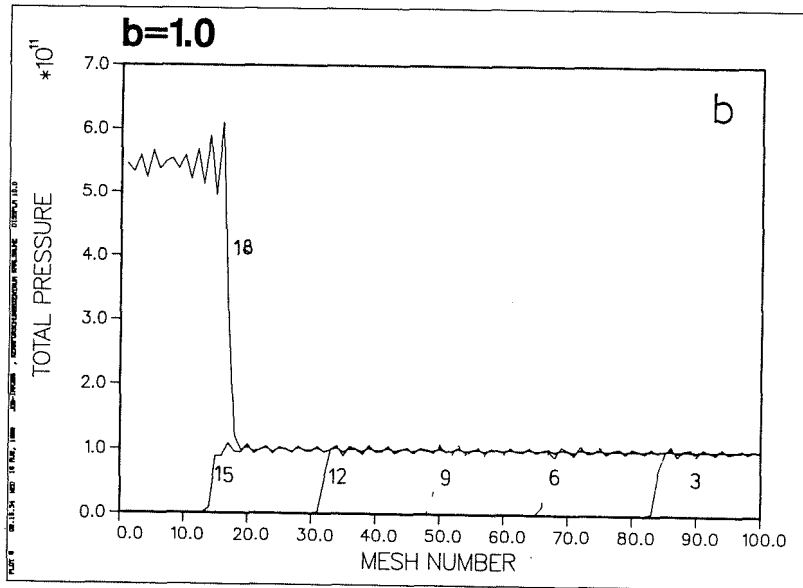
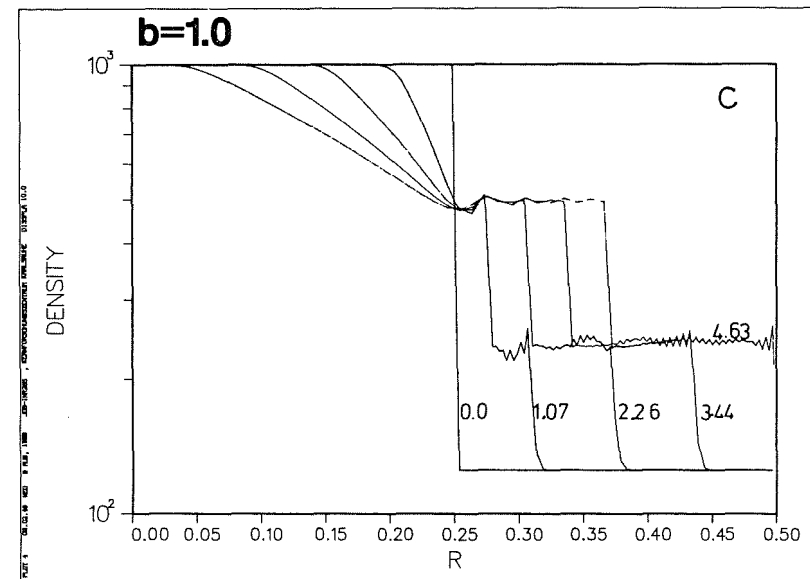
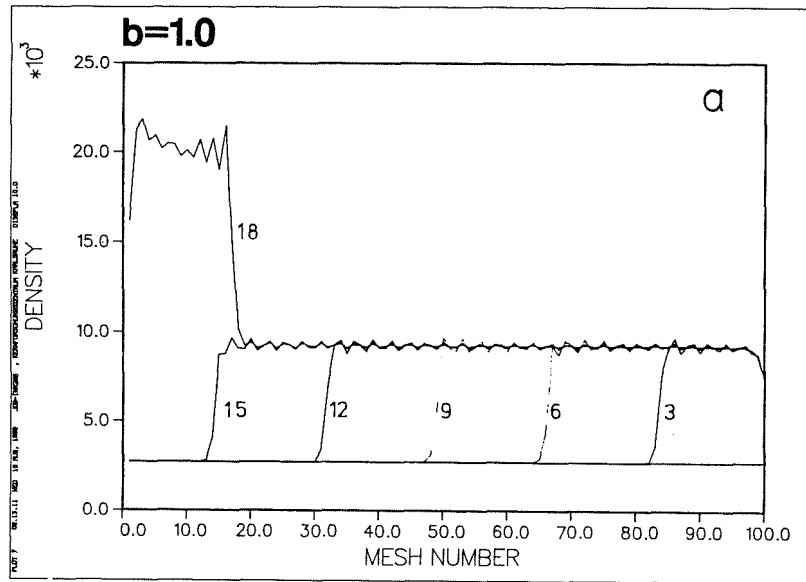


Fig. 1.1: Density and pressure profiles at various time steps for the von-Neumann artificial viscosity parameter $b = 1.0$. Curves a and b are for a constant pressure pulse while c and d represent Sod's problem. Numbers on the curves indicate time.

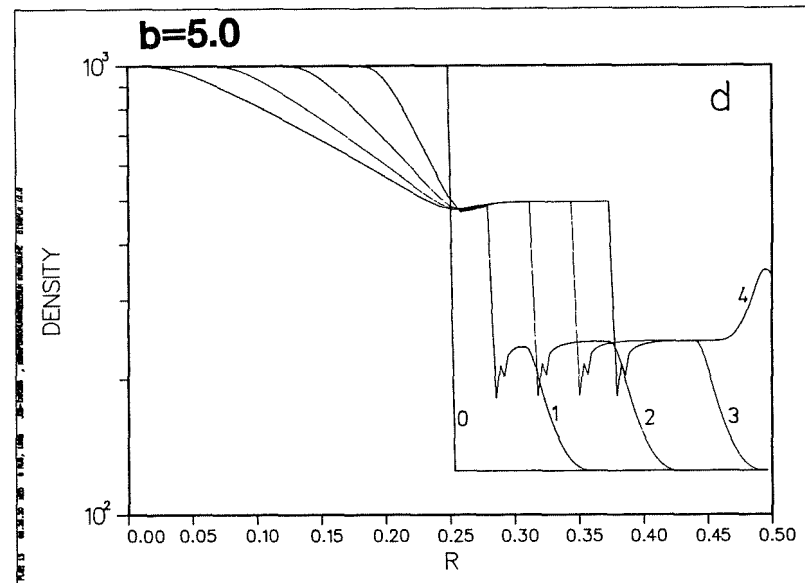
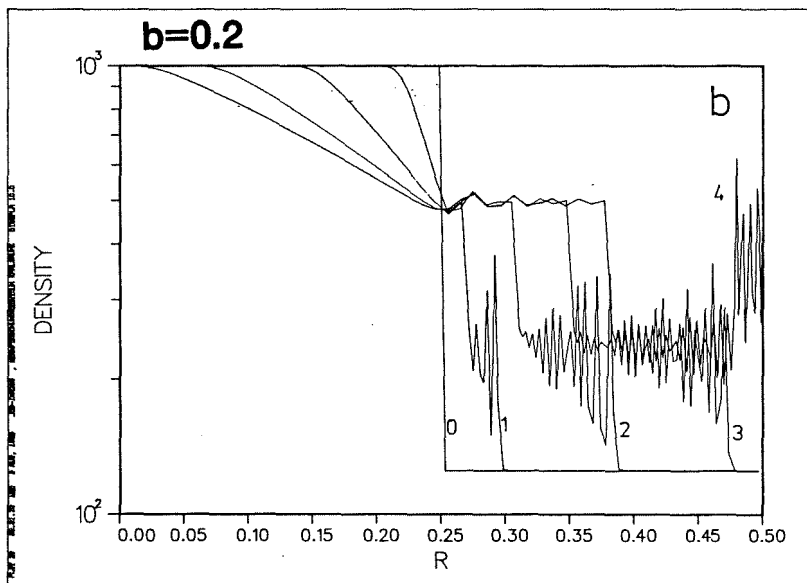
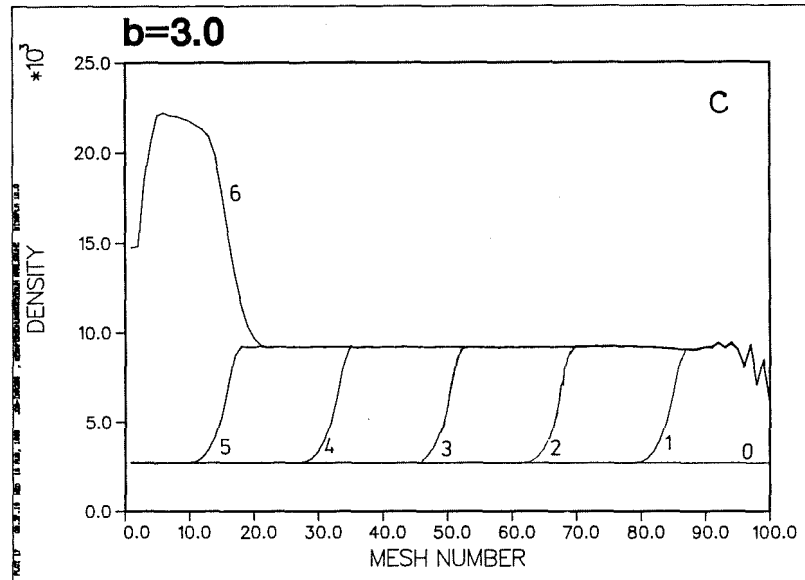
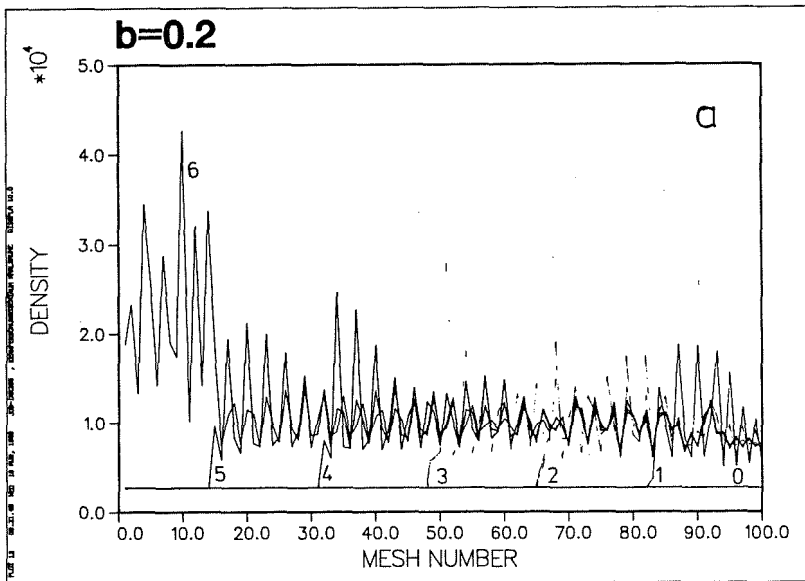


Fig. 1.2: Effects of the variation of the von-Neumann viscosity parameter b on density for the amplitude of oscillations in density for the constant pressure pulse (a and b) and Sod's problems (c and d).

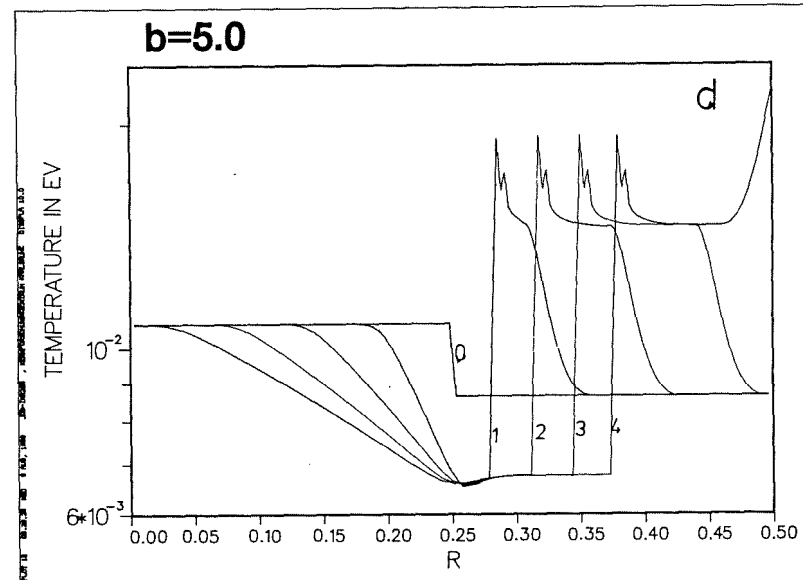
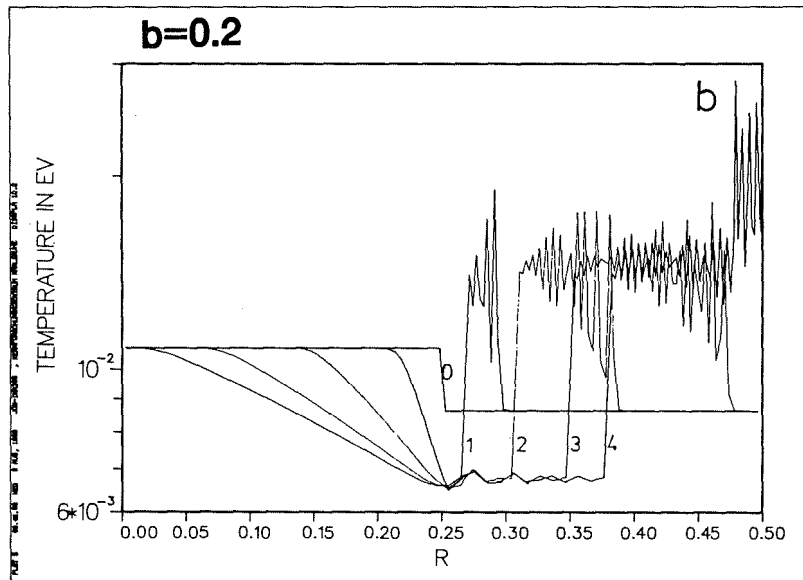
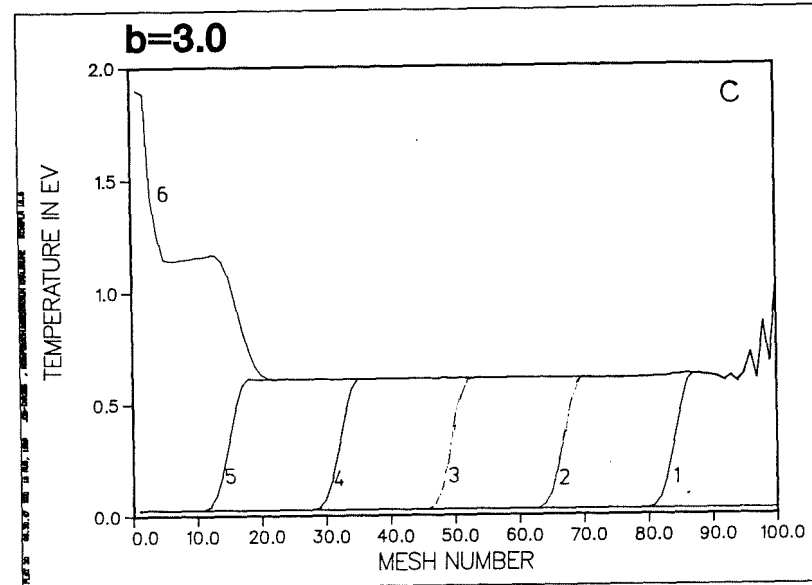
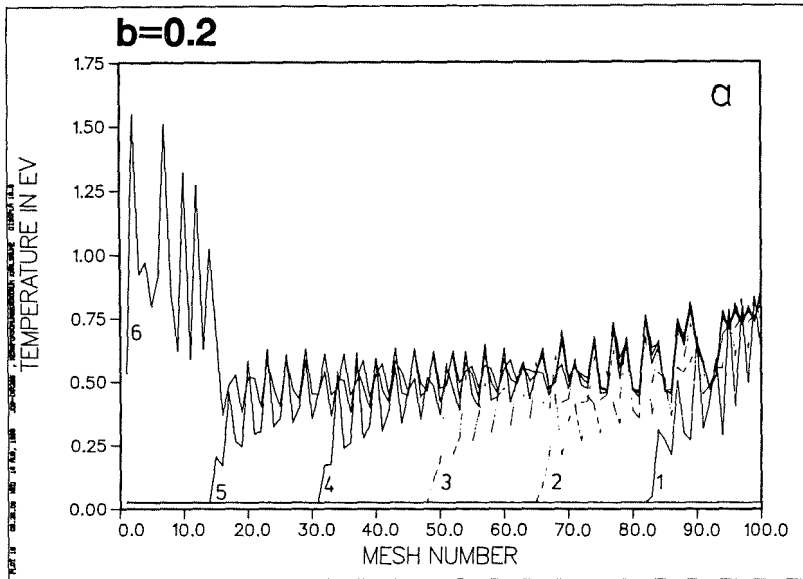
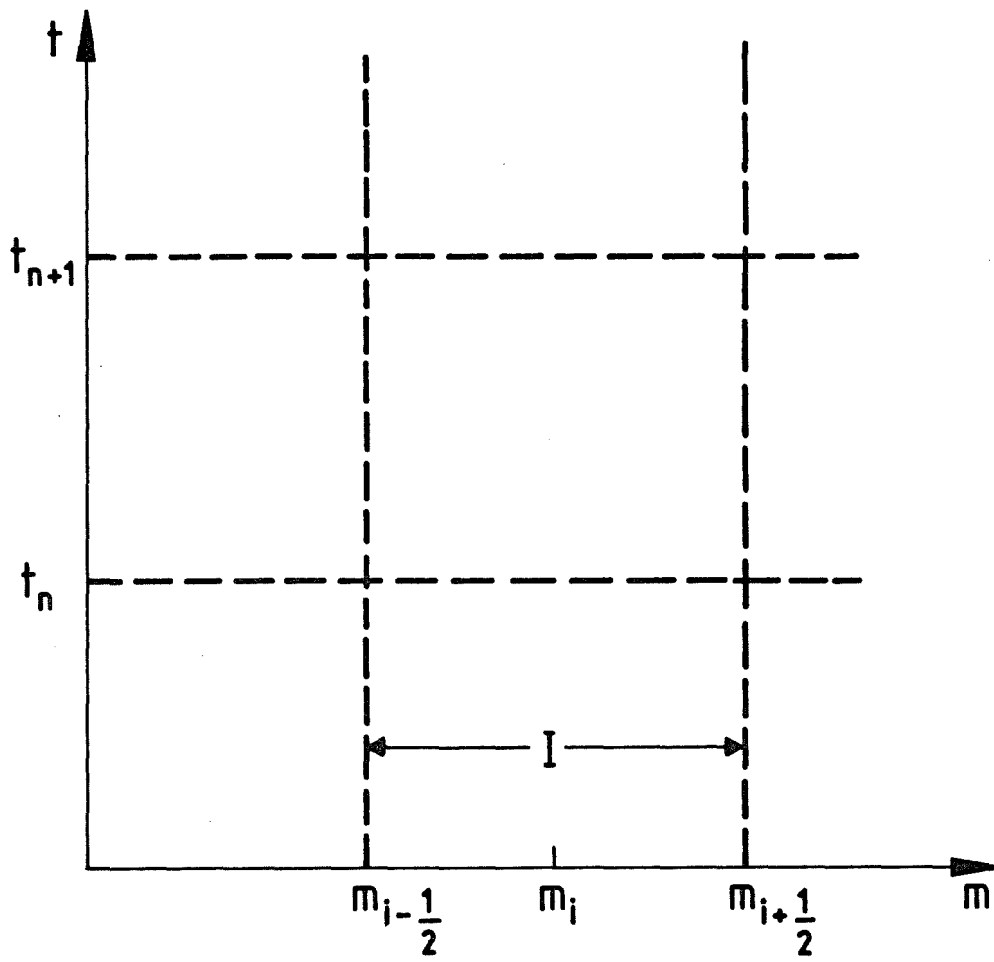
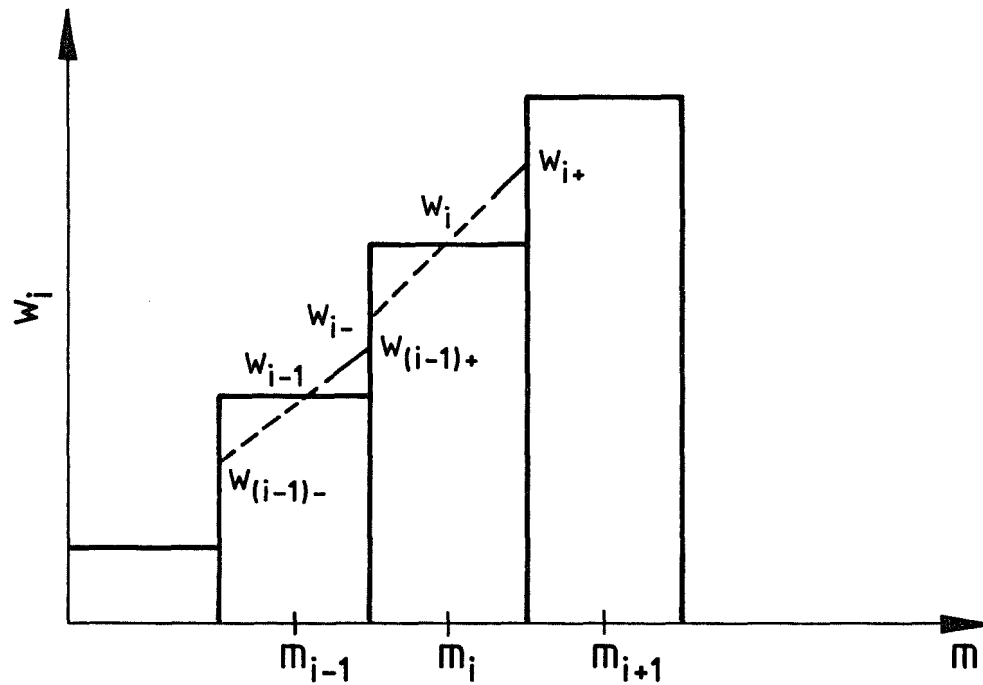


Fig. 1.3: Same as Fig. 1.2 but for temperature.



FINITE DIFFERENCE MESH GRID

Fig. 3.1: The finite difference mesh grid for the upwind scheme.



PIECEWISE LINEAR REPRESENTATION
OF THE CONSERVED VARIABLES

Fig. 3.2: Piecewise linear representation of the conserved variables.

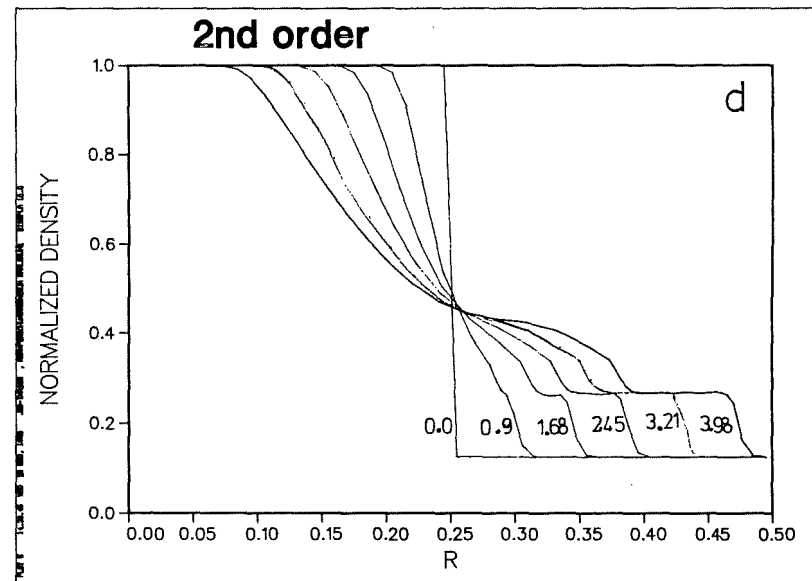
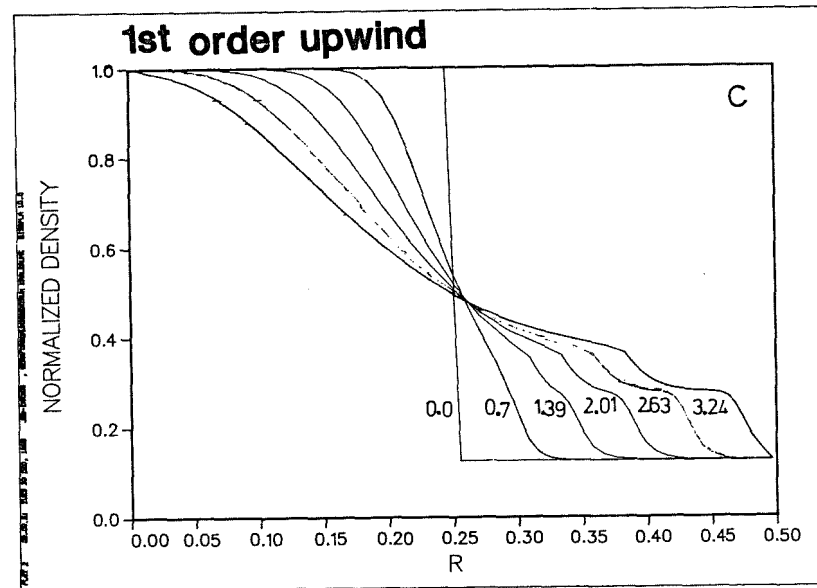
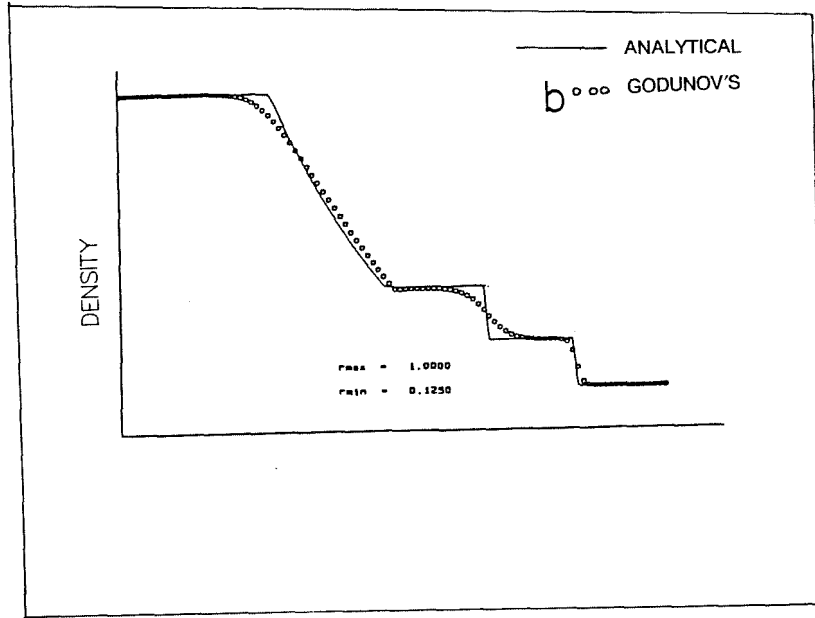
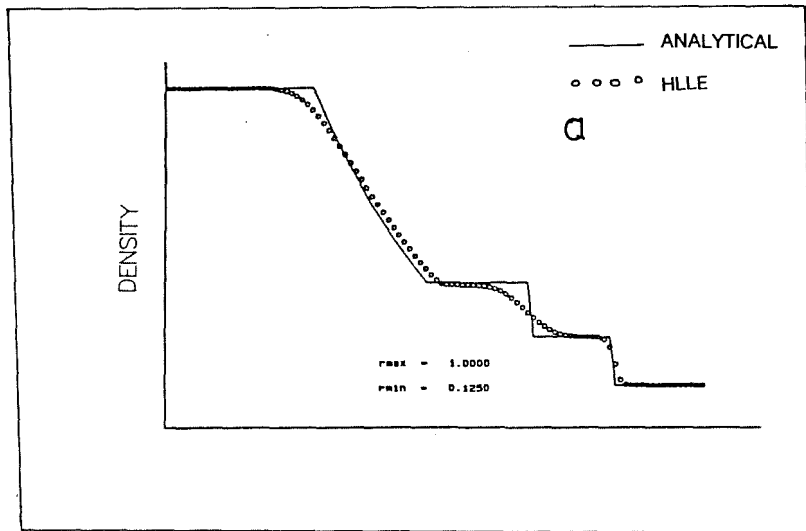


Fig. 5.1: Comparison of density profiles for the Sod's shock tube problem. Numbers marked on each curve represent time in units of 10^{-4} sec.

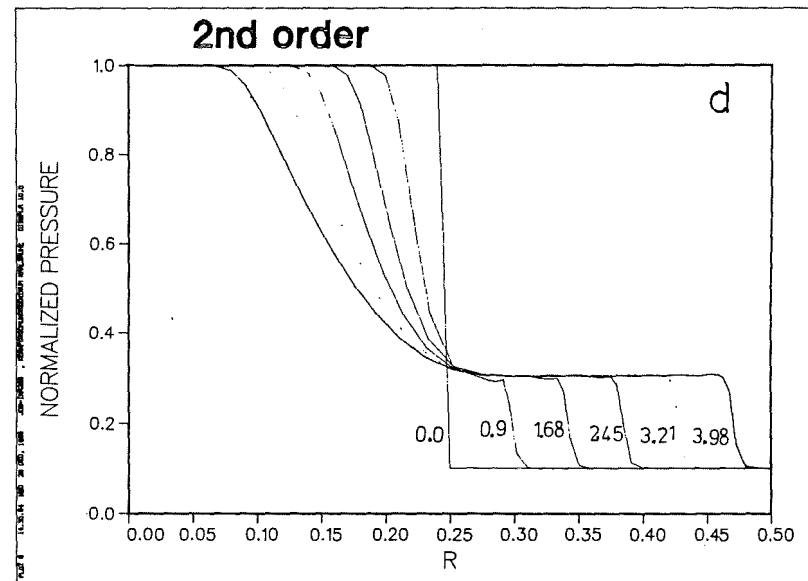
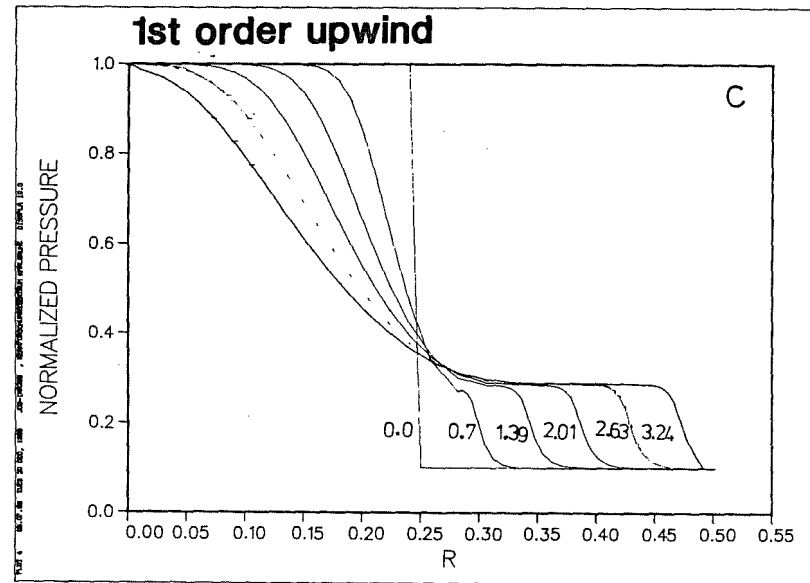
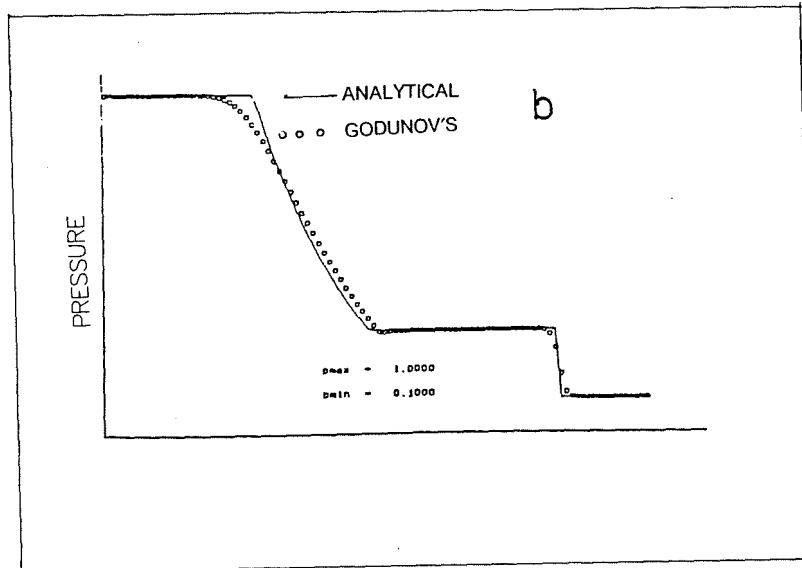
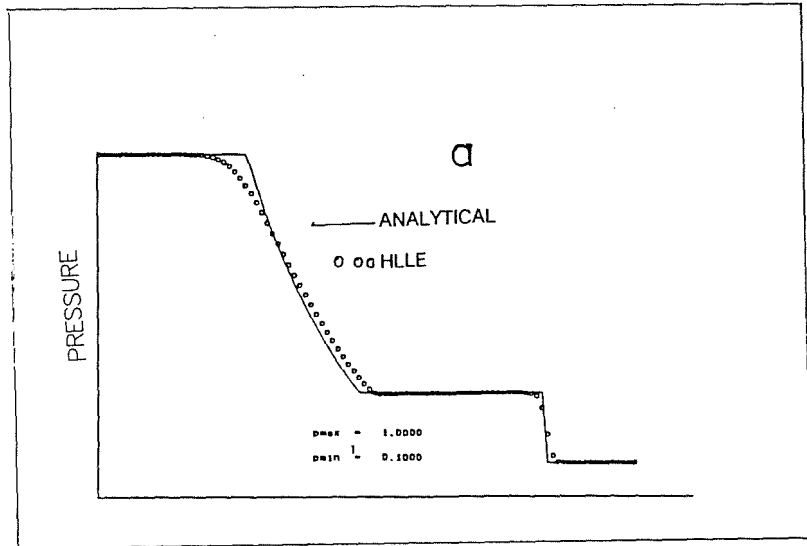


Fig. 5.2: Same as Fig. 5.1 but for pressure.

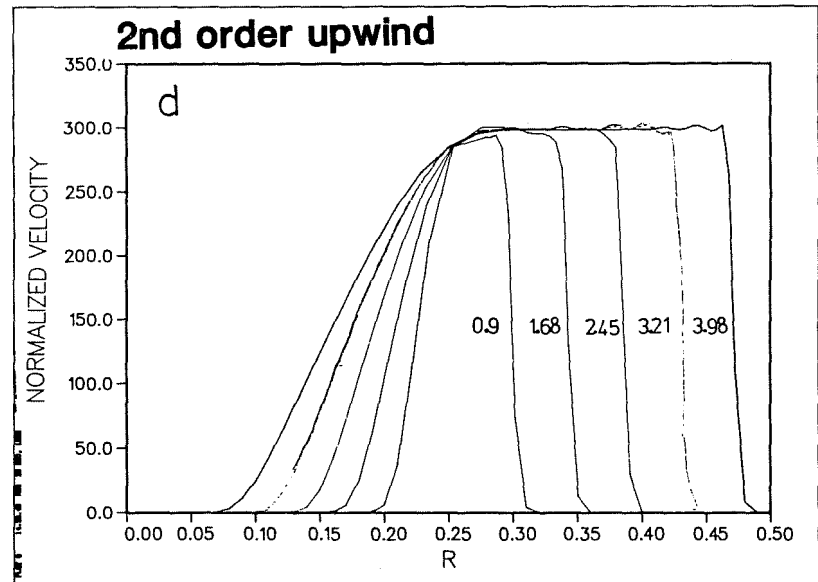
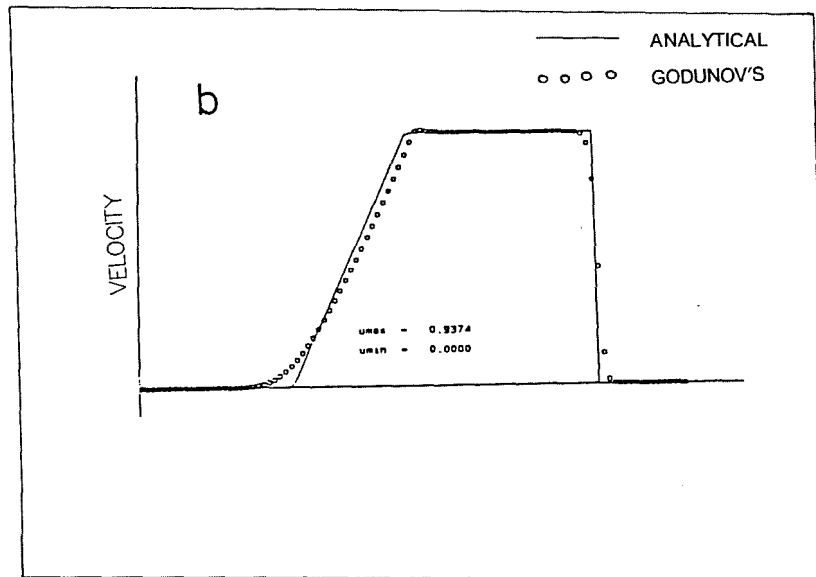
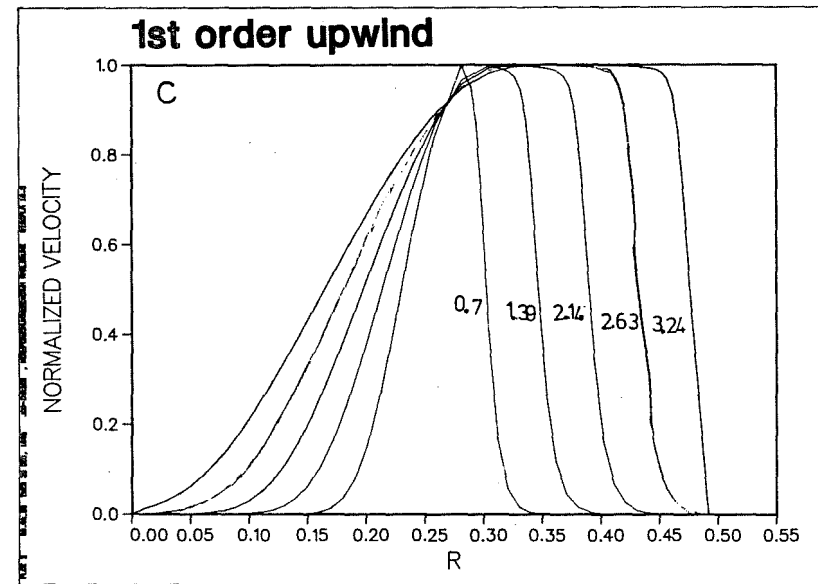
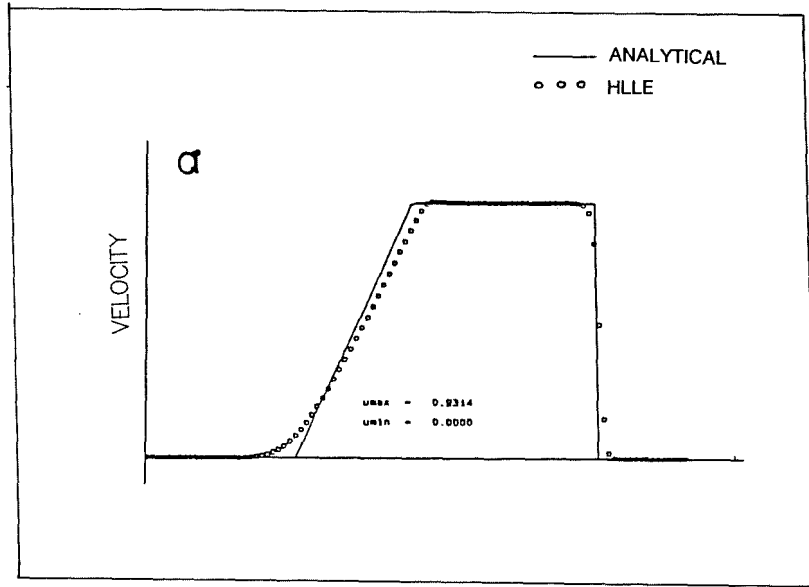


Fig. 5.3: Same as Fig. 5.1 but for particle velocity.

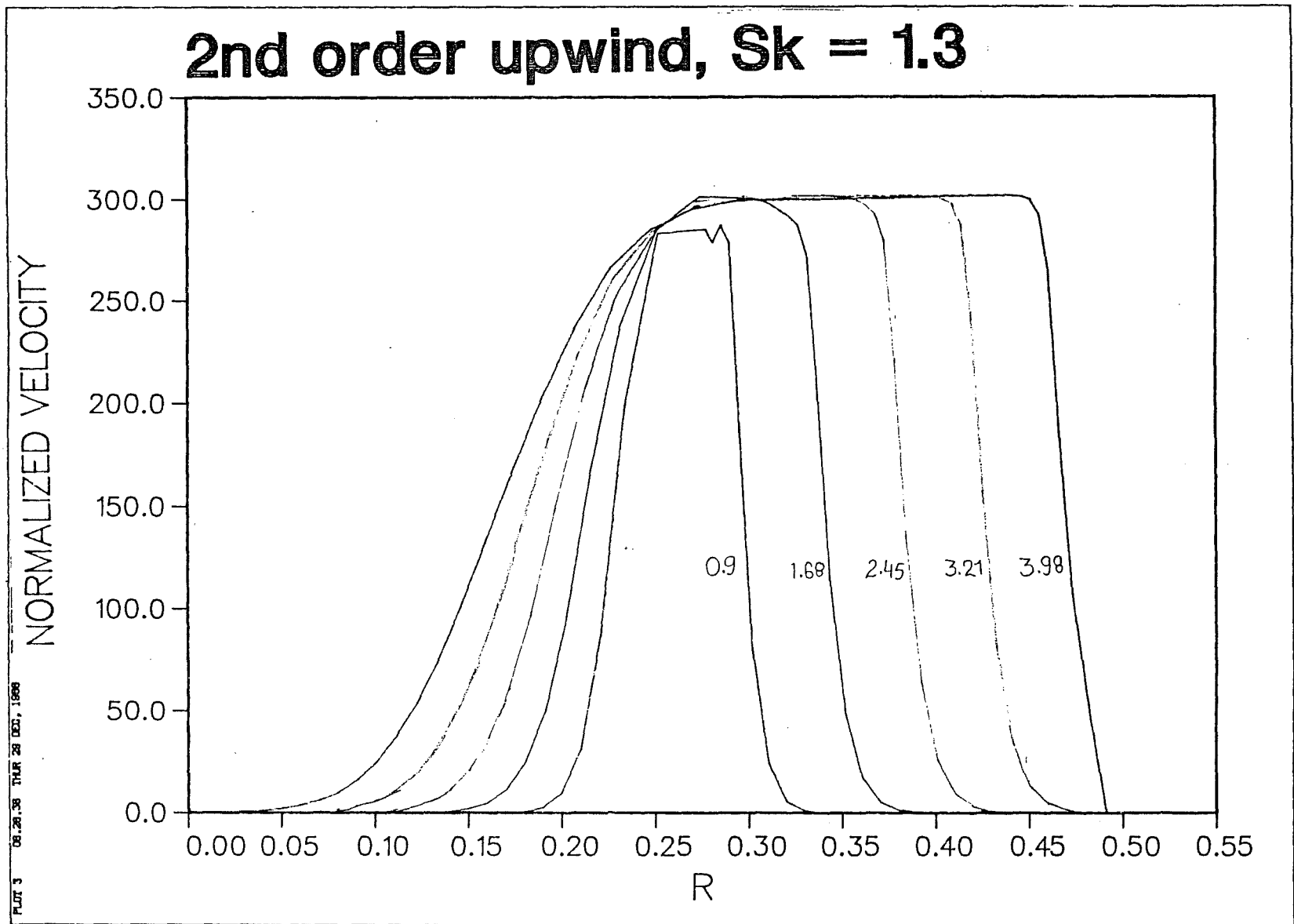


Fig. 5.4: Same as Fig. 5.3d but with the Roe's prescription for the calculation of slopes with constant $s_k = 1.3$.

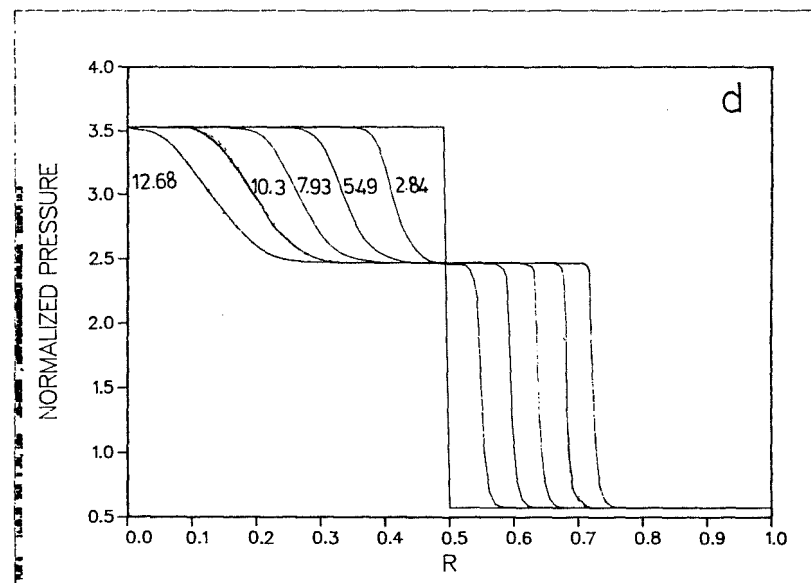
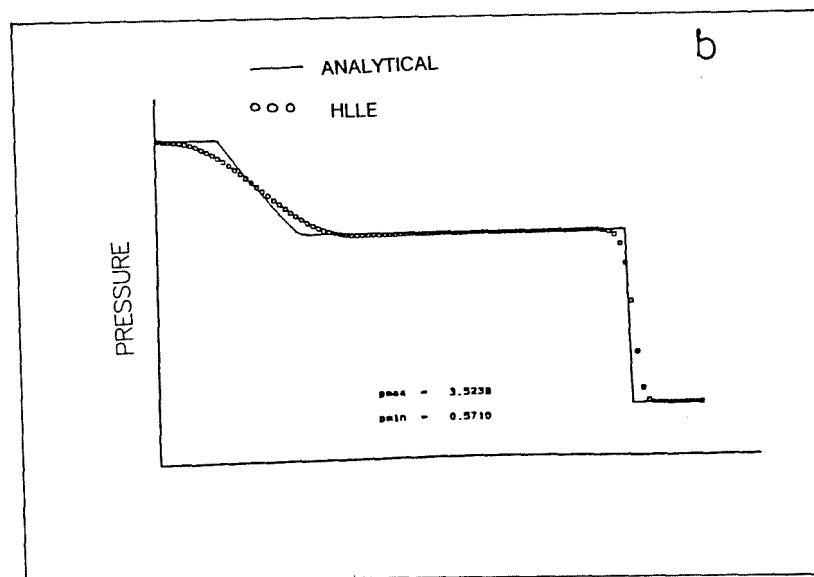
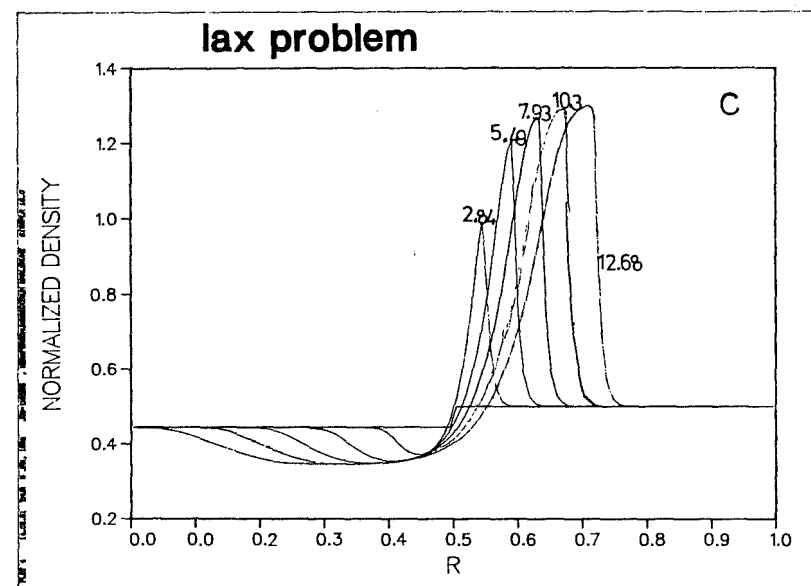
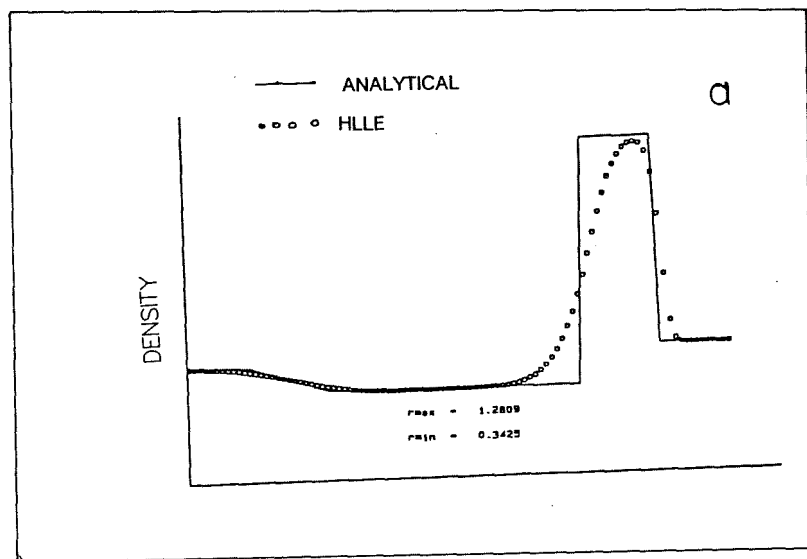


Fig. 5.5: Comparison of the density and pressure profiles for the Lax₄ problem. Numbers marked on each curve represent time in units of 10^{-4} sec.

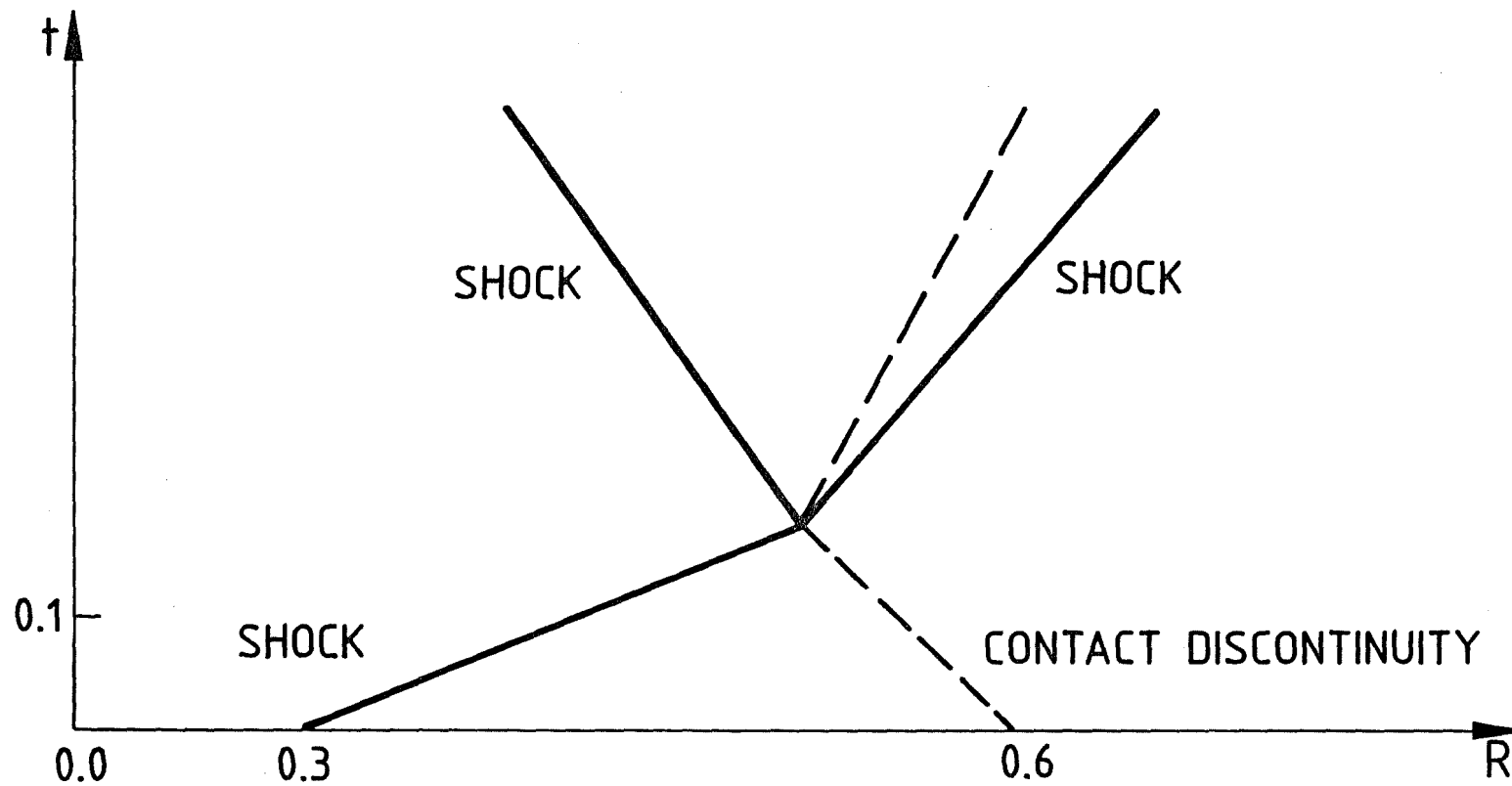


Fig. 5.6: Space-time diagram of a shock wave interacting with a contact discontinuity as generated in the Munz problem.

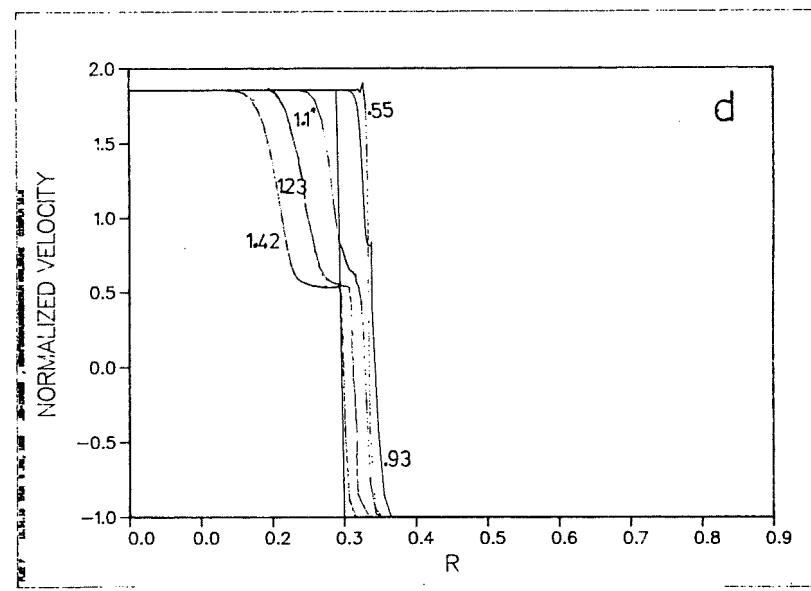
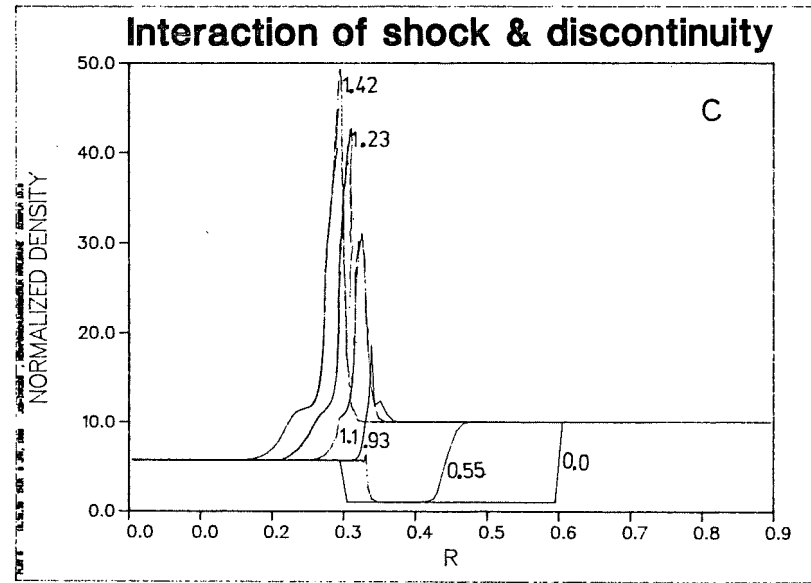
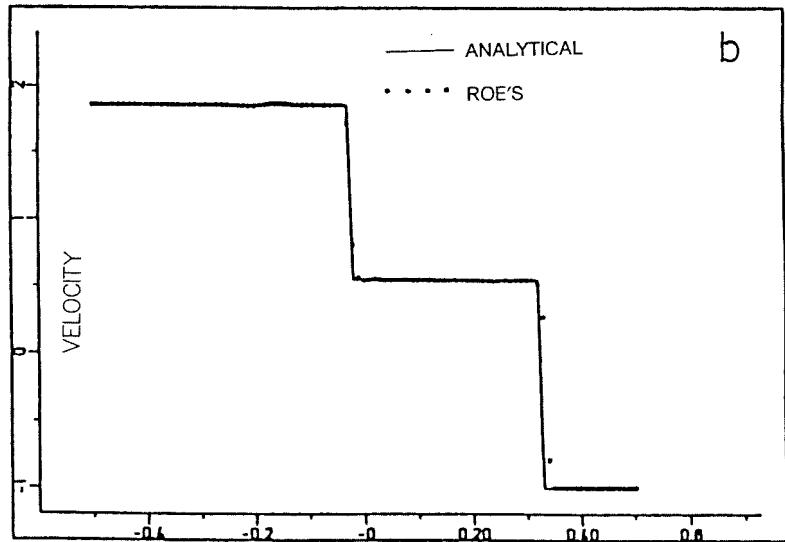
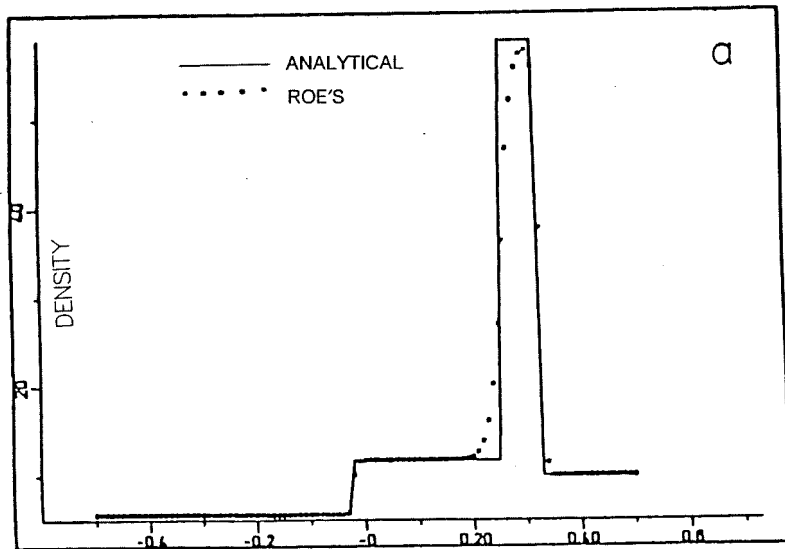


Fig. 5.7: Comparison of density and pressure profiles for the Munz's problem. Numbers marked on each curve represent time in units of 10^{-4} sec. Curves c and d show the 1st order upwind scheme results.

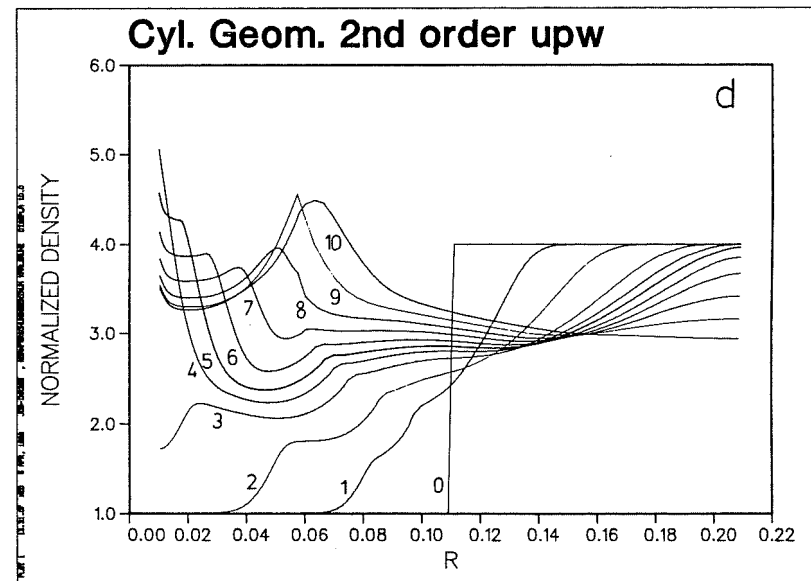
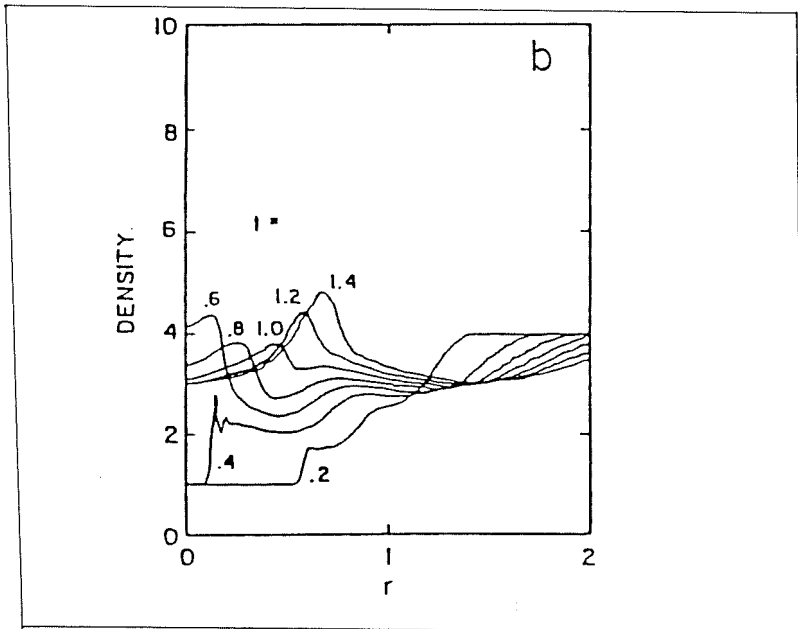
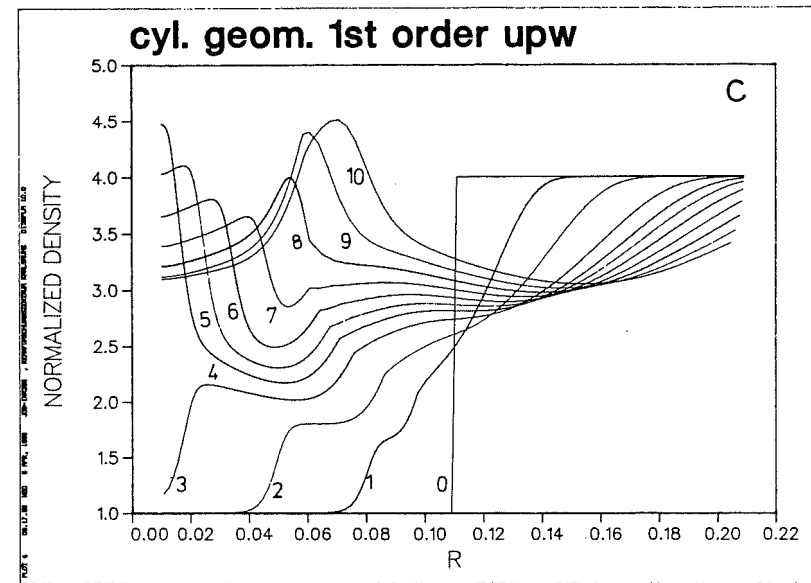
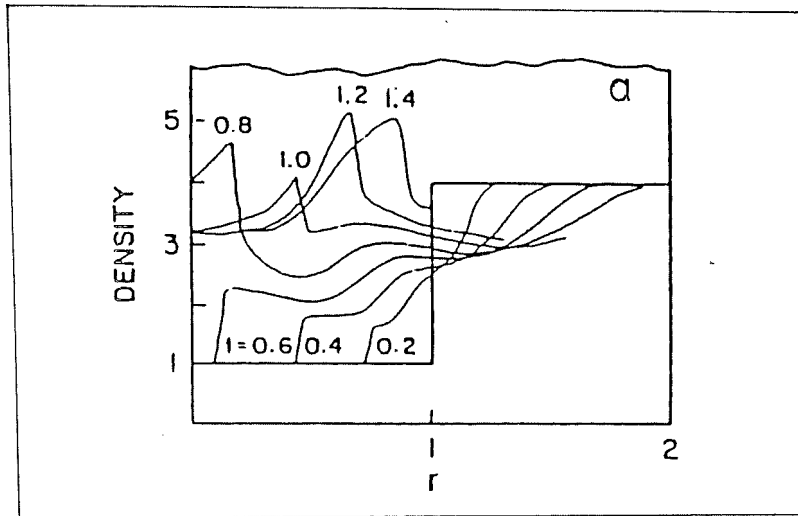


Fig. 5.8: Comparison of density problems for the Payne's problem. Number on curves in figures c and d represent relative time. Curves marked a represent the payne results while those marked b represent Lapidus results.

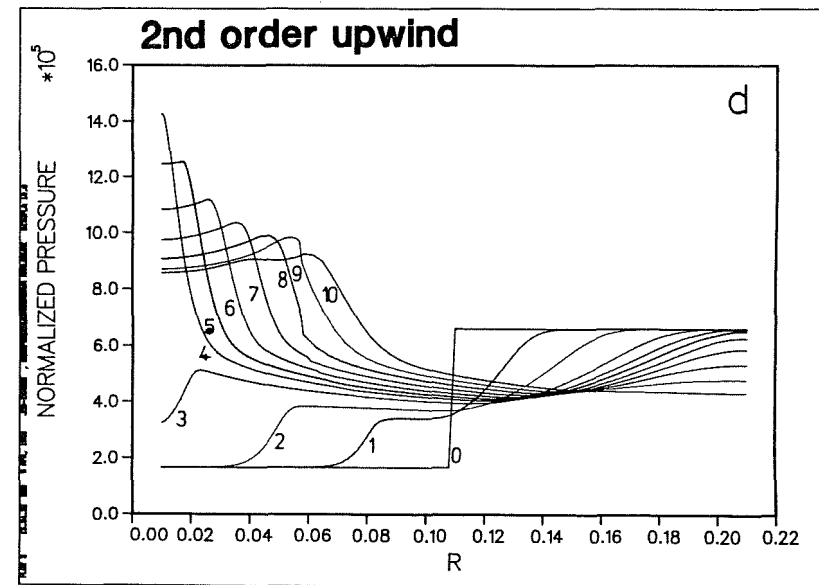
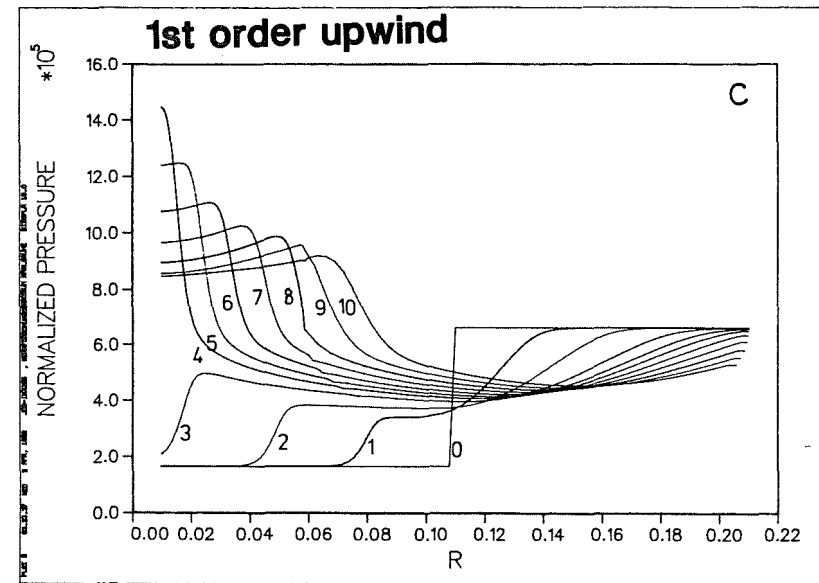
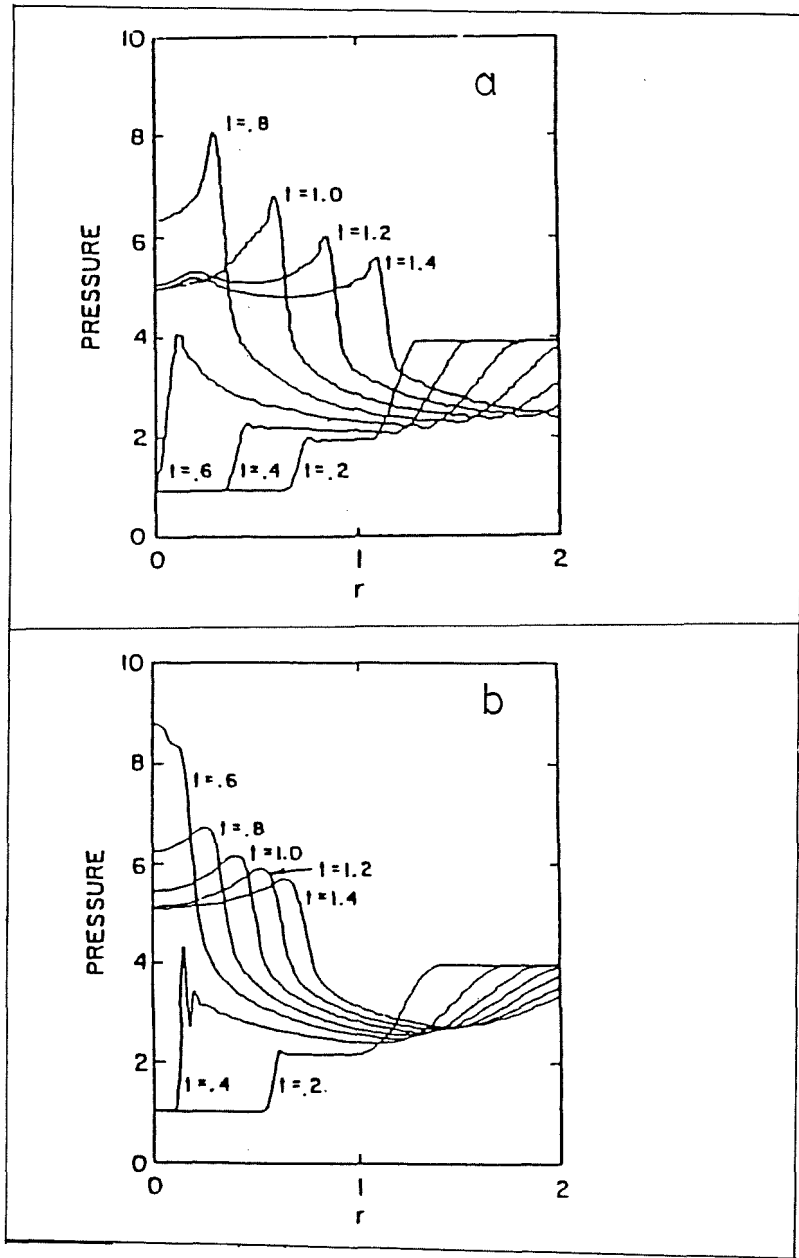


Fig. 5.9: Same as Fig. 5.8 but for pressure.

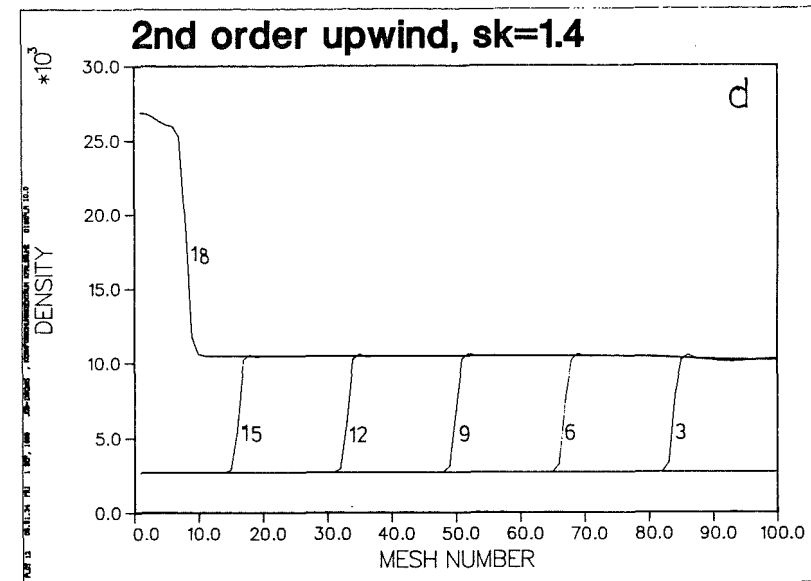
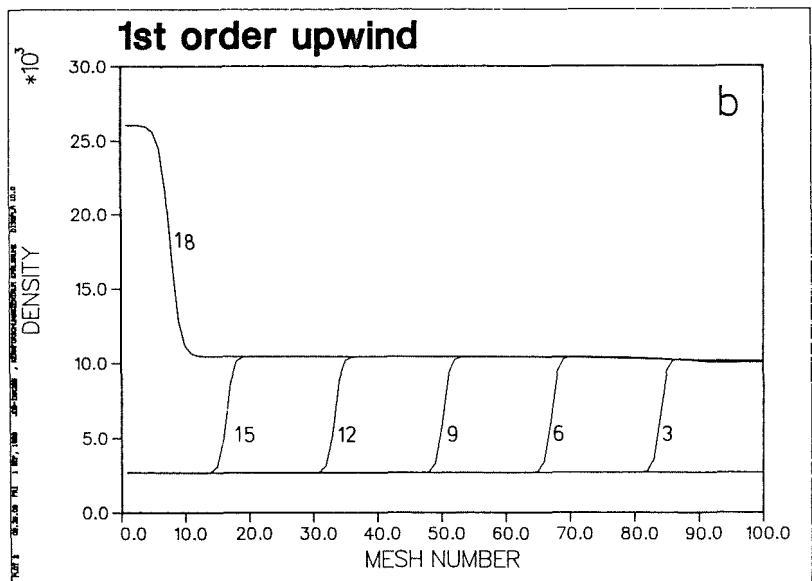
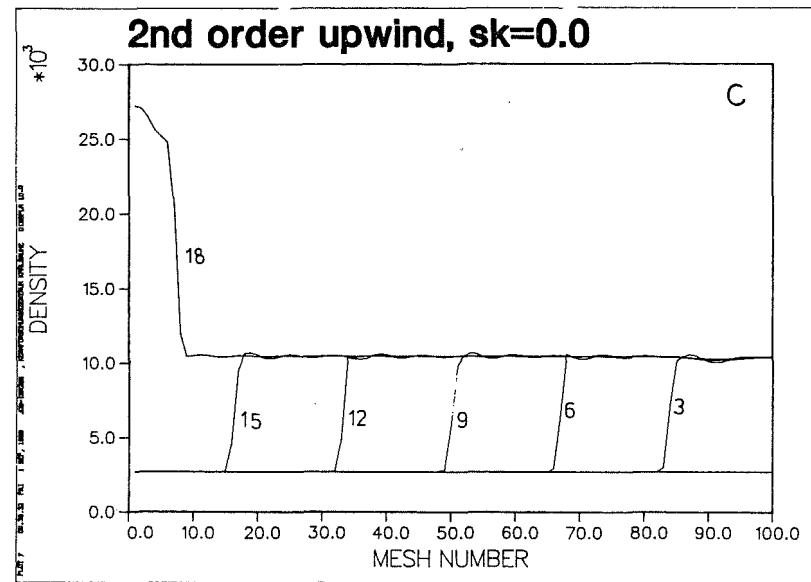
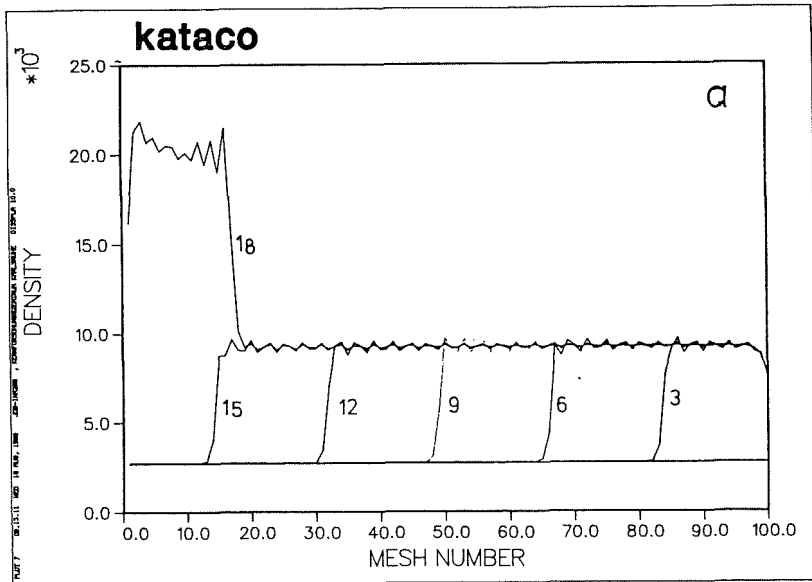


Fig. 6.1: Density profiles for the constant pressure pulse. Numbers marked on each curve represent time in nano-seconds.

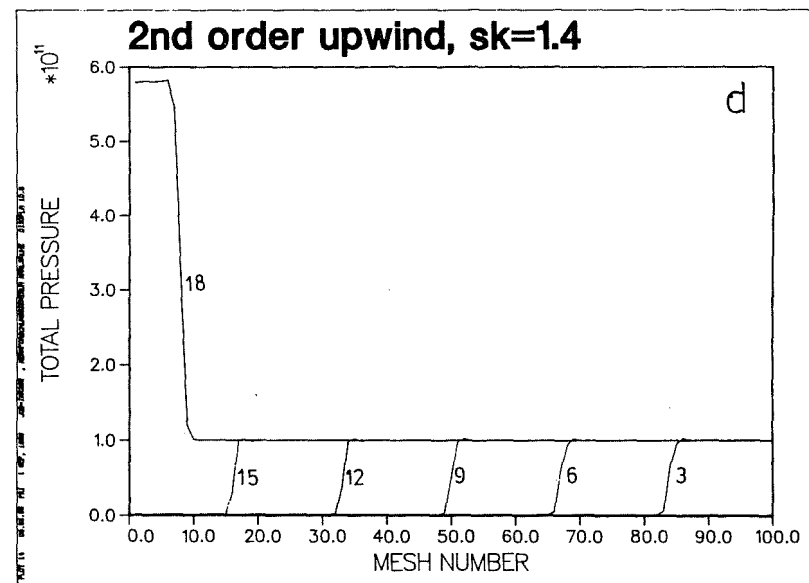
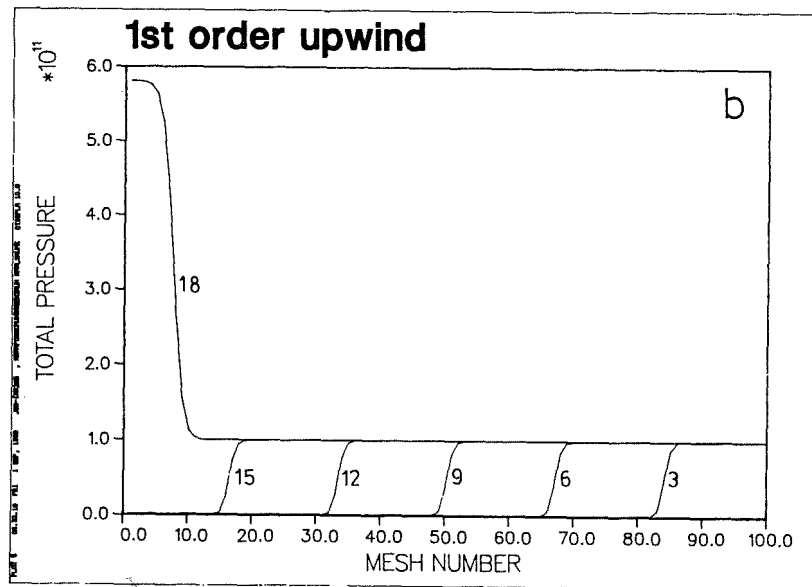
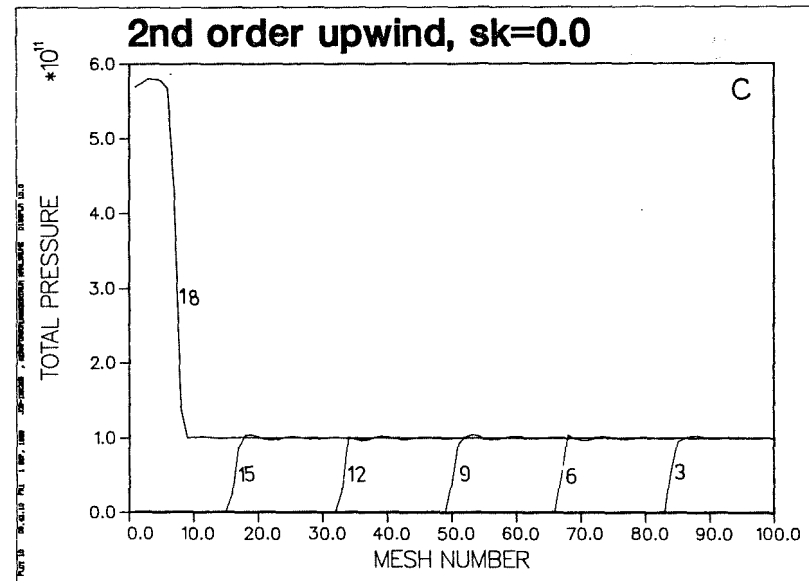
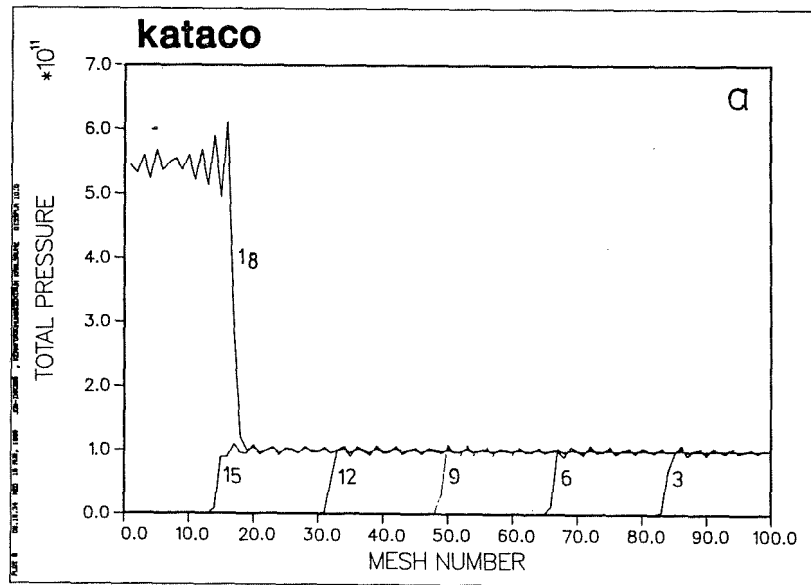


Fig. 6.2: Pressure profiles for the constant pressure pulse. Numbers marked on each curve represent time in nano-seconds.

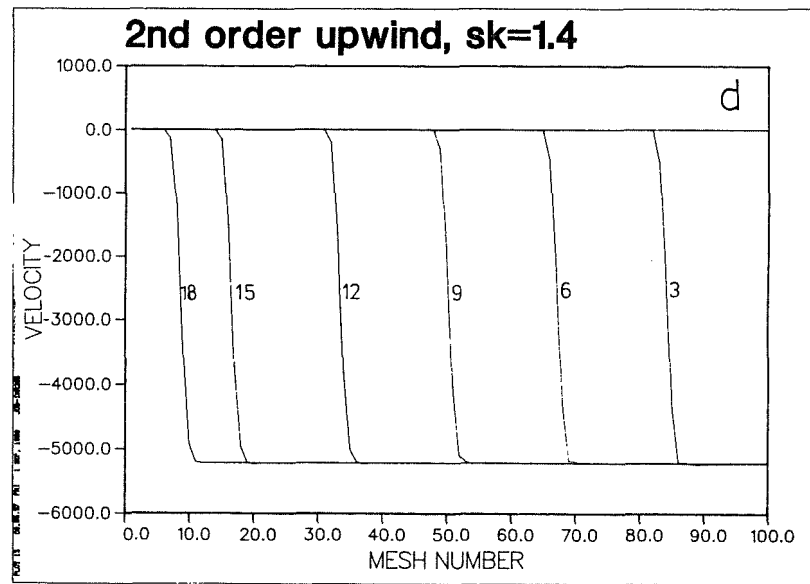
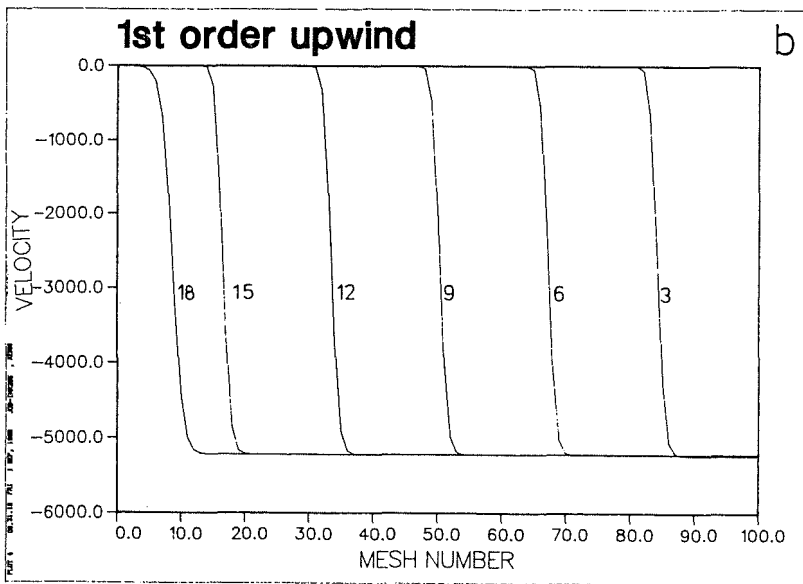
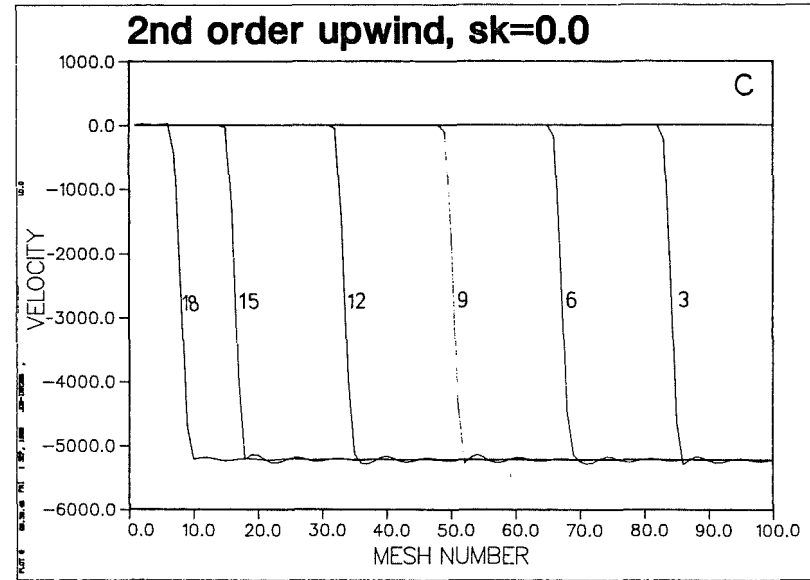
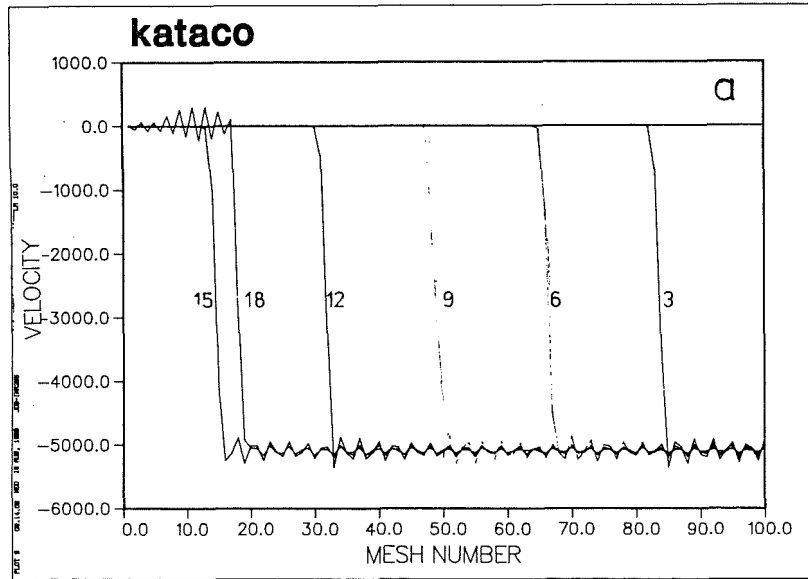


Fig. 6.3: Same as Fig.6.2 but for particle velocity.

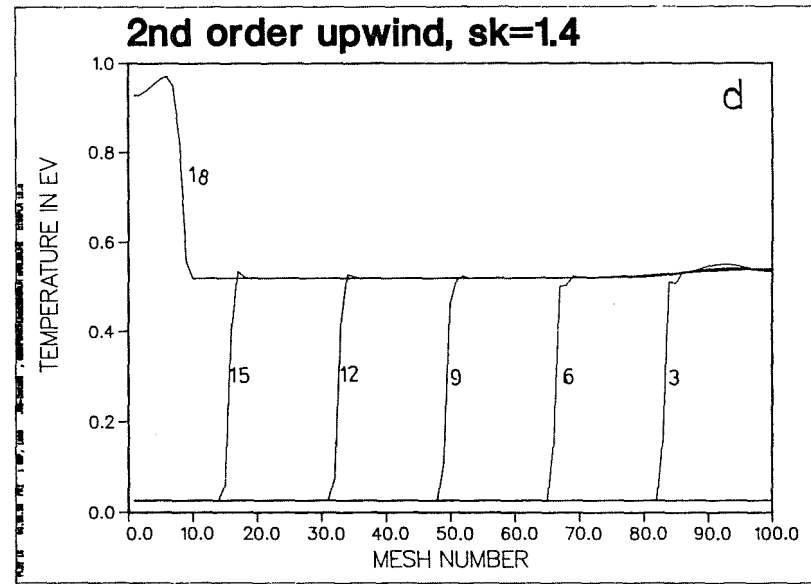
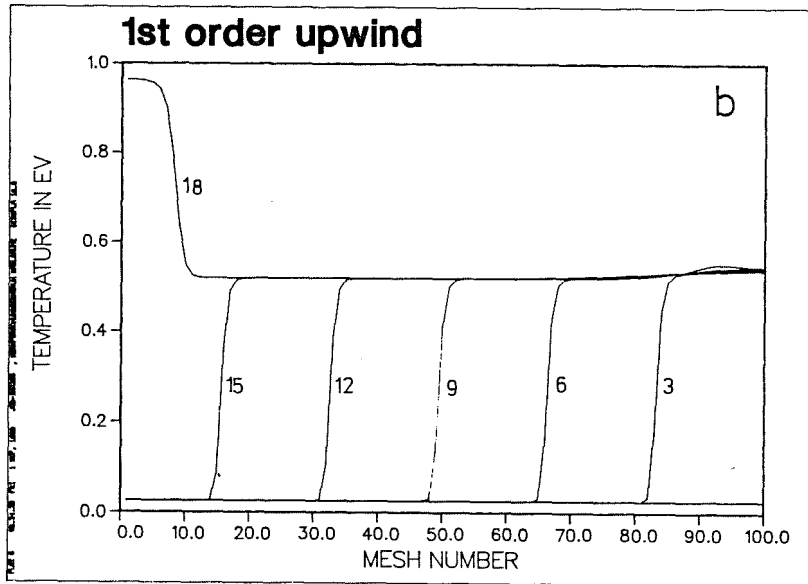
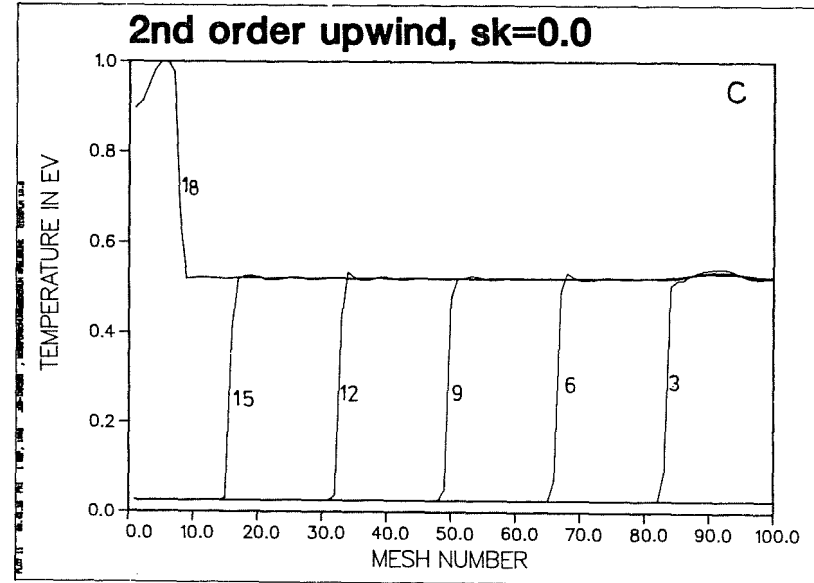
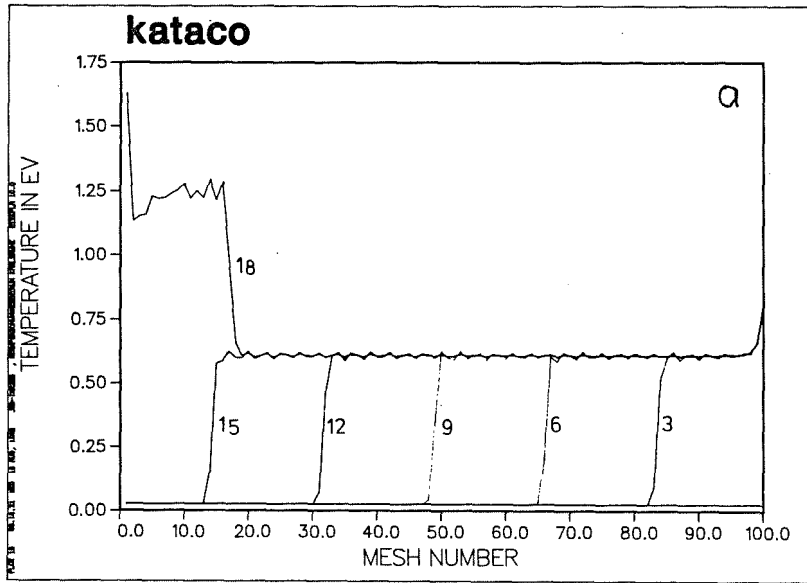


Fig. 6.4: Same as Fig. 6.2 but for temperature.

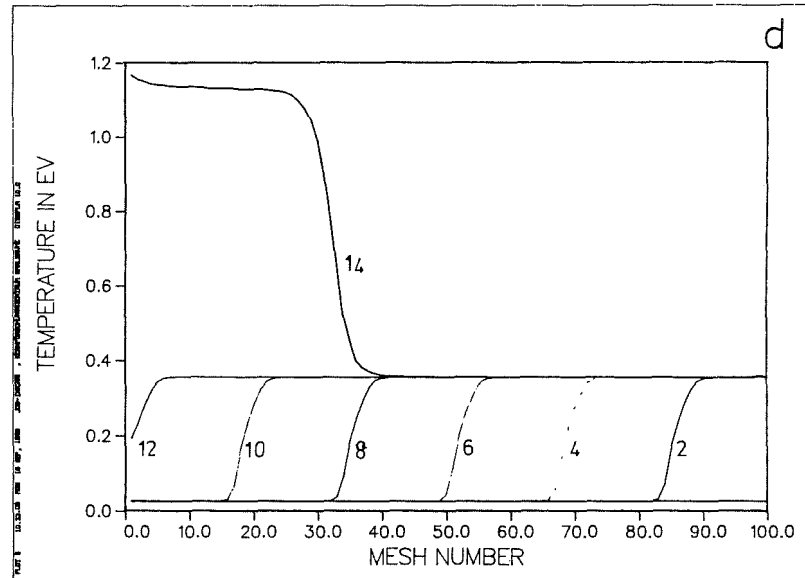
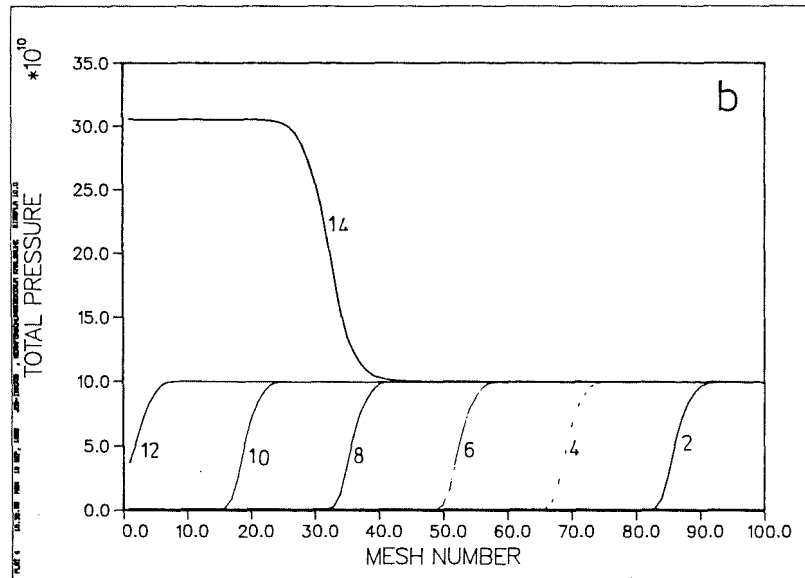
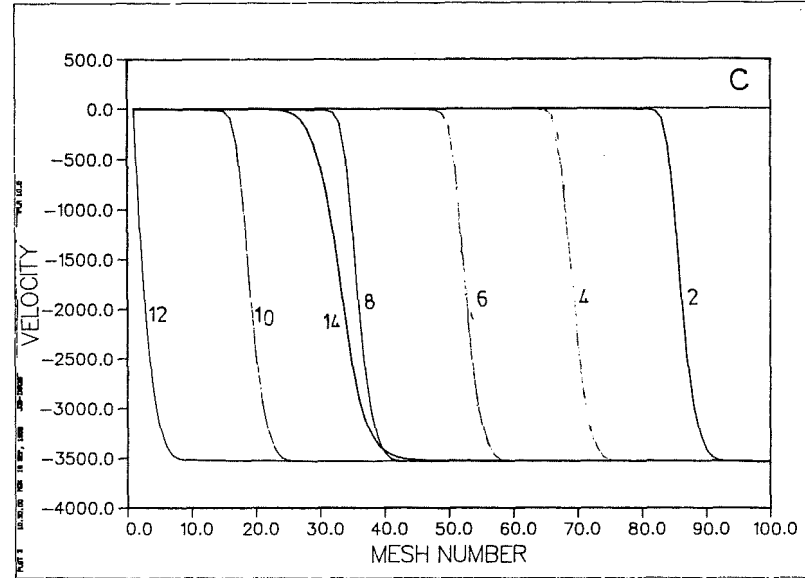
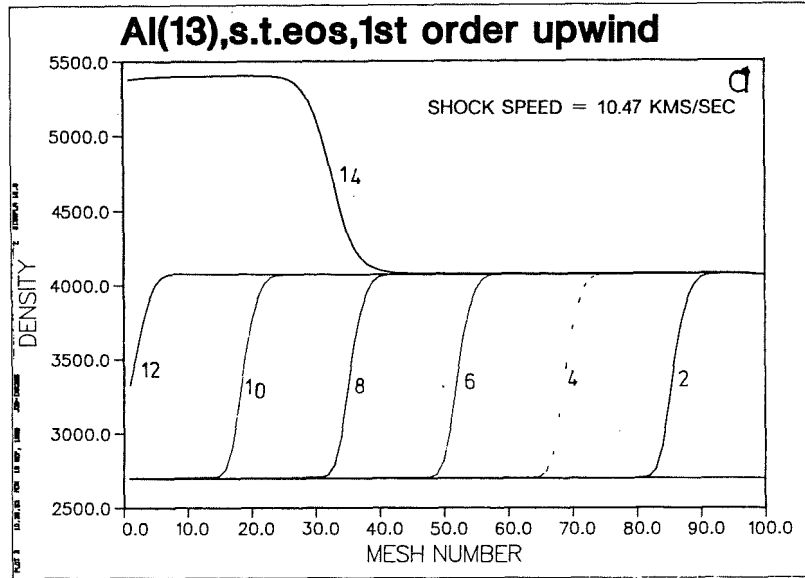


Fig. 6.5: 1st order upwind results for a constant pressure pulse with SESAME EOS. Numbers marked on each curve represent time in nano-seconds.

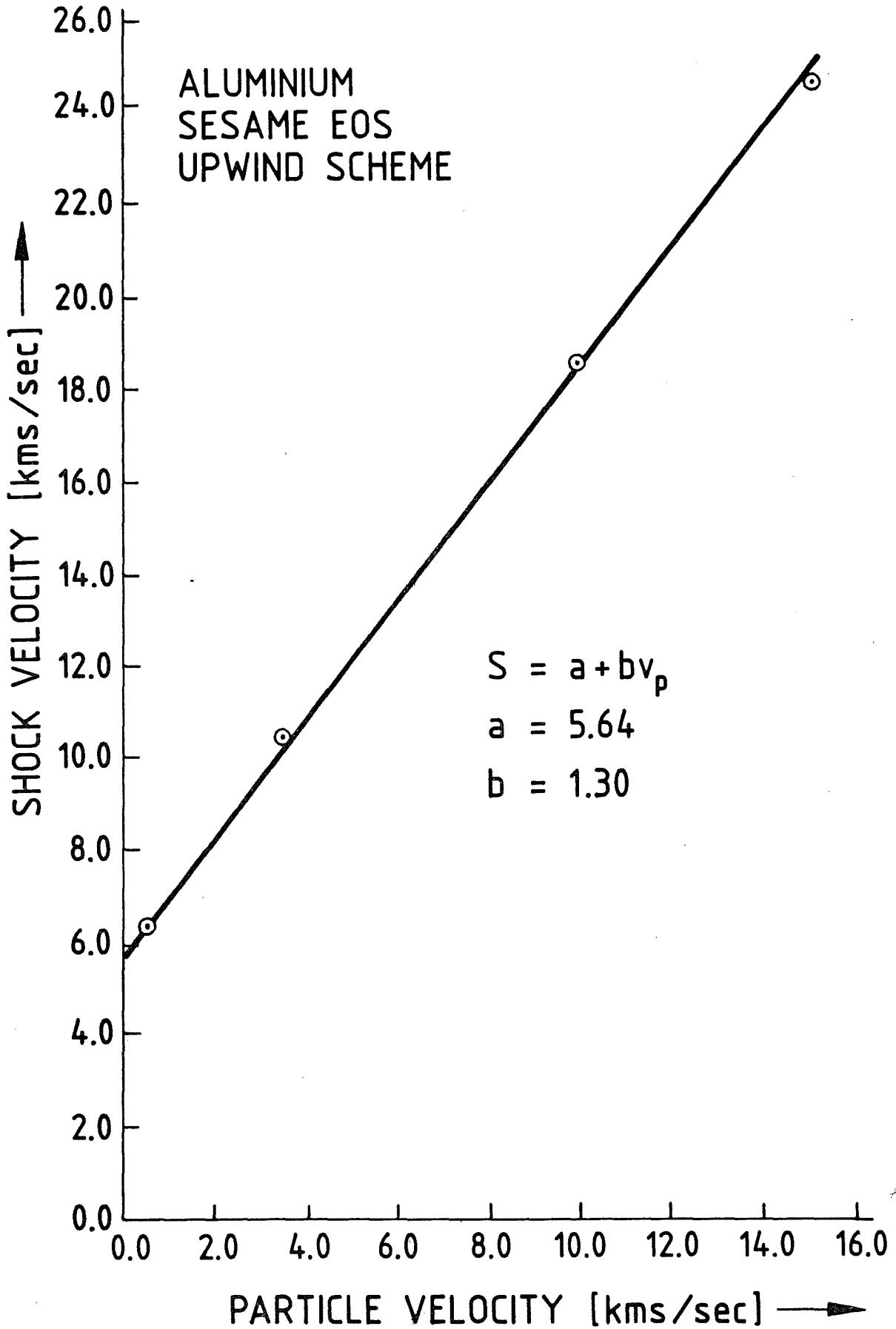


Fig. 6.6: Shock velocity vs particle velocity for an aluminium slab for constant pressure pulses. The four points on the curve correspond to the pressures of 10^{11} , 10^{12} , 10^{13} and 10^{14} Pascal.

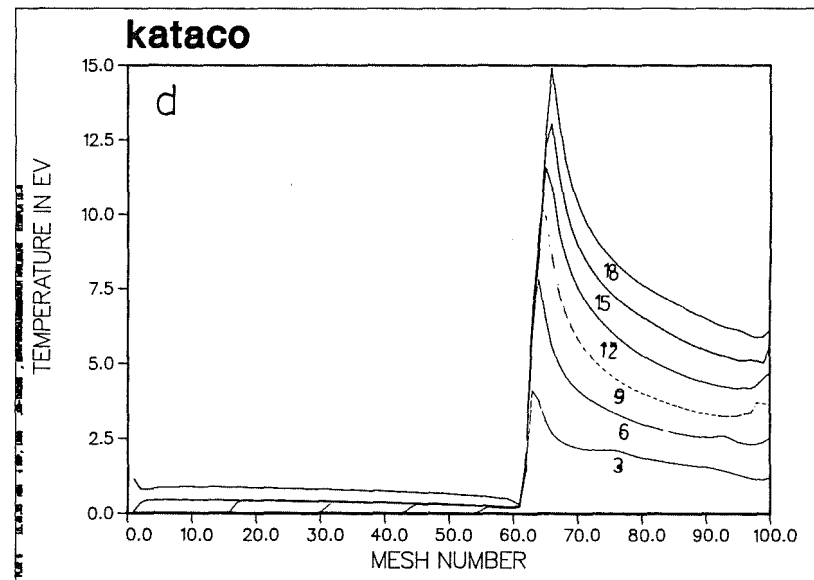
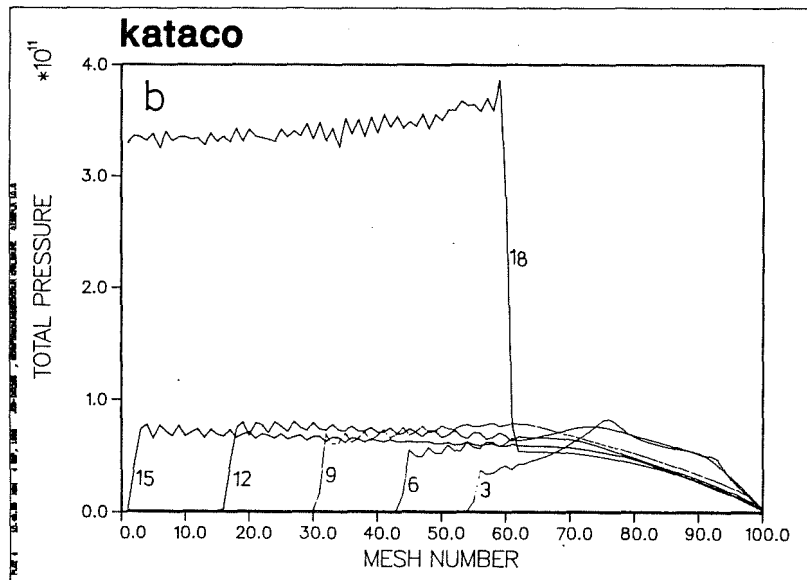
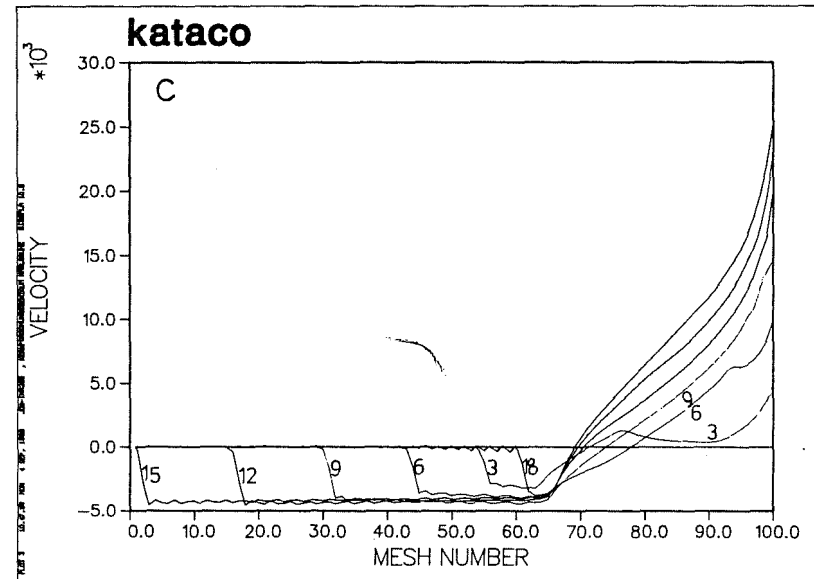
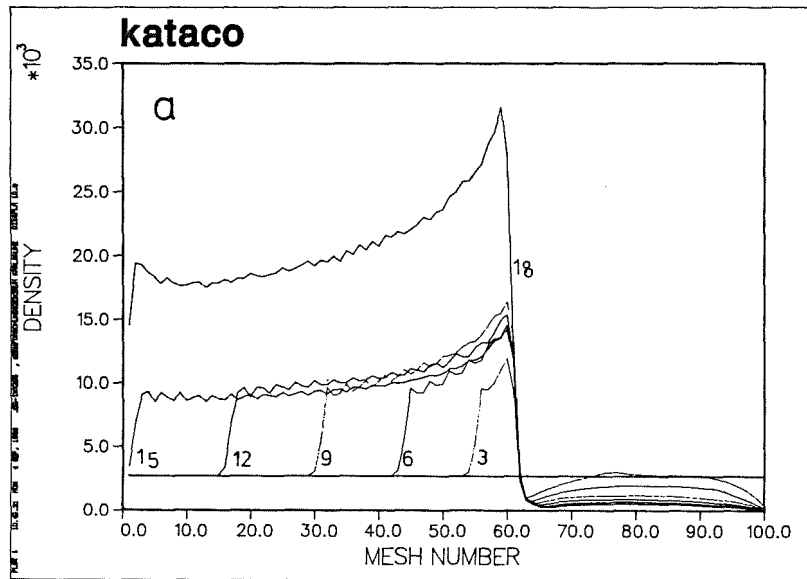


Fig. 6.7: KATACO results for a constant proton beam. Numbers marked on each curve represent time in nano-seconds.

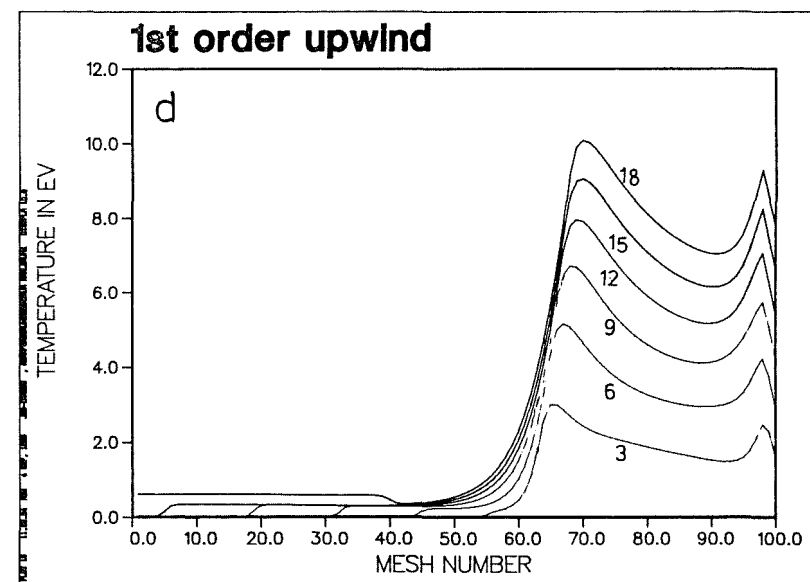
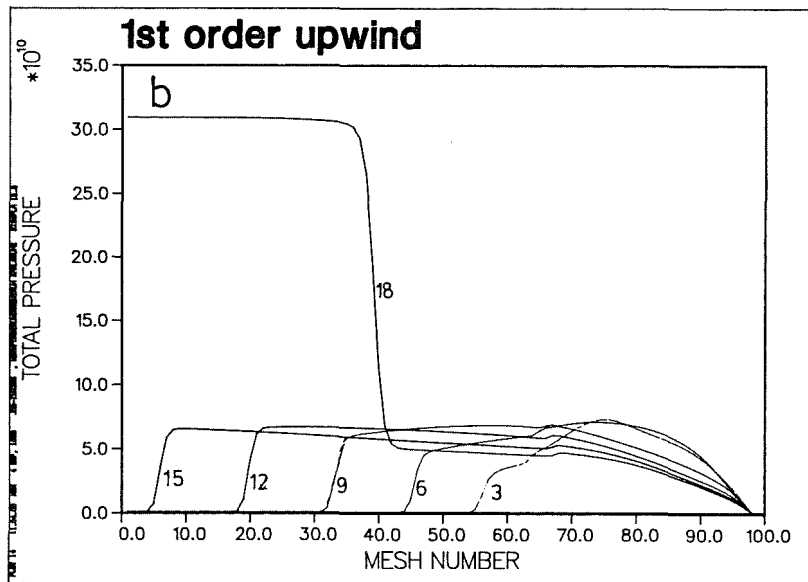
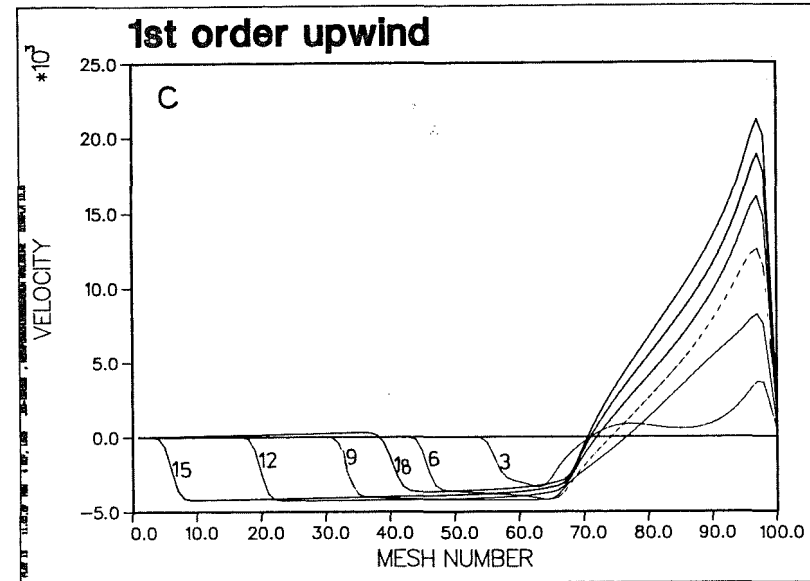
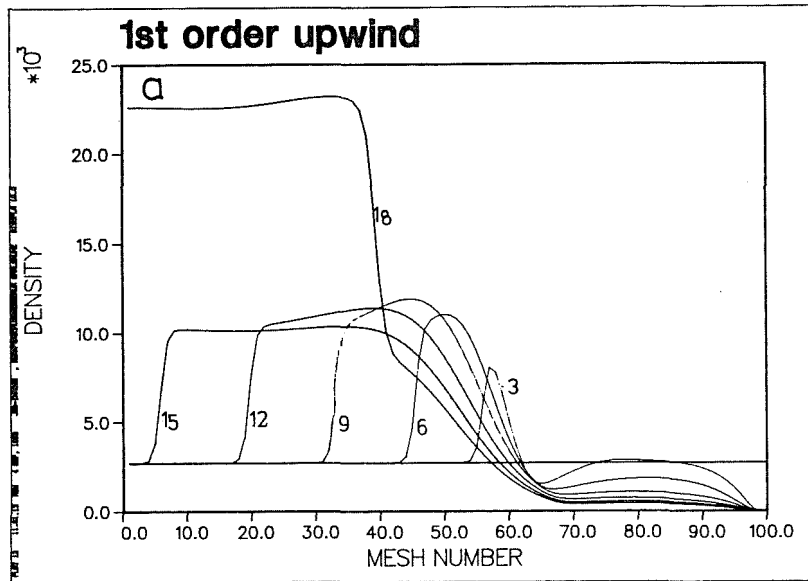


Fig. 6.8: 1st order upwind results for a constant proton beam. Numbers marked on each curve represent time in nano-seconds.

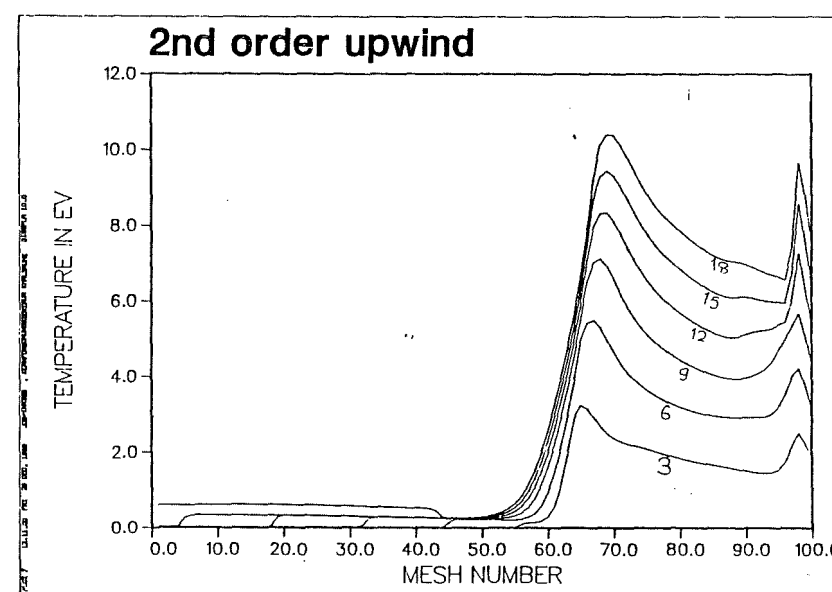
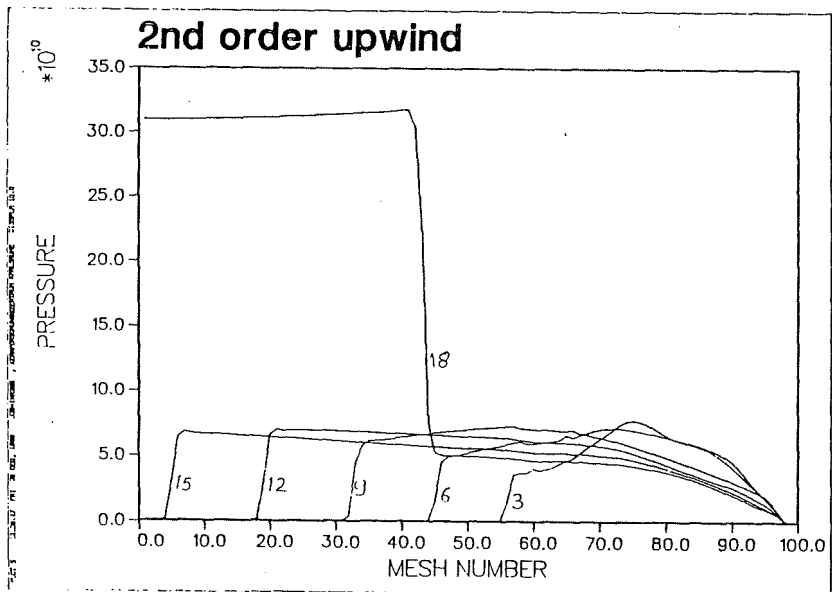
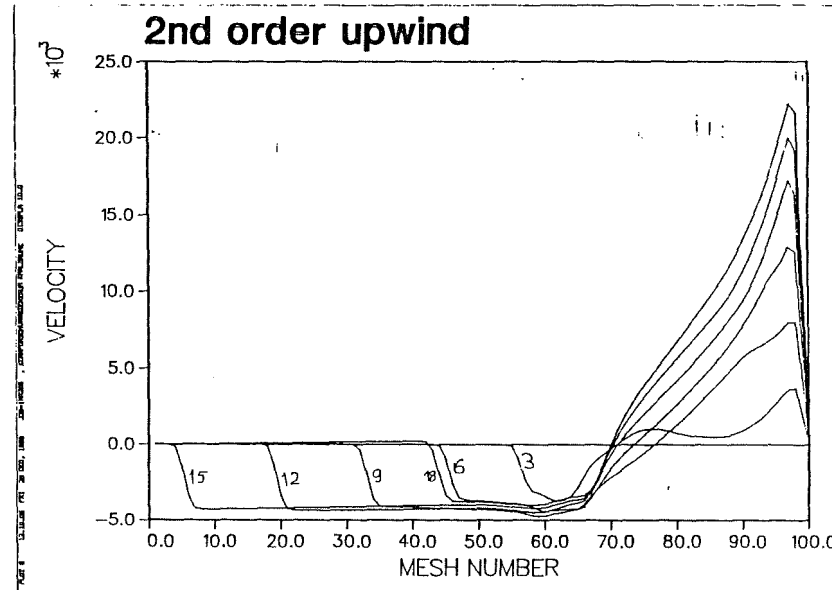
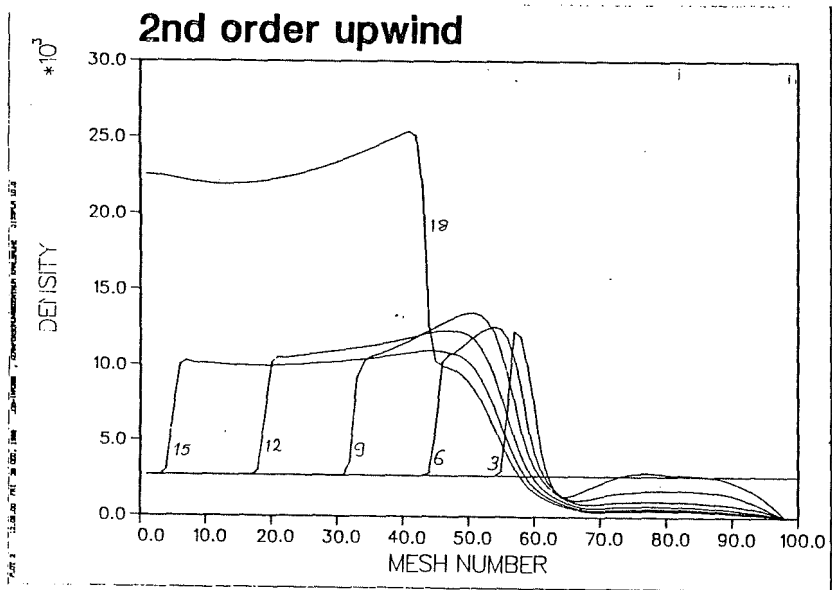


Fig. 6.9: 2nd order upwind results for a constant proton beam. Numbers marked on each curve represent time in nano-seconds.

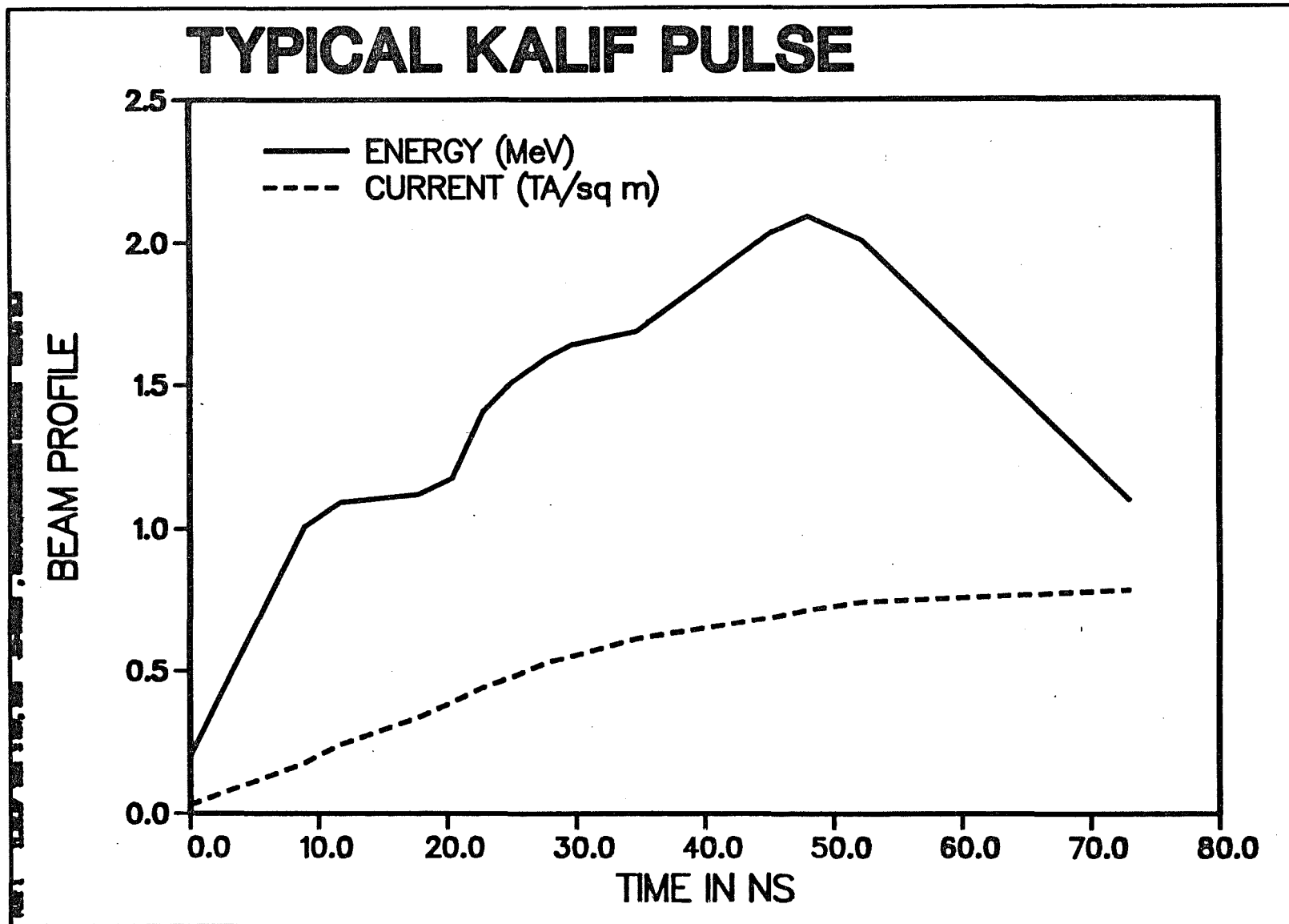


Fig. 6.10: Time profile of Pinch-reflex diode KALIF pulse.

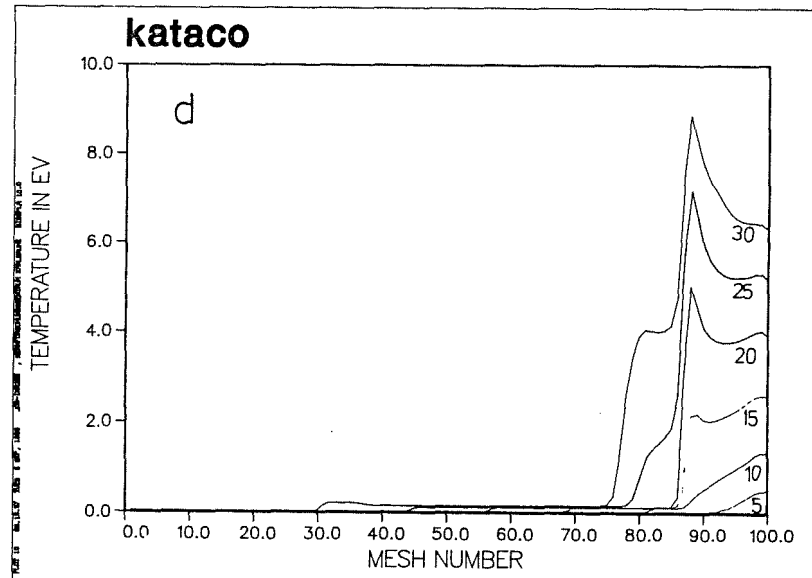
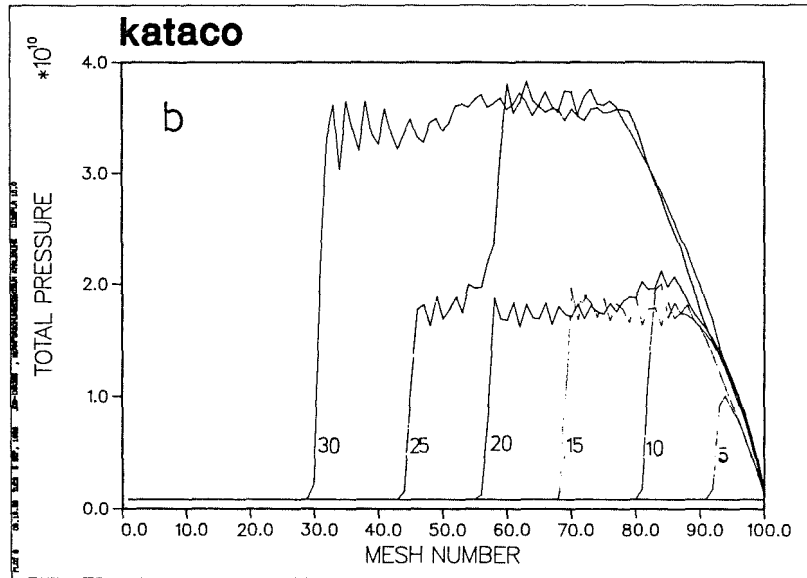
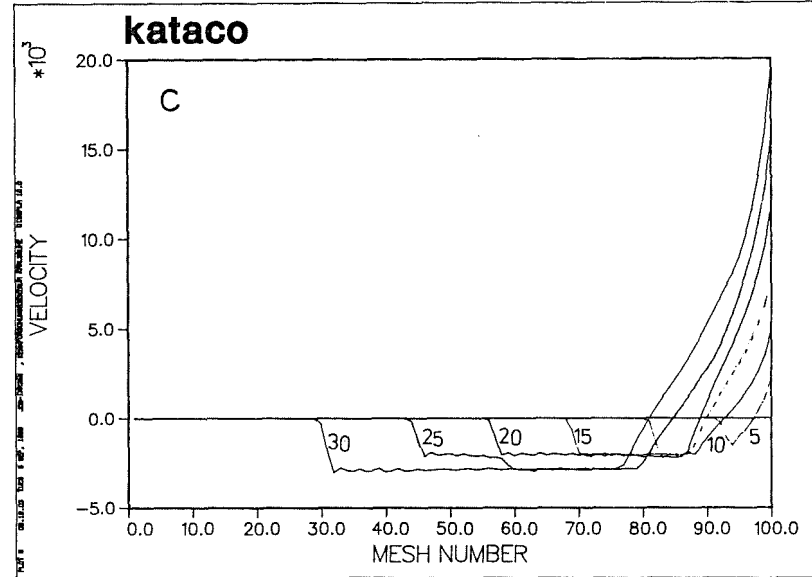
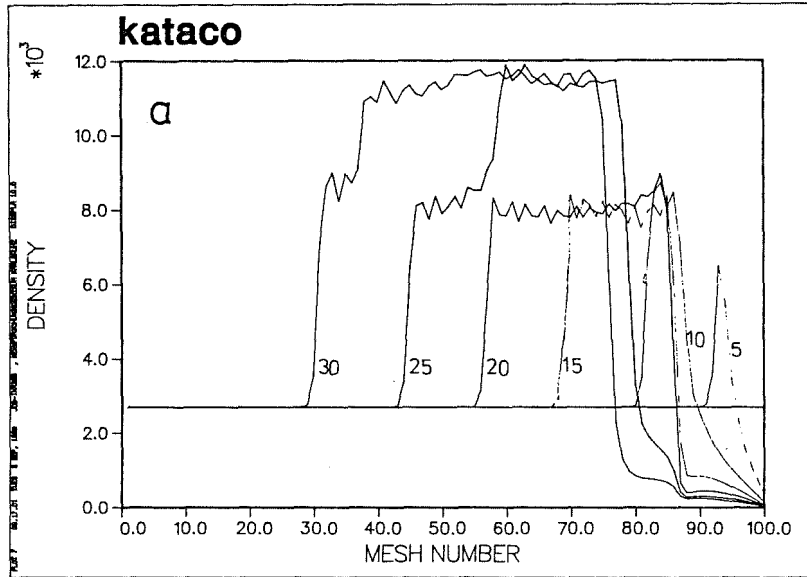


Fig. 6.11: KATACO results for KALIF pulse. Numbers marked on each curve represent time in nano-seconds.

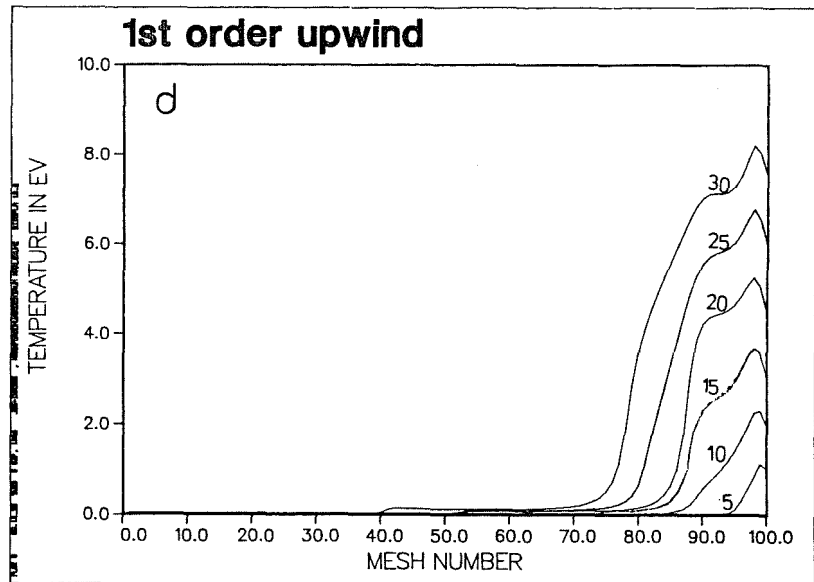
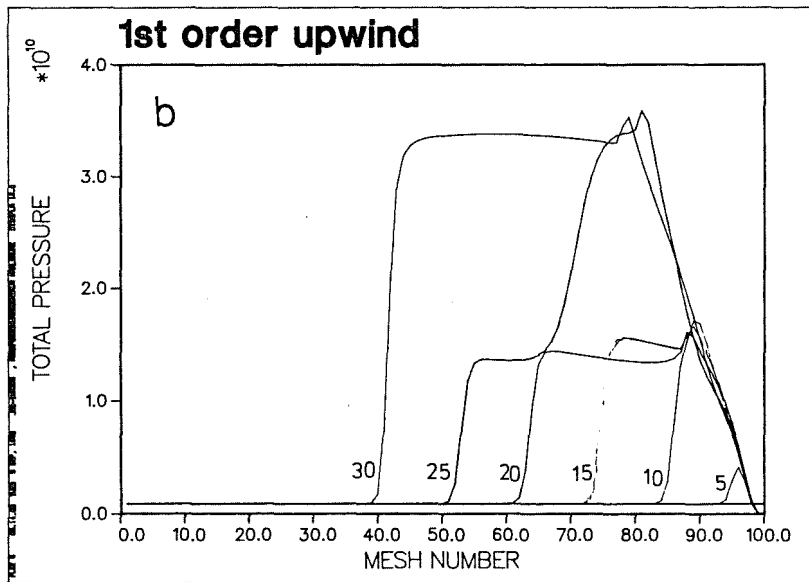
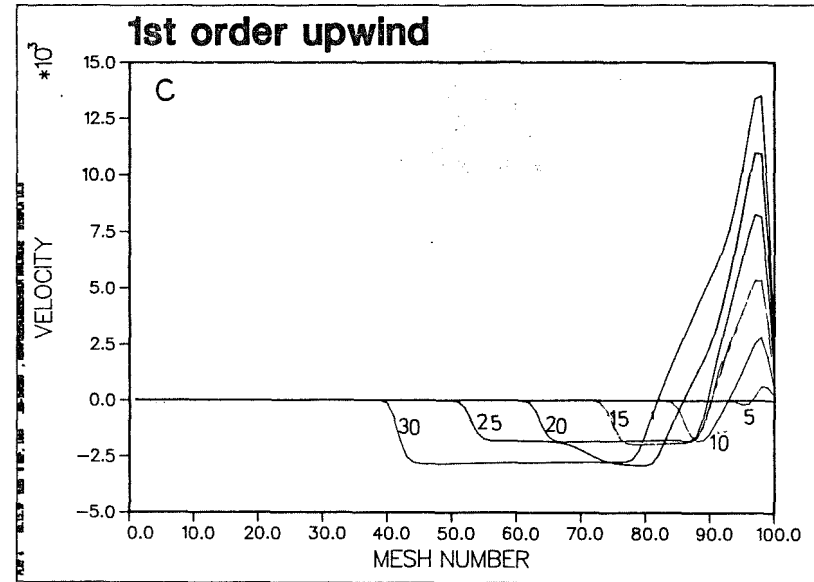
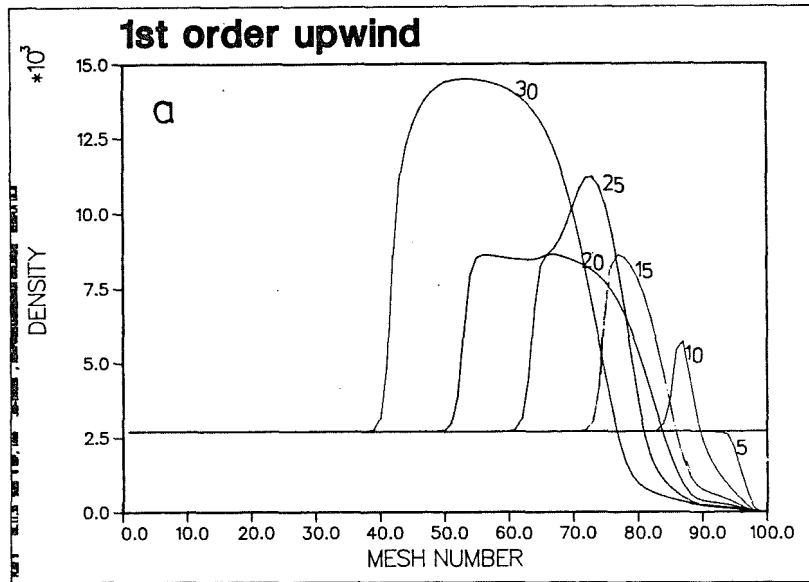


Fig. 6.12: 1st order upwind results for a KALIF pulse. Numbers marked on each curve represent time in nano-seconds.

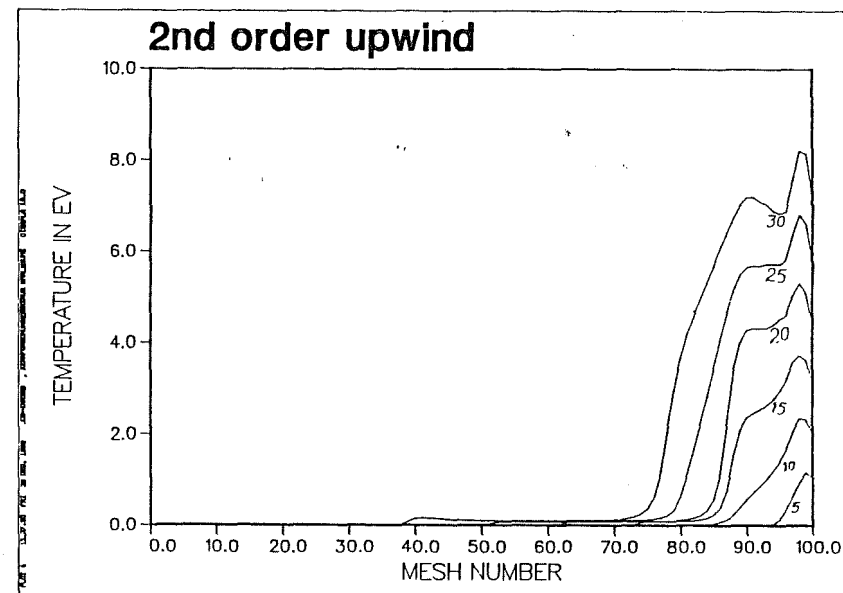
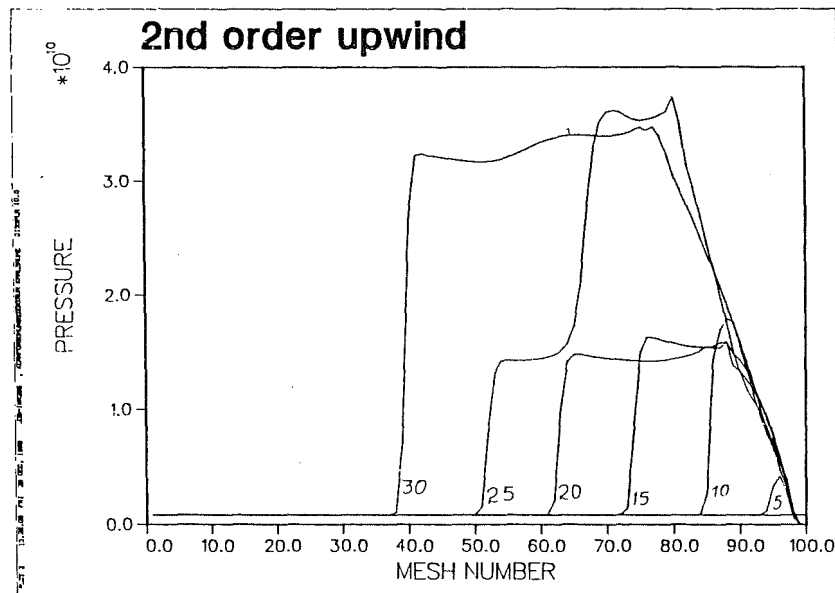
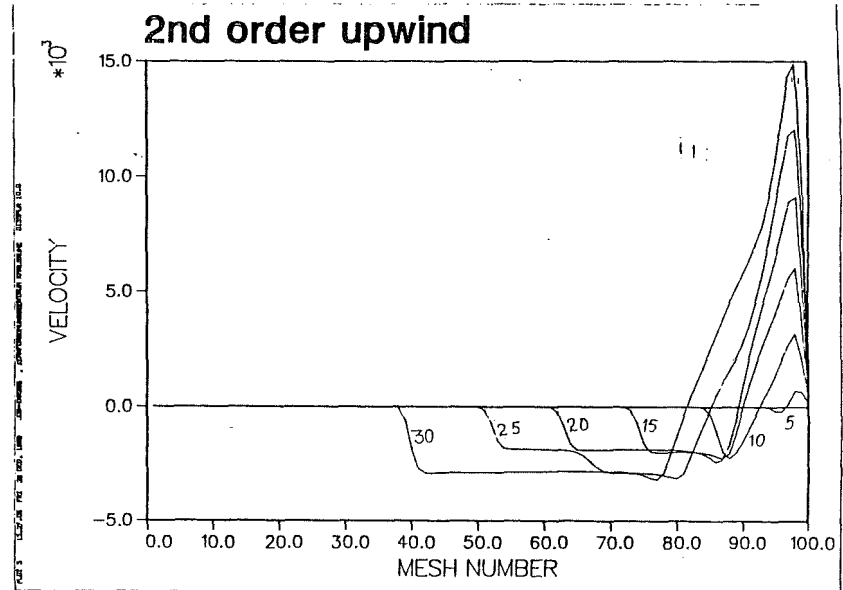
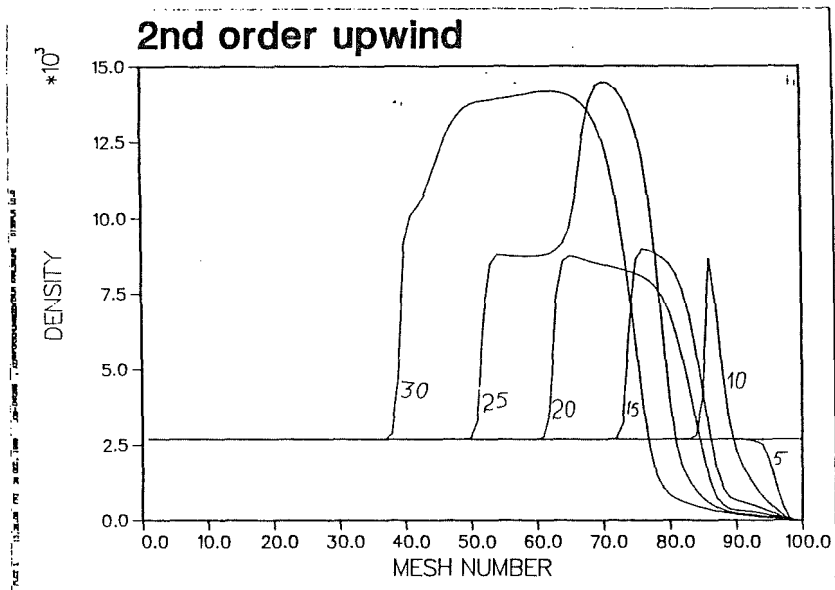


Fig. 6.13: 2nd order upwind results for a KALIF pulse. Numbers marked on each curve represent time in nano-seconds.

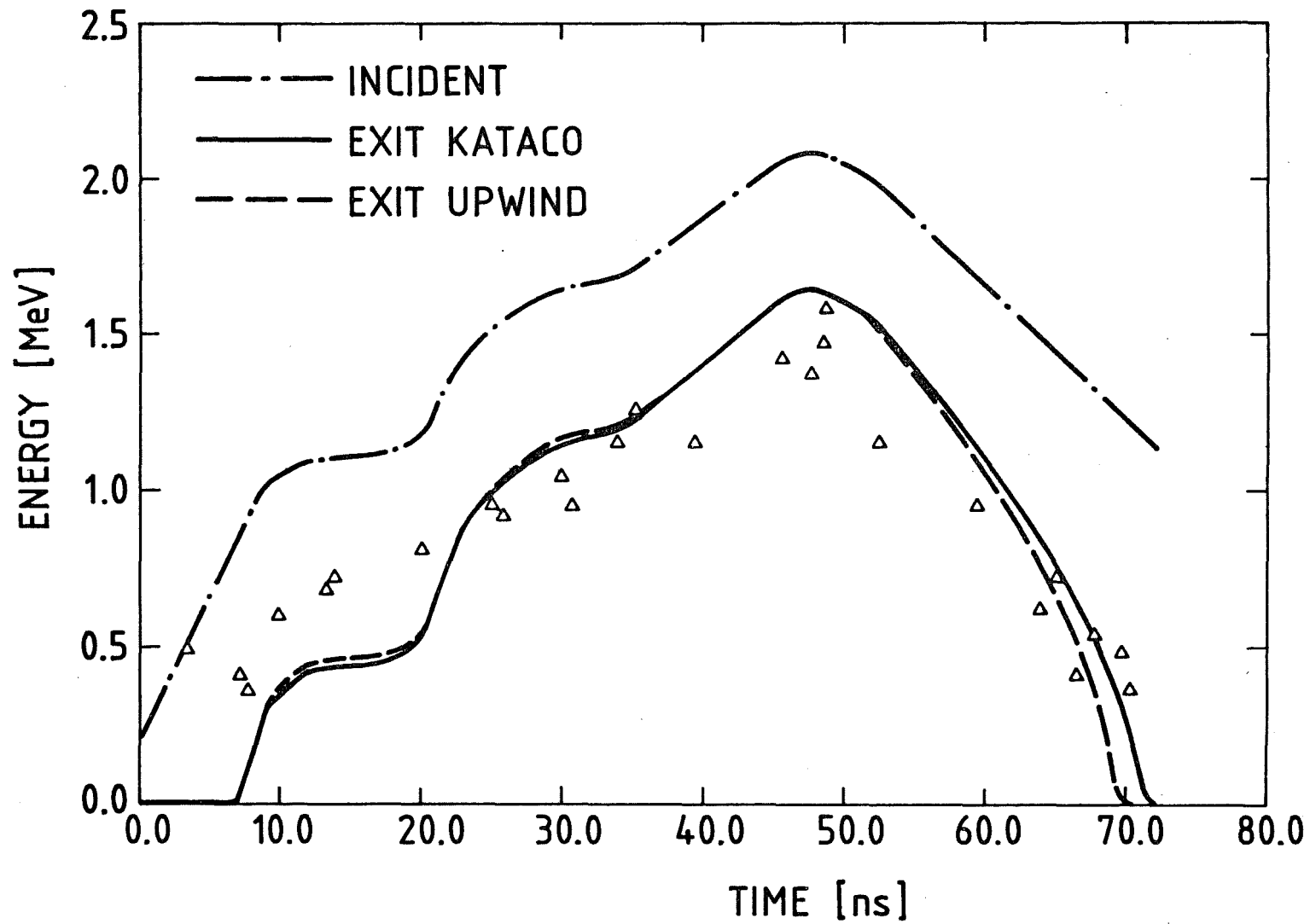


Fig. 6.14: Exit energy as calculated by KATACO and upwind scheme for pinch reflex diode KALIF proton pulse on aluminium slab.